UNIVERSITÀ DEGLI STUDI DI PADOVA

DIPARTIMENTO DI BIOLOGIA

Corso di Laurea magistrale in Biologia Sanitaria

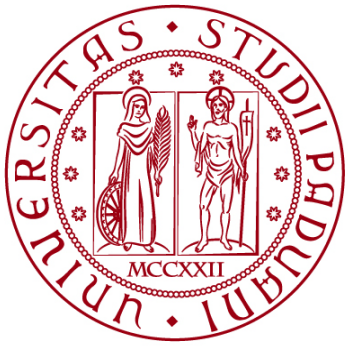

TESI DI LAUREA

Development of a fusion-entry system based on GFP complementation: an innovative approach for the screening of SARS-CoV-2 therapeutics

Relatore: Prof. Alfredo Garzino Demo
Dipartimento di Medicina Molecolare

Correlatore: Dott.ssa Adriana Vitiello
Dipartimento di Medicina Molecolare

Laureanda: Chiara Sandro

ANNO ACCADEMICO 2022/2023

TABLE OF CONTENTS

ABSTRACT

The severe acute respiratory syndrome coronavirus 2 (SARS-CoV-2) is a *Betacoronavirus* that causes COVID-19 disease. The mechanism of viral entry into human host cells consists in the binding of the Spike (S) protein to its receptor, angiotensin-converting enzyme 2 (ACE2), and subsequent membrane fusion. Molecules targeting SARS-CoV-2 entry mechanisms are a promising therapeutic approach since they inhibit the first step of infection. This experimental study provides an innovative assay to screen new antiviral drugs with a fusion-entry system based on Green Fluorescent Protein (GFP) complementation. The system development consists in the production of stable ACE2 or Spike-expressing cell lines, to allow the fusion between membranes. Each cell line also carries a construct encoding a part of the split GFP (GFP1-10 or GFP11); upon membrane fusion, complementation occurs reconstituting GFP. The expression of each component of the system is monitored through flow cytometry allowing the sorting of cells. Pilot cell-cell fusion assays are then performed, and fusion is monitored through fluorescent microscopy, flow cytometry and fluorescence plate reader. The assay, once optimized, will be used to screen new antiviral drugs that target SARS-COV-2 Spike - human ACE2 mediated entry-fusion.

1. INTRODUCTION

1.1 Coronaviruses: taxonomy and evolution

The severe acute respiratory syndrome coronavirus 2 (SARS-CoV-2) is a member of the *Coronaviridae* family (CoVs). *Coronaviridae* family belongs to the order of *Nidovirales* and the suborder of *Coronavirinae*. This family includes the *Orthocoronavirinae* subfamily, that is composed of four genera, based on genetic and serological characterization: *Alphacoronavirus, Betacoronavirus, Gammacoronavirus* and *Deltacoronavirus.* These viruses are thought to have diverged from each other at 2400-3000 BC [1]. *Alphacoronaviruses* and *Betacoronaviruses* infect mammals, including humans, while *Gammacoronavirus* and *Deltacoronavirus* primarily infect birds. The first *Coronavirus* was the avian infectious bronchitis virus, that was discovered in 1931 [2]. The first human *Coronaviruses* were HCoV-229E, discovered in 1966 and originated in bats, and HCoV-OC43, emerged in 1967 [2]. *Betacoronaviruses* can be divided into four lineages: lineage A (*Embecovirus*), B (*Sarbecovirus*), C (*Merbecovirus*) and D (*Nobecovirus*). In the last years, three *Betacoronaviruses* emerged in human population: SARS-CoV (Severe Acute Respiratory Syndrome Coronavirus), originating from China in 2002-2003 and belonging to the B lineage, MERS-CoV (Middle East Respiratory Syndrome Coronavirus), originating from the Middle East in 2012 and belonging to the C lineage of the *Coronaviruses*, and SARS-CoV-2 (Severe Acute Respiratory Syndrome Coronavirus 2), originating in the Wuhan city of China in 2019 and belonging to lineage B. SARS-CoV and SARS-CoV-2 are part of the *Sarbecovirus* subgenus (Fig.1) [1].

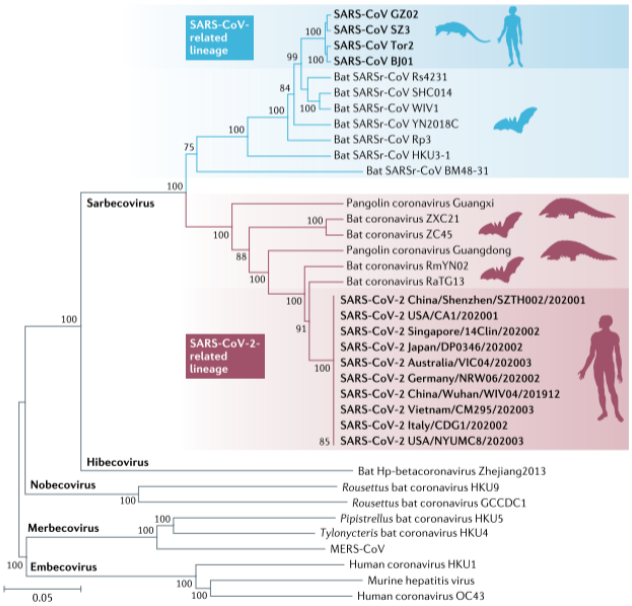

Fig.1: Phylogenetic tree of SARS-CoV and SARS-CoV-2 related lineages, that belong to the subgenus *Sarbecovirus.* In the graph four lineages are represented: *Embecovirus* (lineage

A), *Sarbecovirus* (lineage B), *Merbecovirus* (lineage C) and *Nobecovirus* (lineage D). The fifth lineage *Hibecovirus*, that has been recently added, is also represented. [3]

The symptoms of these three *Betacoronaviruses* include respiratory infections, fever, cough, and in people with a compromised immune system also death. In some cases, infected people are asymptomatic, but they can transmit the virus to other people [2]. Human-to-human transmission occurs through respiratory droplets produced when an infected person (symptomatic or asymptomatic) coughs or sneezes, otherwise through aerosol or contaminated surfaces [4]. Other three Coronaviruses are known to infect humans and to cause mild upper respiratory tract infections: HCoVs OC43, 229E, HKU1 and NL63 [1].

Coronaviruses are positive-sense single-stranded RNA viruses (+ssRNA) with the largest genome among other RNA viruses. These viruses use an RNA-dependent RNA polymerase to replicate, which has a 5'-3' proofreading exoribonuclease: this efficiency of correction is different in different hosts, and this allows the emergence of new variants. SARS-CoV-2 shares 79.6% nucleotide similarity with SARS-CoV and 83% nucleotide similarity (considering synonymous substitution) with bat coronavirus RaTG13 from *Rhinolophus affinis* [1]. Furthermore, SARS-CoV-2 shares also close relations to bat coronavirus ZC45 and ZXC21 [2].
SARS-CoV-2 genome shows more similarities with bat coronavirus RaTG13 in R1, a region that contains ORF1b, R2, a region that includes the 5' region of the Spike protein, and R4, a region that includes the nucleocapsid protein. In R3, that includes the variable loop region of the Spike protein, the genome is more like the Pangolin Guangdong 2019 virus than with RATG13 (Fig.2) [1].

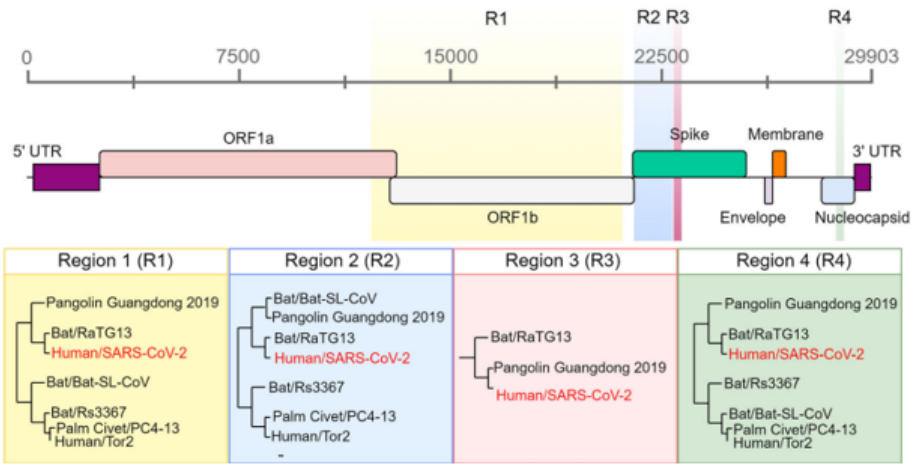

Fig.2: Variations in human SARS-CoV-2 genome in comparison with other coronaviruses. The figure shows four genome regions: R1, R2, R3 and R4 [1]. In R1, R2 and R4 the human coronavirus is more similar to bat coronavirus RaTG13, while in R3 it is more similar to the Pangolin Guangdong 2019 [1].

To enter the host cells, the viral Spike protein binds to host membrane proteins: MERS-CoV binds DPP4 (dipeptidyl peptidase 4, also known as CD26), HCoV-229E

binds APN (alanine aminopeptidase), HCoV-OC43 binds N-acetyl-9-O-acetylneuraminic acid, bat SARS-related coronaviruses, SARS-CoV and SARS-CoV-2 bind ACE2 receptor [5]. Mutations in the protein sequence of the receptor can lead to the generation of new coronaviruses variants and can influence spillover from one species to another species. The fact that bat SARS-related coronaviruses use human ACE2 receptor to enter host cells suggests that SARS-CoV-2 originated in bats and then it was transmitted to humans [5]. The environmental separation between bats and human suggests the existence of an intermediate host. In 2020 several chicken, duck, pigeon, and goose coronaviruses were observed in wet markets in China, and this suggests that these animals could be intermediate hosts for *Coronaviruses*, included SARS-CoV-2 [5]. Moreover, red foxes, hog badgers and common raccoon dogs were sold live at the Wuhan market in November 2019, and they can be potential intermediate hosts of the virus. Pangolin Guangdong 2019 virus and other coronaviruses from pangolins were observed to be in the same clade of coronaviruses from bats, so this can suggest that pangolins may be an intermediate host, but conclusive evidence is lacking [1].
Regarding SARS-CoV-2 Spike protein, the amino-terminal and carboxy-terminal parts are similar to bat coronaviruses ZC45 and ZXC21, while the middle part of the Spike is similar to the SARS-CoV and bat coronavirus WIV1 and RsSHC014 [2]. A variation in the amino acidic sequence of the Spike protein of SARS-CoV-2 is the furin cleavage site (PRRAR, a polybasic cleavage site), which is found to be similar in other human *Coronaviruses* such as MERS-CoV, HCoV-HKU1 and HCoV-OC43, but absent in other *Sarbecoviruses.* Moreover, an independent insertion of amino acids (PAA) at the same region of the Spike has been identified in the bat coronavirus RmYN02. During the pandemic, some scientists hypothesized that the FCS was engineered in laboratory due to the presence of the same sequence RRARSVAS in one of the FCSs of human amiloride-sensitive epithelial sodium channel α subunit (ENaC). This hypothesis was not confirmed because five of the amino acids present in the PRRARSVAS sequence were also found in other bat *Coronaviruses,* moreover, in the SARS-CoV-2 Spike sequence there is an insertion of 12 nucleotides, and every codon except one was different in the two sequences. The PRRAR leads to the protein cleavage and to the resulting conformational transitions and enhanced infection. Furthermore, it broadens the range of permissive cells because human furin is ubiquitous. Therefore, the Spike protein of SARS-CoV-2 is more efficient at binding ACE2 and can infect more permissive cells than previous *Coronaviruses*, and this can explain its high transmission into the human population. [2].

In conclusion, there is molecular evidence that *Coronaviruses* have spilled from bats into humans because of Spike similarities of different viruses that infect the two hosts and entry with ACE2 receptor. These spillover events must be prevented to avoid new coronavirus outbreaks, for example controlling hygienic conditions in wet markets.

1.2 SARS-CoV-2: genome replication and biology

SARS-CoV-2 is the etiological agent of coronavirus disease 2019 (COVID-19). It is an enveloped positive-sense single-stranded RNA (+ssRNA) virus with a genome of about 29.903 bp. It has the largest known RNA genome among all RNA viruses [6]. The genome (Fig.3) has a m^7G 5' cap structure and a 3' poly-A tail with 30-60 nucleotides. The 3' end has the function of preventing cellular exoribonuclease digestion and increasing viral genome stability. The 5' untranslated region (UTR) has 265 nucleotides and contains a 5' leader sequence of about 72 nucleotides, a transcription regulatory core sequence (TRS_L), some *cis* elements that confer resistance to degradation of viral messenger RNAs and regulate viral translation, sub-genome synthesis and viral genome packaging. The 3' UTR has 337 nucleotides and contains the binding site of the replication and transcription complex (RTC). ORF1a and ORF1b (also known as ORF1ab), two large Open Reading Frames partially overlapping located near the 5' end of the viral genome, encode 16 non-structural proteins (nsps). These 16 nsps derive from the cleavage of the two polyproteins by two self-activating viral proteases: Papain-like protease (also known as nsp3) and 3-chymotrypsin-like protease (also known as nsp5 or Mpro). Furthermore, the genome encodes 4 structural proteins (E, M, S and N) and 6 accessory proteins (from ORF3a, ORF6, ORF7a, ORF7b, ORF8 and ORF9b), which are translated from newly synthesised individual genomic RNAs (sgRNA). Based on computer predictions, additional ORFs might exist in the genome: for example, ORF10 and other ORFs overlapping S, ORF3a and N in alternative positive sense reading frames may encode functional proteins [7].

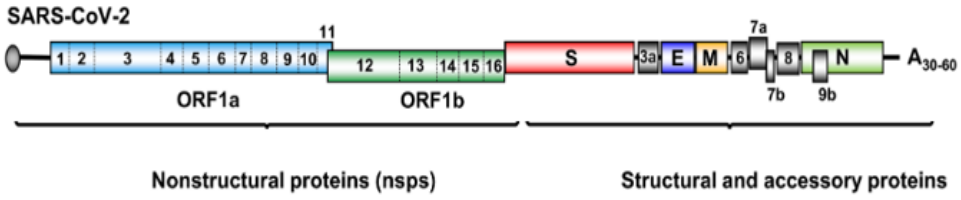

Fig.3: SARS-CoV-2 genome structure. At the 5' there is a cap. ORF1a and ORF1b near the 5' encode 16 non-structural proteins (nsps). At the 3' there is a poly-A tail (A30-60). Near the 3' are located genes that encode 4 structural proteins (E, M, S and N) and ORF3a, ORF6, ORF7b, ORF8 and ORF9b that encode accessory proteins. Additional ORFs that are not represented may exist [6].

The virion (Fig.4) consists of viral nucleocapsid proteins (N) and an envelope membrane with lipids and viral proteins Spike (S), membrane (M) and envelope (E). The N protein has the function of packaging the viral RNA (gRNA) into a ribonucleoprotein complex (RNP) and of interacting with other structural proteins

during viral particles assembly. The most abundant structural protein is the M protein, a transmembrane glycoprotein with three transmembrane domains involved in viral morphogenesis and budding. The E protein is the smallest integral membrane protein, and its functions are unclear. It has been shown that E protein exists in a monomeric form that interacts with cellular proteins to alter secretory and intracellular signaling pathways, and it can also form oligomers. In the homo-pentameric form it is thought to act like an ion channel for cations (viroporin), like Ca2+, in the viral membrane and its function is to regulate the host cell microenvironment and to facilitate releasing of viral particles from host cells. Inflammatory-mediated lung damage is correlated with the transport of Ca2+ through E pentamer. The channel activity of E also leads to trafficking of virions [8].

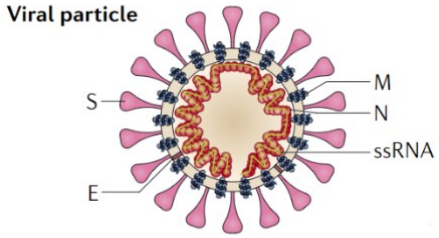

Fig.4: Viral particle of SARS-CoV-2 with Spike (S), envelope (E), membrane (M), and nucleocapsid (N) proteins. Spike proteins protrude from the virus surface, and they appear like a crown. The viral genome is a positive-sense single-stranded RNA (+ssRNA) encapsidated by nucleocapsid proteins (N) [2].

The Spike protein of SARS-CoV-2 is involved in the recognition of angiotensin-converting enzyme 2 receptor (ACE2) and in the entry in host cells. It is synthetised as a single-chain precursor and then trimerized. As mentioned above, it is cleaved by the cellular protease furin in the PRRAR, resulting in enhanced infection, and expanded cell tropism. Proteolytic cleavage of the Spike can also be realized by the protease TMPRSS2 at the cell surface, which is a type II transmembrane serine protease of the TTSP family, or by cathepsin B/L in the endosome, or by other trypsin-like proteases and this results in the release of the viral RNA into the cell cytoplasm. Also, TMPRSS13 and TMPRSS11D, that are other members of the TTSP family, can cleave the Spike protein but with less efficiency than TMPRSS2 [9].

The first step of infection involves the binding between the Spike and the ACE2 receptor (Fig.5). ACE2 is also recognized as an entry receptor by other human coronaviruses, like hCoV-NL63 and SARS-CoV. A recent study underlies the function of different cofactors in facilitating the viral entry into the host cells, like neurophilin-1 (NRP-1), CD147, phosphatidylserine receptors, heparan sulphate proteoglycans, sialic acids, and C-type lectins [10].

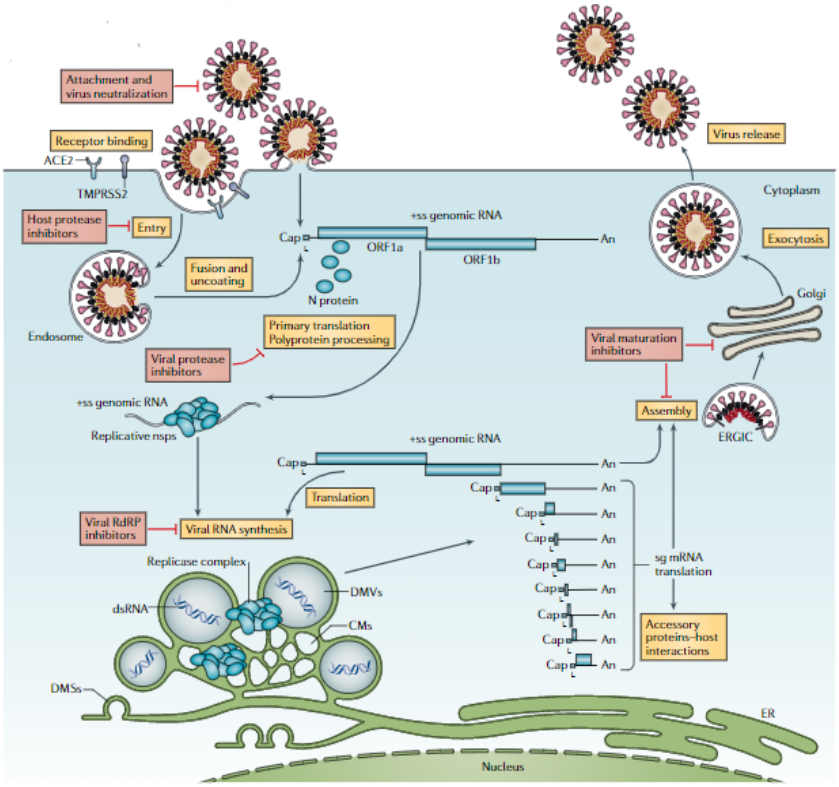

Fig.5: SARS-CoV-2 life cycle. The first step of infection consists in the recognition between the viral Spike protein and the ACE2 receptor. The virus enters through a fusion process and the formation of an endosome. Subsequently, the RNA genome is released in the host cell cytoplasm, then two polyproteins from ORF1a and ORF1b region are translated into two polyproteins, pp1a and pp1ab, that are then processed into 16 non-structural proteins (nsps). Viral genomic replication and transcription of subgenomic mRNAs (sg mRNAs) occur into double-membrane vesicles (DMVs). Structural proteins move to the ER-to-Golgi intermediate compartment (ERGIC), where there is the assembly of viral proteins and viral RNA genome into new virions. Virions are then released through exocytosis. Potential drugs, that target different virus life cycle stages, are indicated in red [2].

In the cytoplasm, the viral genome is unpacked from bound viral N proteins by cellular proteases. The genome replication takes place in the cell cytoplasm and the viral genome functions as a messenger RNA to translate two polyproteins from ORF1a and ORF1b region and as a template RNA for negative RNA transcription. The interaction of nsps leads to formation of the RTC, a virus-encoded complex, on the positive RNA and then to the transcription of gRNA and the synthesis of sgRNAs inside double-membrane vesicles (DMVs). RNA synthesis is performed by the RNA-dependent RNA polymerase (RdRP or nsp12), nsp7 and nsp8 (two cofactors). DMVs are ER-derived and interconnected perinuclear double-membrane structures and their role is to create a protective environment to evade host innate immunity. The sgRNAs released from DMVs encode accessory and structural proteins. Only one newly generated +gRNA is packed into a virion and then released from the cells via lysosomal trafficking pathway [2].

The synthesis of -gRNA is performed by continuous 5'-3' transcription: the RTC binds to the +gRNA 3' end and transcribes the intermediate -gRNA, then this is used for the transcription of +gRNA. In contrast, the production of -sgRNAs is made by discontinuous 5'-3' transcription (Fig.6) where the RTC pauses on transcription regulatory sequence (TRS) and there is a template switch due to the highly structured 3' end. This mode of transcription results in the skipping of a part of the genome. It has been proposed that this could be caused by the interaction of TRS_B and TRS_L. -sgRNAs are used for the synthesis of +sgRNAs. About 10% of sgRNAs are probably produced in a TRS_B-independent or TRS-independent way.

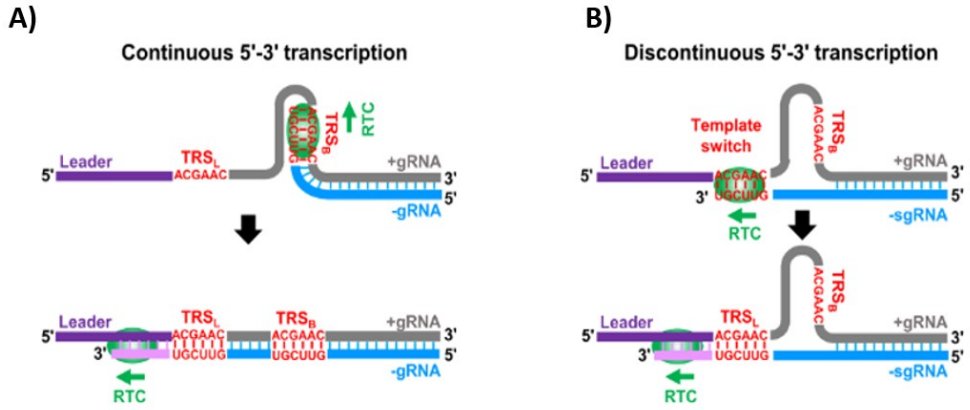

Fig.6: A) Continuous 5'-3' transcription: the replication and transcription complex (RTC) binds to the 3' end of the +gRNA and synthetizes the -gRNA. B) Discontinuous 5'-3' transcription: the RTC binds to the 3' end of the +gRNA and synthetizes -sgRNAs. The template switch from a body transcription regulatory sequence (TRS-B) to the leader TRS (TRS-L) is illustrated [6].

Through all these processes, SARS-CoV-2 can infect both the upper and the lower respiratory tract in humans. As mentioned above, the most common symptoms are fever, dry cough, and dyspnea, like other human *Betacoronaviruses*. These symptoms are developed in the first stage of infection. In the second stage, the infection develops into acute lung inflammation and pneumonia and patients may require oxygen supplementation because of hypoxia and shortness of breath. In some cases, the infection can progress into a third stage characterized by acute respiratory distress syndrome (ARDS), systemic inflammatory response syndrome (SIRS), coagulation problems, cardiac failure and in some cases also death. The patient can have several manifestations affecting various end organs, for example central nervous system symptoms like taste disorders, confusion, and encephalopathies [11]. Older people or people with a dysfunctional immune system have a higher risk of developing severe infection because of co-morbidities. Some individuals may have post-acute sequelae of COVID, for example multi-system inflammatory syndrome and "long COVID".

1.3 SARS-CoV-2 variants

Despite the presence of proofreading activity in the viral replication machinery, the large viral RNA genome of SARS-CoV-2 easily acquires mutations because the RNA-dependent RNA polymerase is prone to the introduction of errors during genome replication [11]. Mutations in the SARS-CoV-2 genome can be deleterious, neutral, or can influence infectivity, disease severity or can have interactions with the human immune system. Mutations that contribute to virus adaptation and fitness are less than low-effect or no-effect neutral amino acid mutations. SARS-CoV-2 variants originate from the accumulation of adaptive mutations because of the positive selection while the virus continues to circulate in the population. There are various mutations altering antigenic properties of the Spike protein and contributing to immune escape. Amino acid substitutions that alter the epitope can cause a reduction in antibody binding, amino acid substitutions can increase receptor-binding avidity and substitutions that introduce additional glycans can mask epitopes from antibody binding. Moreover, changes in the NTD of the Spike can affect recognition by neutralizing antibodies: this because amino acids deletions and insertions can alter epitope conformation, otherwise, amino acid substitutions can have allosteric structural effects that change the epitope disposition [21].
One of the first variants of the Spike protein is the D614G Spike, which became the most prevalent in the pandemic since April 2020. This mutation confers enhanced Spike cleavage and more efficient entry. This variant is characterized by a substitution of aspartic acid (D) with glycine (G) at 614 site. Furthermore, this variant has a higher affinity for ACE2 receptor than the parental strain and it increases replication capacity and susceptibility.

Because of the global spread of the virus in billions of individuals, virus variants originated and spread quickly, often taking over previous variants in a Darwinian fitness manner. Therefore, variants are continually monitored, and are catalogued according to 3 categories: variant under monitoring (VUM), variant of interest (VOI), and variant of concern (VOC). A VUM is a variant with genetic changes that are suspected to affect virus characteristics and growth advantage but for which evidence of phenotypic or epidemiological impact remains unclear, requiring enhanced monitoring. A VOI is a variant with genetic changes that are predicted or known to affect virus characteristics such as transmissibility, virulence, antibody evasion, susceptibility to therapeutics and detectability and that has a growth advantage with increasing relative prevalence alongside increasing number of cases over time, or other apparent epidemiological impacts to suggest an emerging risk. A VOC is a variant with similar characteristics of a VOI, but which has more impact on the transmission, morbidity, and mortality. A VOC is

characterized by a change in clinical disease severity, a change in epidemiology and a significant decrease in the effectiveness of available vaccines.
During the pandemic, major VOIs were Epsilon, Zeta, Eta, Theta, Iota, Kappa, Lambda and Mu variants. Major VOCs were Alpha (also known as B.1.1.7, it was first isolated in United Kingdom in December 2020), Beta (B.1.351, it was first isolated in South Africa in December 2020), Gamma (P.1, it was first isolated in Brazil in November 2020), Delta (B.1.617.2/AY sublineages, it was isolated in India in October 2020) and Omicron (B.1.1.529/BA sublineages: BA.1, BA.2, BA.3, BA.4 and BA.5, it was first isolated in South Africa in November 2021). These variants are characterized by amino acid changes in the FCS (Fig.7), and in many of the innate immune system antagonists like NSP1, NSP3, NSP6, ORF3a, ORF6a, ORF7b, ORF8 and N protein, probably to better evade the immune system [22].
These variants are characterized by multiple convergent mutations that may have arisen in previously infected individuals or in individuals with chronic infections. The evolutionary success of Alpha and Delta variants is linked to an enhanced Furin Cleavage Site (FCS), while the evolutionary success of the Omicron variant is linked to endosomal entry and immune escape.

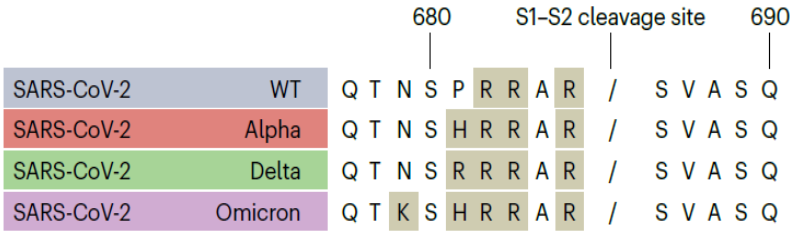

Fig.7: Comparison of FCS in wild-type SARS-CoV-2, Alpha, Delta, and Omicron variants. Amino acids of the polybasic cleavage site are shaded. The mutations affecting FCS function are P681H in Alpha variant, P681R in Delta variant, P681H/N679K in Omicron variant [21].

In Alpha and Omicron sublineages BA.4 and BA.5 there is an upregulated expression of innate immunity suppressing viral proteins, such as ORF6. ORF6 inhibits nuclear transport of transcription factors that control the expression of antiviral proteins and pro-inflammatory mediators.
Regarding the Omicron variant, there are 18.261 mutations in the entire SARS-CoV-2 genome. Most mutations are detected in the coding region and are indels, non-synonymous, and synonymous SNPs, while the minority is present in the extragenic region. The Omicron variant has a bigger number of mutations in the Spike protein than the other variants (Fig.8). Unlike other VOCs, Omicron had evolved diversity before first detected, and is divided into five major lineages (BA.1, BA.2, BA.3, BA.4 and BA.5), with many more sublineages that are accumulating further antigenic changes.

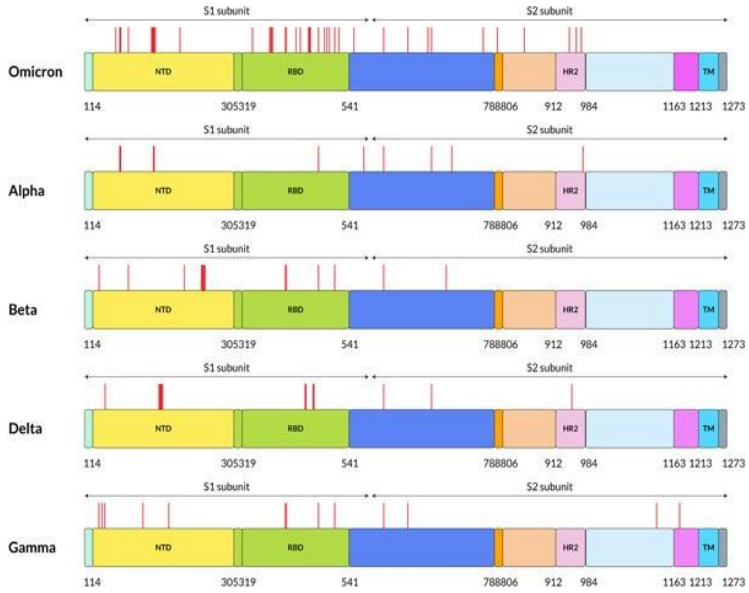

Fig.8: Representation of the Spike protein of the five VOCs (Omicron, Alpha, Beta, Delta, and Gamma variant). The Omicron variant has a bigger number of mutations than other variants: it has more than thirty mutations in the Spike protein (mutations are indicated with red lines) and many of these mutations are in the RBD [23].

The Omicron variant is more transmissible than the wild type virus or other VOCs. Indeed, there are more than thirty mutations in the Spike protein by which the virus protein recognizes host cells, and these mutations can increase transmission by evading the immune response. H655Y and N679K amino acid substitutions are present near the FCS and increase Spike cleavage, in this way the virus is more contagious. P681H multiplies virus transmissibility by increasing the Spike protein cleavage. The Omicron variant efficiently infects human cells through the ACE2 receptor because there are some mutations in the RBD of Spike protein that are responsible for higher affinity to the ACE2 receptor. The Omicron variant is characterized by a lower disease severity in the human host than other previous variants, probably because of reduced fusogenicity of the Spike protein. This variant leads to less tissue damage and the tropism is restricted to the upper respiratory tract due to altered TMPRSS2 use. Omicron variant has a lower efficiency in using TMPRSS2 than other VOCs, as mutations in the Spike gene determine its inefficient cleavage by the host protease. Furthermore, Omicron lineages are poorly neutralized by pre-Omicron infection-derived antibodies and by the first and second doses of Pfizer/BioNTech and Moderna mRNA vaccines, while the third dose of these vaccines is efficient to neutralize the variant.
The previous infection with other variants confers low protection against Omicron lineages, and there is immune escape by Omicron from neutralization antibodies produced in response to vaccines. Recombination events occur when two RNA viruses co-infect the same cell and the RNA polymerase switches from one RNA to

the other, resulting in the formation of a new recombinant virus with a recombined RNA sequence from the two viruses. A high degree of immune evasion can be seen in Omicron recombinants like XBB, a recombinant of BA.2.10.1 and BA.2.75 sublineages, which is emerged in August 2022 and has been reported in at least 26 countries. XBB subvariant is more elusive, more transmissible, and less virulent [24]. The Omicron lineages show multiple intra-COV recombination events, for example BA.3 is thought to be the recombinant progeny of ancestral BA.1 and BA.2: this because BA.1 and BA.3 contain near identical 5' ends of the genome until the Spike gene, while in the 3' end they show big divergence, suggesting a recent recombination. Example of recombinant lineages are XA from B.1.1.7 and B.1.177 recombination, XC from Alpha and Delta recombination, XD from Delta, and BA.1, XE from BA.1 and BA.2, XAY from BA.2 and Delta. The number of recombinants increases when there is the co-circulation of more variants in the population [22].

In conclusion, SARS-CoV-2 continues to evolve and to acquire adaptations, so it is important to study the phenotypes of emerging variants and their effects in infectivity, transmissibility, virulence, and antigenicity. Over time, SARS-CoV-2 is expected to cause less severe diseases and less mortality due to adaptation to human host.

1.4 Spike Protein

Spike protein is a homotrimeric class I fusion glycoprotein that induces fusion between viral membrane and host cell membrane, with the result of increased infection and virulence. It also induces the fusion between infected and uninfected cells, resulting in syncytia formation. There are three classes of viral fusion glycoproteins, and they all are trimers of hairpins with a central N-terminal trimeric core surrounded by C-terminal regions that carry the fusion peptide and transmembrane domain. Fusion glycoproteins can be in the native fusion competent state and after specific triggers (for example pH) they can change their state through different conformational transitions: there are stages of close apposition, hemifusion, formation of small fusion pores and large fusion pores. During this process there is an extension towards the host cell membrane and the insertion of a hydrophobic fusion peptide in the host membrane [17].
Class I fusion glycoproteins, like Spike protein of SARS-CoV-2 and HA of Influenza virus, are trimers with a central N-terminal trimeric α-helical coiled coil with three C-terminal helices forming a 6-helix bundle. Class II fusion glycoproteins, like E protein of flaviviruses or E1 protein of alphaviruses, have β-sheets with fusion loop at the tip of the β-sheet and they are arranged in three connected domains. The difference between class I and class II is in the presentation of the fusion peptide

in the cell membrane host: while in class I there is secondary structure refolding, in class II there is the rearrangement of the three domains. Class III fusion proteins, like the B glycoprotein of herpes simplex virus 1 and the G glycoprotein of the Vesicular Stomatitis virus (VSV-G), are trimers with a central α-helical coiled-coil, with a potential helical extension during fusion peptide insertion in the membrane host, and internal fusion loops located at the tip of β-sheets [17].

The SARS-CoV-2 Spike is a protein with 1273 amino acids and is composed of two subunits: the receptor-binding fragment S1 and the fusion fragment S2 (Fig.9).

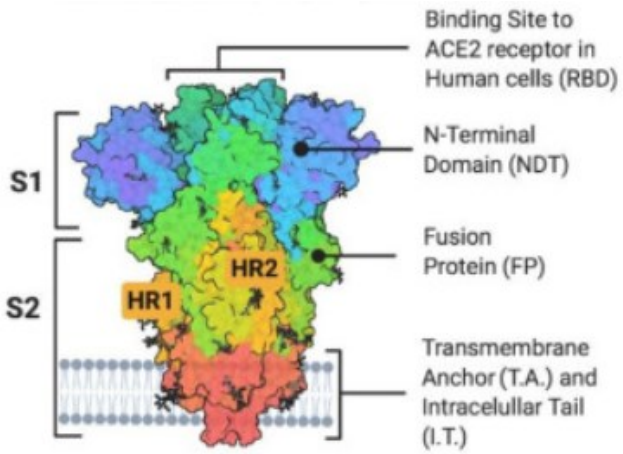

Fig.9: Crystallographic 3D-structure of SARS-CoV-2 Spike protein, with structural location of the receptor-binding fragment S1 and the fusion fragment S2. The S1 subunit is characterized by the binding site to human ACE2 (RBD) and by a N-terminal domain (NTD), which are represented in the image, and by two C-terminal domains CTD1 and CTD2, which are not represented in the structure. Indeed, the S2 subunit is characterized by a fusion protein (FP), two heptad repeat subdomains (HR1 and HR2), a transmembrane anchor (TMD, T.A. in the image), and a C-terminal tail (CT, I.T. in the image) [4].

S1 subunit is involved in host receptor binding, while S2 subunit is responsible for membrane fusion and endosomal escape. In the prefusion form, the surface-exposed S1 domain folds into four domains that wrap around S2: the N-terminal domain (NTD), the receptor-binding domain (RBD), which is involved in the engagement of the ACE2, and two C-terminal domains CTD1 and CTD2 (Fig.10). The NTD is characterized by four β-sheets and connecting flexible loops, bearing some N-linked glycans. The RBD is composed of five-stranded antiparallel β-sheets covered with connecting α-helices on both sides and a Receptor Binding Motif (RBM) that makes contact with ACE2 receptor. Between two antiparallel β-strands of CTD1 there is the RBD, and between two antiparallel β-strands of CTD2 there is CTD1. CTD1 is composed of β-structures, and it is packed underneath the RBD. CTD2 is composed of two stacked β-sheets, each composed of four strands, with a fifth strand in one sheet contributed by the connecting strand between the NTD

and the RBD. In the other sheet, there is an interstrand loop with the FCS and one strand is the N-terminal segment of S2.

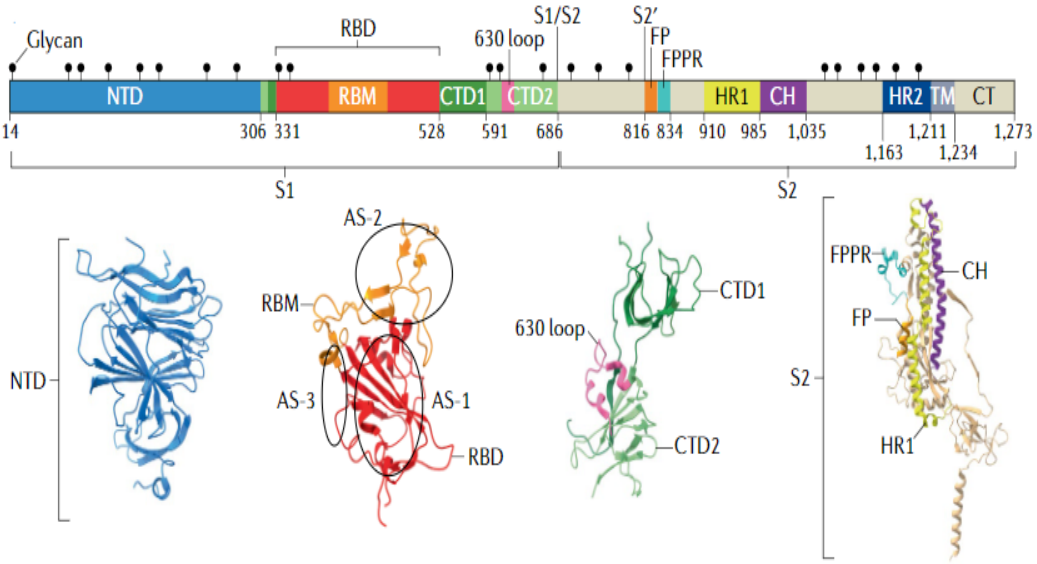

Fig.10: Structure of Spike protein and 3D-representation of its subdomains: NTD (in blue), RBD (in red) with three antigenic sites (AS-1, AS-2 and AS-3) and with the RBM (in orange), CTD1 and CTD2 (both in green), which are connected by a 630 loop (in pink), HR1 (in yellow), HR2 (in blue), CH (in purple), FP (in orange), FPPR (in light blue) [18].

The transmembrane S2 domain contains a fusion peptide (FP) subdomain which facilitates the fusion of viral and cellular membranes, two heptad repeat subdomains (HR1 and HR2), a transmembrane subdomain (TMD), and a C-terminal tail (CT) (Fig.10). The exact location of FP has recently been reported [19]. Before this study, three adjacent regions were thought to be the fusion peptide: the N-terminal FP (residues 770-788) upstream of the S2' cleavage site, the *bona fide* FP (residues 798-816/835) downstream of the S2' cleavage site, and the internal FP upstream of HR1 (residues 858-886). The study is based on the in vitro reconstruction of the full-length Spike in lipid-based nanodiscs. Lipid nanodiscs provide a native-like environment to membrane proteins, which is useful to study membrane biophysics. In this case, the nanodisc technology was used to study the interaction of the Spike protein with host membrane and then conformational changes from the pre-fusion to the post-fusion state. The study is also based on the induction of the conformational changes using soluble ACE2 to obtain the post-fusion form of the Spike and then on the cryogenic electron microscopy to determine post-fusion structure. According to the data presented in the study, the fusion peptide includes residues from 866 to 910 [19].

Spike protein undergoes conformational transitions that promote fusion between viral and cellular membrane and in this process the fusion glycoprotein passes from a pre-fusion state to a lower energy post-fusion conformational state. This passage is fundamental to overcome the kinetic barriers caused by repulsive

hydration forces between viral and host membranes [19]. In the pre-fusion conformation, S1 surrounds S2, which forms a central helical bundle with HR1 bending back towards the viral membrane. In the pre-fusion form, the Spike can have a closed conformation with three RBDs down or an open conformation with one RBD up. The viral attachment to the host cells occurs when the RBD in the up conformation binds ACE2, this allows the exposure of the S2' cleavage site upstream the fusion peptide. Pre-fusion trimers can have a stochastic conformation, either closed or open. In the down conformation the RBM is partially occluded because it packs against the central helical bundle of S2 and two other RBDs, while leaning on CTD1 from the same protomer and the NTD from a neighbouring protomer. When the RBD passes to up conformation and exposes one RBM, this causes a shift of CTD1 and NTD. After conformational changes, HR1 undergoes a conformational transition with the FP insertion into the cell membrane, there is a detachment of S1 from S2 and this leads to the post-fusion conformational state. In the post-fusion state HR1 and CH form a central three-stranded coiled coil and part of HR2 adopts a helical conformation. A region in the S1/S2-S2' packs against CH to form a six-helix-bundle (6HB-1). The N-terminal region of HR2 packs against HR1 to form a six-helix-bundle (6HB-2) (Fig.11).

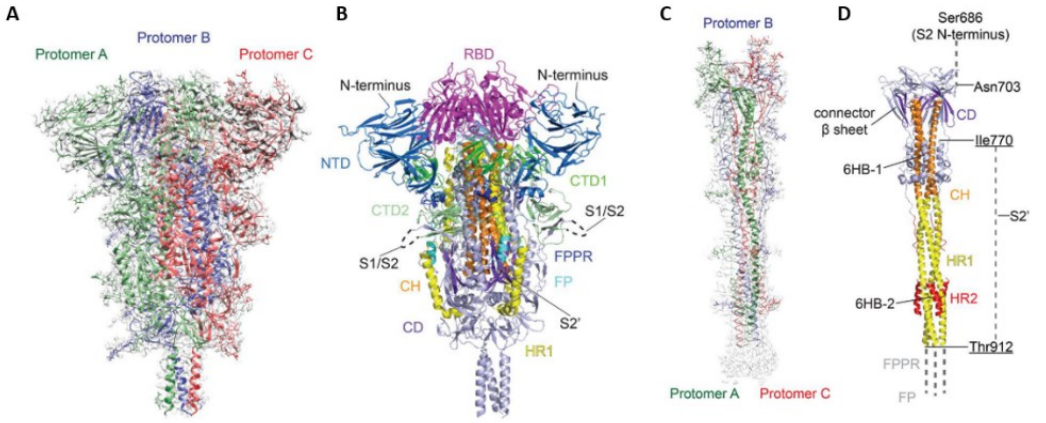

Fig.11: Cryo-EM structure of the Spike protein with its three protomers (protomer A, B and C). A, B) Spike protein in the pre-fusion form with cleavage site (S1/S2 and S2') and with structural components (RBD, NTD, CTD1, CTD2, FP, FPPR, HR1, CH, CD). C, D) Spike protein in the post-fusion form, after conformational changes. The post-fusion form is represented with the cleavage site S2' and with its structural components (CD, CH, HR1, HR2, FPPR, FP). HR1 and CH form a long central three-stranded coiled coil. The two six-helix-bundles (6HB-1 and 6HB-2) at the extremities of the central three-stranded coiled coil are also represented [20].

During the infection phase, Spike protein is cleaved by two human cellular proteases. As mentioned above, the Spike has a cleavage site, the S1/S2 site, cleaved by furin or furin-like proprotein convertase in the Golgi apparatus during biosynthesis and maturation. The furin recognizes a multibasic site (Arg-Arg-Ala-Arg). Another cleavage site is the S2' site. This site is cleaved by TMPRSS2 at the plasma membrane when the virus enters with a membrane fusion process and this

allows the formation of the fusion pore; otherwise, it is cleaved by cathepsin L in the endolysosome when the virus enters through an endosomal process. The virus enters through a clathrin-mediated endosomal process when the target cell expresses low levels of TMPRSS2. In both ways of entry, the cleavage of the S2' site exposes the fusion peptide (FP) and dissociation of S1 from S2 induces conformational transitions in the S2 subunit, especially in HR1, moving forward the fusion peptide into the target membrane, initiating membrane fusion. The fusion-peptide proximal region (FPPR), the 630 loop (which connects the CTD1 and the CTD2), and CTD2 are components of the Spike fusion machinery. The FPPR, which is directly connected with the fusion peptide, passes underneath CTD1 of the neighbouring protomer and makes contact with CTD2 of the same protomer. The FPPR and the 630 loop contribute to maintain the RBDs in the down conformation and they move when the adjacent RBD passes to up conformation. The FPPR shift helps exposing the S2' cleavage site, while the 630 loop shifts from the CTD2 helps exposing the S1/S2 cleavage site. All these passages lead to Spike protein cleavages and then to the transition to post-fusion form. Subsequently to the fusion pore formation, the viral RNA is released into the cell cytoplasm (Fig.12).

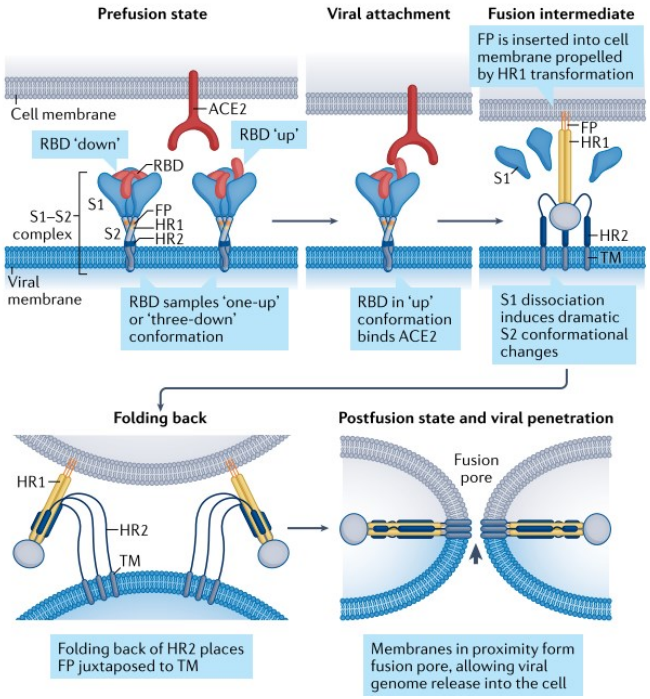

Fig.12: Conformational changes in the Spike protein and membrane fusion. In the pre-fusion state, the Spike can have one RBD up or three RBD down. Viral attachment occurs when the RBD in the up conformation binds ACE2 receptor, and this leads to the exposure of the S2' cleavage site. Cleavage at the S2' site releases FP, FP is inserted into cell membrane thanks to S1 dissociation. Folding back of HR2 places FP juxtaposed to TM. Membranes in proximity form fusion pore and then the release of viral genome into the host cell occurs [18].

1.5 Angiotensin-converting enzyme 2 (ACE2)

ACE2 is a cell surface metalloprotease expressed in a variety of human tissues, including arterial and venous endothelial cells, alveolar cells, and enterocytes. ACE2 is part of the Renin-Angiotensin system (RAS system), which is important in lung tissue because it regulates pulmonary circulation and blood pressure, and it contributes to normal pulmonary function and development. ACE2 and ACE are the main regulators of RAS system and are highly expressed in the pulmonary vascular endothelium [12]. The RAS system starts with the proteolytic conversion of liver-derived angiotensinogen (AGT) to angiotensin I (ANG I) by renin, that is a hormone produced by juxtaglomerular cells in the afferent arterioles of the kidneys. On the surface of vascular endothelial cells, ANG I is converted into angiotensin II (ANG II) by ACE. The binding of ANG II to AT1R receptor has effects of vasoconstriction, oxidative stress, inflammation, fibrosis, apoptosis and water and sodium retention. ACE2 cleaves ANG I into ANG 1-9 which is then converted into ANG 1-7 by ACE; furthermore, it hydrolyses ANG II into ANG 1-7, in opposition of the adverse effects of ACE2. ANG 1-7 binds to Mas receptor (MasR) and activates signaling pathways that lead to vasodilation, anti-inflammatory, anti-fibrotic and anti-apoptotic effects (Fig.13).

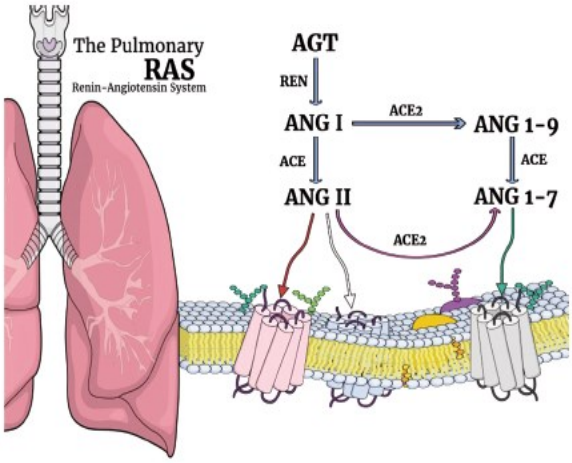

Fig.13: Role of ACE2 in Renin-Angiotensin system (RAS). The first step of the cascade is the conversion of angiotensinogen (AGT) into angiotensin I (ANG I) by renin. ANG I is converted into angiotensin II (ANG II) by angiotensin-like converting enzyme (ACE). ACE2 is involved in the conversion of angiotensin I (ANG I) into angiotensin 1-9 (ANG 1-9), that is subsequently converted into angiotensin 1-7 (ANG 1-7) by ACE, and in the conversion of angiotensin II (ANG II) into ANG 1-7. The resulting ANG II binds AT1R receptor, leading to inflammatory signals and thrombosis, while the resulting ANG 1-7 binds Mas receptor, leading to protective signals [13].

The ACE2 gene, which has a size of 112,671 bases and contains 20 introns and 19 exons, encodes a type I transmembrane glycoprotein of 805 amino acids (Fig.14A)

in the X chromosome (Fig.14B). It is composed of two domains: a carboxypeptidase domain at the N-terminal and a collectrin domain at the C-terminal.

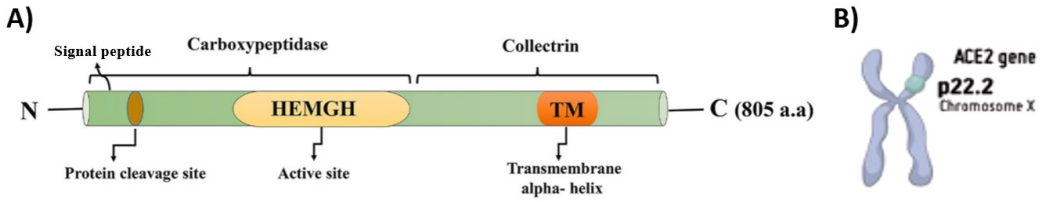

Fig.14: A) Representation of ACE2 metalloprotease with 805 amino acids, which is composed of a carboxypeptidase domain near the N-terminal region and a collectrin-like domain near the C-terminal region. In the carboxypeptidase domain there are a signal peptide, a protein cleavage site and a zinc binding motif (HEMGH), which is the active site, while in the collectrin-like domain is present the transmembrane alpha-helix region (TM) [14]. B) Location of ACE2 gene in X chromosome. Cytogenetic band: Xp22.2 [13].

The carboxypeptidase domain is composed of a N-terminal signal peptide region of 17 amino acids residues, a protein cleavage site, and a zinc-binding motif (HEMGH), which is the active site that cleaves one peptide bond on the C-terminus of ANG II with high affinity and ANG I with lower affinity. The collectrin-like domain (CLD) is composed of a ferredoxin-like fold neck domain, a transmembrane alpha-helix region of 22 amino acids (TM) and an intracellular cytoplasmic tail of 43 amino acids (Fig.14A, Fig.15). ACE2 gene shows similarities with the ACE gene located at chromosome 17q23, which is composed of two HEMGH motifs instead of one.

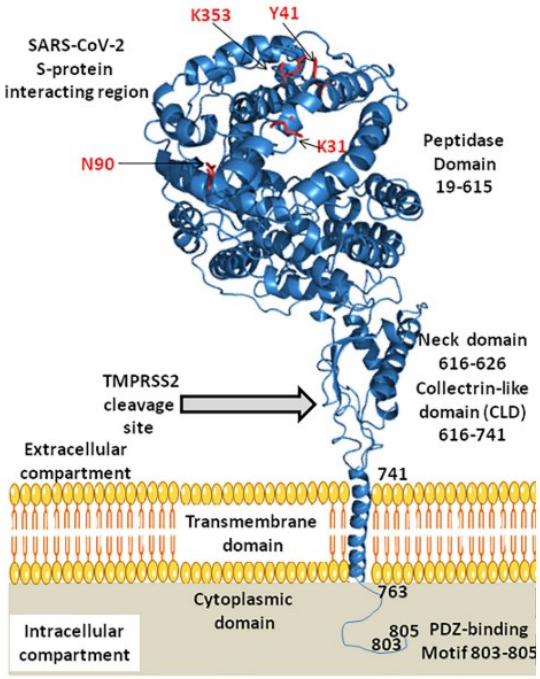

Fig.15: Human ACE2 3D structure. The carboxypeptidase domain comprises residues from 19 to 615 and it includes Spike interaction regions. Amino acids important for SARS-CoV-

2 binding are indicated in red: N90, K353, Y41 and K31. The collectrin-like domain comprises residues from 616 to 741 and it includes a TMPRSS2 cleavage site and a neck domain (residues 616-626). ACE2 is also characterized by a transmembrane domain from 741 to 763 residues and a cytoplasmic domain from 763 to 805 residues. Residues from 803 to 805 (threonine, serine, and phenylalanine) form a PDZ-binding motif which is involved in the binding with proteins that act in protein trafficking [12].

The transmembrane form of ACE2 is recognized by SARS-CoV-2 Spike to enter respiratory tract cells. The virus causes ACE/ACE2 balance disruption and RAS activation, with an imbalance between the two axes ACE/ANG II/AT1R and ACE2/ANG1-7/MasR. The Spike protein is an antagonist for ANG II and inhibits the enzyme's function. The final effect is the downregulation of the protective ACE2/ANG1-7/MasR axis and a pathological ACE/ANG II/AT1R up-regulation with vasoconstriction and inflammation. During infection, surface ACE2 is downregulated due to the internalization of the virus and the ACE2 by endocytosis, resulting in accumulation of ANG II. Therefore, there is an increase in ANG II mediated vasoconstriction and a decrease in ANG1-7 mediated vasodilation [15].

Numerous single nucleotide polymorphisms (SNPs) of the ACE2 gene have been shown to have an impact on SARS-CoV-2 infection by modifying ACE2 expression levels and binding affinity with the Spike (Fig.16) [16]. ACE2 variants among different populations can be indicative of their epidemiological status and are the main genetic risk factor for COVID-19 [14]. One of the most studied polymorphisms is the rs2285666, a splice region variant (G>A, Intron 3/4) associated with hypertension, coronary disease, and diabetes. The A polymorphic allele in homozygosity causes increase in gene expression. The GG genotype, which is associated with lower expression levels, is strongly associated with an increased risk of viral infection, severe disease, or death. In contrast, the A allele is associated with decreased risk of infection and death. Even though rs2285666 is associated with comorbidities like hypertension and cerebral stroke, a meta-analysis study in patients suggest that this SNP is linked to an increased severity of COVID-19 disease [16]. Another variant is the rs190509934, which is characterized by a lower ACE2 expression in individuals with the C allele and this is associated with reduced risk of infection. Also, other ACE2 polymorphisms, such as rs182366225, rs2097723, rs536092258 and rs370596467, that increase its expression, are associated with a reduced risk of infection and death. In contrast, ACE2 polymorphisms such as rs4646114 and rs4646115, as well as the G allele of rs2285666, are associated with an increased risk of infection and death [13].

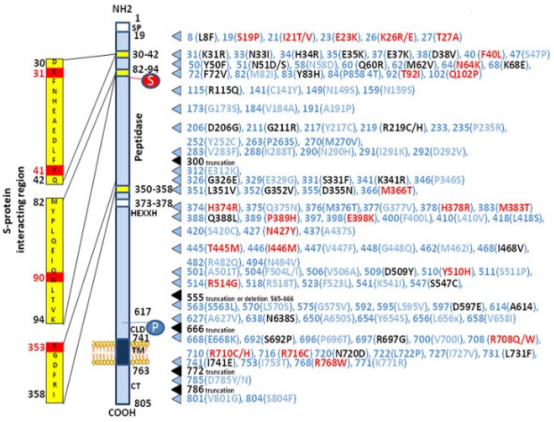

Fig.16: Human ACE2 protein polymorphisms: main 125 substitutions reported for 805 amino acid position. ACE2 substitutions in light blue are neutral, substitutions in red increase cell susceptibility to SARS-CoV-2, substitutions in black decrease cell susceptibility to the virus. Polymorphisms in intronic regions may cause ACE2 dysregulation [12].

An *in silico* study demonstrated the existence of six ACE2 missense variants with higher affinity to Spike protein, that increase viral entry, and 11 variants with lower affinity, that are protective against viral entry. Missense mutations can disrupt ACE2-Spike interactions in different ways: changing chemical characteristics, peptidase activity, affinity with the RBD of the Spike, leading to conformational changes of the secondary and tertiary structure of ACE2. Furthermore, some mutations in ACE2 seem to inhibit the interaction with Spike. Some mutations modulate conformational changes that modify interactions with the receptor-binding domain (RBD) of the Spike because they are near sequences important for Spike binding. Other variations located at the ACE2 proteolytic cleavage site can influence virus infection [14]. There are also polymorphisms in regulatory and non-coding regions, like promoters or 3'-UTR, that can change expression levels of ACE2 (Fig.17).

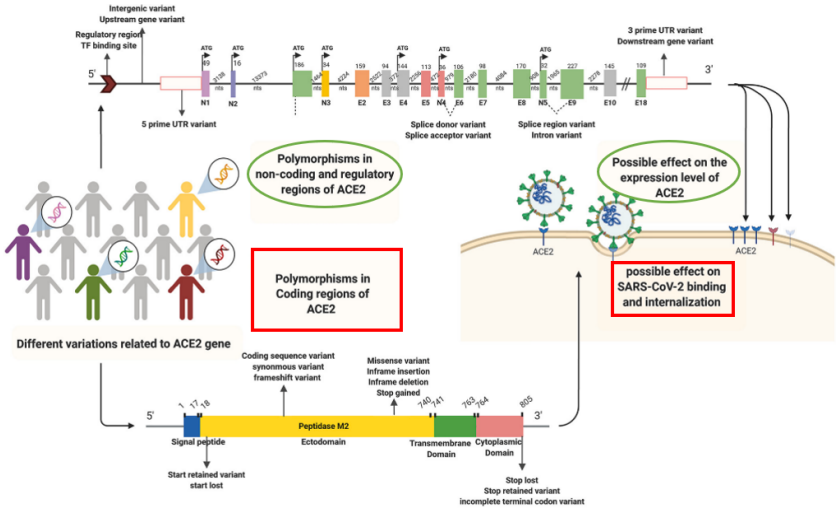

Fig.17: Different variants related to ACE2 gene and possible effects. Polymorphisms in the coding regions of ACE2 (red rectangles) can be start retained or start lost variants, coding

sequence variants, synonymous or frameshift variants, missense variants, in-frame insertions or deletions, stop gained variants, stop lost or stop retained variants and incomplete terminal codon variants. These polymorphisms can have potential effects on SARS-CoV-2 binding and internalization. Instead, polymorphisms in the non-coding and regulatory regions of ACE2 (green ovals) can be variants in the regulatory regions, intergenic or upstream gene variants, 5'prime UTR variants, splice donor or acceptor variants, splice region or intron variants, 3' prime UTR or downstream gene variants. These polymorphisms can have potential effects on the ACE2 expression levels [14].

In the end, the impact of variants depends on the functional and structural context of mutating residues and on the physicochemical characteristics of the mutant residue. The study of ACE2 polymorphisms is fundamental to understand what variants can increase susceptibility to SARS-CoV-2 and to identify patients at high risk. Unfortunately, there are contradictory results for the impact of ACE2 polymorphisms in COVID-19 disease. Other studies are needed to understand whether multiple variants of ACE2 may have synergistic effect on disease outcome or whether some rare variants may have a major impact on infection.

1.6 Cell-cell fusion assays

One of the first cell-cell fusion assays was performed in 1990 by Edward A. Berger and Bernard Moss with cells that express gp120, which is the HIV envelope glycoprotein and other cells that express the CD4, which is the HIV human host receptor, to study membrane fusion mediated by the interaction between these two proteins. This process is facilitated by the presence of HIV envelope glycoprotein gp41. In the assays by Berger and Moss, suspension cells were transduced with vaccinia virus vector containing gp160 gene, which is the precursor of gp120 and gp41, under the control of a vaccinia virus promoter, and other suspension cells were transduced with a vaccinia virus vector containing CD4 gene under the control of the bacteriophage T7 promoter and a vector containing T7 RNA polymerase gene under the control of a vaccinia virus promoter. After transduction, they performed immunofluorescence to detect protein expression (CD4 and gp160) on the cell surface. Then, cells expressing gp160 and cells bearing CD4 were mixed in the same cell plate for 10-14 hours of incubation. The result was the formation of syncytia, *i.e*, a multinucleated giant cell, after 1-3 hours of incubation [25], [26] (Fig.18). These assays were instrumental for studies of the process of entry-fusion of HIV, its kinetic, and eventually allowed for the discovery of chemokine receptors as co-receptors for HIV on susceptible cells.

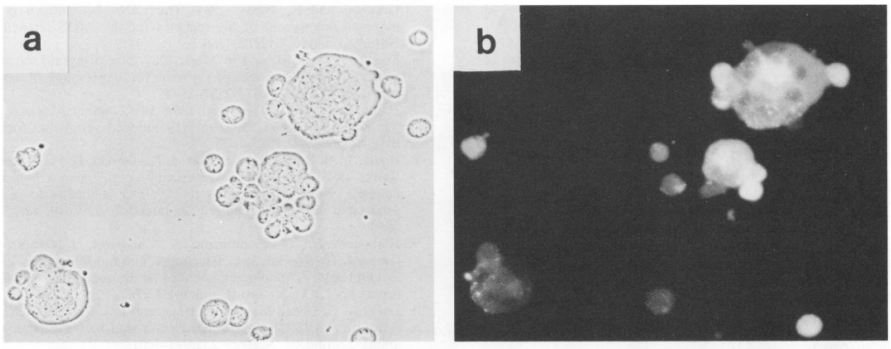

Fig.18: a) Light microscopy images and b) fluorescence microscopy images of syncytia formation after mixing of CD4-expressing cells and gp160-expressing cells. FITC labelling was used for fluorescence microscopy [25].

Regarding SARS-CoV-2, some quantitative cell fusion assays have yet been set up for the screening of inhibitors of SARS-CoV-2 that interfere with the Spike-ACE2 recognition and virus-cell fusion. For example, a system based on luciferase reporter gene has been developed, to monitor and quantify the fusion between stable ACE2-expressing cell lines and stable Spike-carrying cell lines. Spike-carrying cells have integrated the HIV LTR (long terminal repeat)-Firefly luciferase gene and the HIV LTR LacZ cassettes and ACE2-carrying cells have been transduced with a vector containing the HIV Tat (transactivator gene codifying a protein that induces gene expression). The LTRs of HIV are Tat-responsive, in other words they can be *trans*-activated by the HIV Tat, resulting in enhancement of processive transcription. In this way, when the two cellular lines are mixed and the cellular fusion occurs, Tat will induce luciferase expression and there will be a luminescent signal. Furthermore, if cell lines are in a medium containing X-gal and if the fusion occurs, there will be a blue signal because Tat induces LacZ expression. These two types of cells are mixed 1:1, and the fusion can be observed after 24 hours through luminometry to quantify luciferase activity. The efficiency of this system has been evaluated with convalescent and acute phase sera and with antibodies: firstly, 10^4 Spike-expressing cells/well were seeded in a 96-well plate, after 24 hours 70 µL of antibodies have been added in every well and then after 1 hour of incubation 10^4 ACE2-expressing cells have been added in every well, at last, after 24 hours luminescence was detected. In this case, if antibodies inhibit Spike-ACE2 recognition and then fusion between cells, the luminescence will decrease (Fig.19) [27].

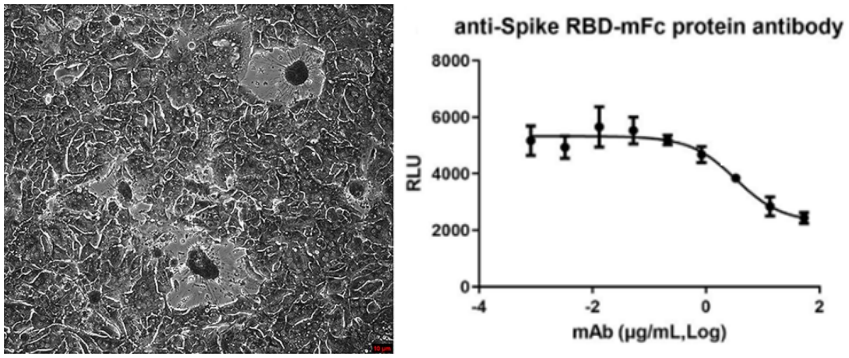

Fig.19: Microscopy image of fusion between ACE2-expressing cells and Spike-expressing cells. Graph about fusion inhibition between ACE2-expressing cells and Spike expressing cells due to the incubation with anti-Spike RBD-mFc protein antibody. When the concentration of the antibody increases, the RLU (Relative Light Unit, based on the detection of the luciferase signal) decreases because Spike-ACE2 recognition is inhibited [27].

To detect fusion between cells of interest, a fluorescent protein complementation system can be used, like an assay based on GFP split protein. The GFP is a protein of the Pacific Northwest jellyfish Aequorea Victoria. It is composed of 11 β-strands that form a barrel structure, which encloses an α-helical region with a chromophore. This split protein can be divided into two parts: one part corresponding to the first to tenth β-strands (GFP1-10, that includes residues from 1 to 215) and a part corresponding to the eleventh β-strand of GFP (GFP11, that includes residues from 216 to 230) (Fig.20). These two parts can spontaneously self-associate when they are near each other. The GFP complementation system is based on the spontaneous fusion of GFP1-10 and GFP11 and it was initially developed to detect expression of soluble protein constructs. This system can also be used to visualize proteins tagged with GFP11 by adding the GFP1-10 fragment [28].

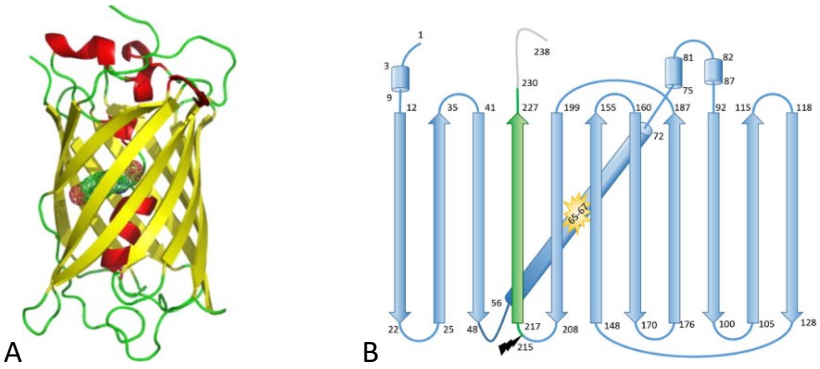

Fig.20: A) GFP 3D structure. β-strands are drawn in yellow, α-helices in red and loops in green [29]. B) Representation of GFP strands. α-helices are represented with arrows, β-strands with cylinders and linker sequences with lines. The chromophore contained in GFP protein is shown in yellow. GFP1-10 strands are drawn in light blue, GFP11 strand in green and the GFP tail in grey [28].

When the two parts are separated, there is no fluorescence. In contrast, when the two parts are in proximity for sufficient time (t1/2 = 60 seconds) they associate spontaneously, and fluorescence can be detected. This happens because GFP1-10 does not have the structure for chromophore formation and only GFP11 binding confers the necessary structure by complementation [28].

1.7 Antiviral drugs against viral entry-fusion

The COVID-19 pandemic highlighted the unmet need for effective antivirals. The first therapy for COVID-19 was infusion of anti-RBD IgG convalescent plasma. Starting 10 months into the pandemic, monoclonal antibodies (mAbs) become available: for example, among the mAbs against Spike, Etesevimab is an inhibitor that binds the RBD of the Spike, used in combination with the human IgG1 Bamlanivimab, which is a Spike antagonist and a synthetic antibody derived from a patient. One problem associated with drug development is fast-emerging resistant mutations in the RBM. To minimize the impact of monoclonal antibodies escape mutations, monoclonal antibodies with epitopes that are highly resistant to viral escape have to be developed. Within two years from the beginning of the COVID pandemic, two oral therapeutics, that do not target the entry-fusion, received emergency use authorization (EUA), Molnupiravir and Nirmatrelvir. The antiviral Molnupiravir is a ribonucleotide analogue that inhibits SARS-CoV-2 replication (RNA-dependent RNA polymerase inhibitor), while Nirmatrelvir blocks protease (Mpro or 3C-like protease) activity blocking virus replication [31]. However, there is still a strong need for new antivirals against SARS-CoV-2.

The viral entry-fusion is a good target for antivirals development because it is the first step of infection and because the viral protein and the host cell receptor are accessible from the extracellular space. Unfortunately, only a small number of antivirals against viral entry-fusion has been developed [30].
Current therapeutic efforts to reduce COVID-19 morbidity and mortality include molecules that target viral fusion-entry (for example, targeting the binding between the RBD of the Spike or targeting the HR regions in the S2 subunit), such as protein chimeras, peptide analogues and small molecules. [30]. An example of protein chimera that has a high affinity for the RBD is a recombinant protein that has been developed connecting the extracellular domain of ACE2 to the Fc region of IgG1. An example of peptide analogue that targets the Spike S2 subunit is a HR2 analogue that can inhibit viral membrane fusion events. Small molecules are the best application in drug development because they can reach remote areas in the body and they are more stable, so they can be more effective than other drugs. Drugs that target Spike protein are more specific, but they easily lose efficacy when virus spike mutations occur.

Drugs that potentially target ACE2 are more toxic than Spike-inhibitors because ACE2 is a human cell receptor, but the efficacy can be higher even if the virus mutate. For example, chloroquine and hydroxychloroquine can inhibit Spike-ACE2 interaction through binding to ACE2, but they cause undesired secondary effects like ventricular arrhythmias. Also, antibodies targeting ACE2 could have some toxicity because of the potential to dysregulate the RAS system. Some applications include the use of soluble human ACE2 as a decoy for the spike protein, with viral Spike binding soluble ACE2 and not membrane ACE2. However, currently there are no drugs targeting ACE2 receptor in clinical or preclinical trials for COVID treatment [30].

In conclusion, while there are drugs against SARS-CoV-2 entry in preclinical trials, it is critical to develop new safe and effective molecules against SARS-CoV-2, possibly focusing on highly conserved targets to reduce drug resistance due to escape mutations. It is essential also to set up new antiviral screening systems for preparedness for outbreaks of new Coronaviruses or other viruses.

2. AIM OF THE EXPERIMENTAL STUDY

The COVID-19 pandemic was caused by severe acute respiratory syndrome coronavirus 2 (SARS-CoV-2), a *Betacoronavirus* that causes symptoms like fever, cough, and respiratory infections. From its origins in late 2019 to now, the SARS-CoV-2 virus has spread across many countries and its genome has mutated giving rise to numerous variants. While severe respiratory symptoms and mortality associated with COVID-19 have decreased in subjects that were previously infected with, or were vaccinated against SARS-CoV-2, severe symptoms still occur especially in immunologically naïve and in immunocompromised people. The search for treatment approaches against SARS-COV-2 is essential to lower disease severity and mortality. Numerous antiviral drugs are now in pre-clinical and clinical stages of development, but few of them target SARS-COV-2 Spike - human ACE2 mediated entry-fusion, for which there is no high-throughput screening system. Currently, tests for antiviral drugs screening rely on infectivity assays with infectious SARS-CoV-2 performed in BSL-3 laboratories and on assays with pseudotype viruses that are labor-intensive and are affected by low standardization.

The aim of this experimental study is to set up an innovative cell-cell fusion system based on GFP complementation for the screening of new therapeutics against SARS-CoV-2 that target ACE2-receptor, Spike protein or Spike-ACE2 mediated fusion, that can be easily perform in a BSL-2 laboratory. The system is based on the generation of a Spike-expressing cell line that carries the GFP1-10, and another stable ACE2-expressing cell line that carries the GFP11. When separated, neither GFP-subunit is fluorescent. When mixing the two cell lines, cells fuse together due to the Spike-ACE2 binding and, in this way, GFP1-10 is complemented by GFP11. The result is green fluorescence that can be detected by fluorescent microscopy or by a plate reader. If the binding is inhibited by antiviral drugs, the complementation does not occur, and no fluorescent signal is detected (Fig.21).

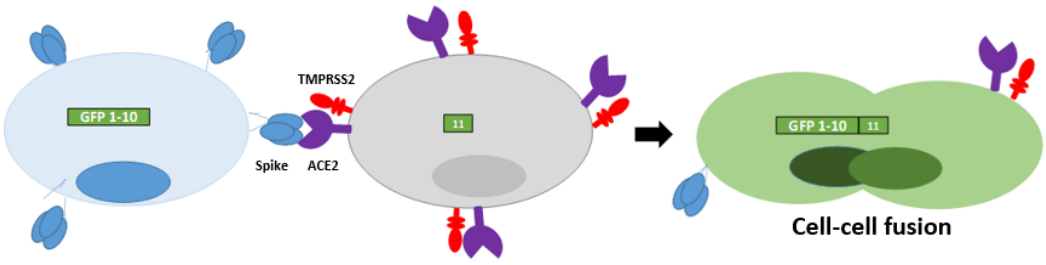

Fig.21: Mechanism of the fusion-entry system based on GFP reporter gene complementation. One cell line expresses the Spike protein, while the other cell line expresses the ACE2 receptor. Moreover, each cell line carries one of the two parts of the split GFP: one part corresponding to the first to tenth β-strands (GFP1-10) and a part corresponding to the eleventh β-strand of GFP (GFP11). If the recognition between Spike

and ACE2 occurs, there is membrane fusion and fluorescence can be detected by fluorescence microscopy.

The first step of this experimental study is the generation of lentiviral vectors expressing GFP1-10, GFP11 or Spike Wuhan through transfection protocol. These lentiviral vectors have been used to transduce HEK 293T or HEK 293T ACE2 cells. In this way, cell lines for fusion tests and cell lines carrying different combinations of the proteins of interest for controls have been obtained. To verify the expression of GFP1-10 or GFP11, cells have been transiently transfected with a plasmid expressing the counterpart of the GFP and visualized through fluorescence microscopy. Fluorescence-activated cell sorting (FACS) has been used to obtain cell lines which stably and permanently express the proteins of interest, allowing system standardization. After obtaining all the cell lines with all possible combinations of the proteins of interest, pilot fusion tests have been performed and the fluorescence signal has been easily monitored through time. These tests set the stage for further optimization and testing of compound libraries and neutralizing antibodies.

3. MATERIALS AND METHODS

3.1 Materials

3.1.1 Cell lines

Two initial cell lines have been employed in this experimental study, HEK 293T and HEK 293T ACE2.

HEK 293T (ATCC® CRL-3216™) is an epithelial cell line isolated from embryonic kidney tissue. This cell line is a derivative of the HEK 293T cell line, optimized for DNA transfection protocols and with the ability to permanently express exogenous proteins. It is characterized by the expression of the tsA1609 allele of SV40's large T antigen, containing the SV40's origin of replication. This cell line has been used to produce other cell lines trough transduction with lentiviral vectors and can be used as a negative control in cell-cell fusion assays.

HEK 293T ACE2 (ATCC®, BEI Resources catalogue number NR-52511) is a HEK 293T cell line which stably and permanently expresses the human-ACE2 receptor. This cell line was kindly provided by Katharine H. D. Crawford and Jesse D. Bloom of the University of Washington (USA). To obtain this cell line, HEK 293T were transduced, in the presence of 5 µg/mL of polybrene (hexadimethrine bromide; Sigma-Aldrich, No. H9268), a polycation that reduces charge repulsion between the virus and the cellular membrane functioning as a transduction enhancer, with a lentiviral vector expressing hACE2 under a human elongation factor-1α (EF-1α) promoter, which is a constitutive promoter that is used to drive robust, constitutive, and long-term gene expression in vitro, especially when other types of promoters (like cytomegalovirus promoter, CMV) have a diminished activity. The EF-1α promoter is derived from the human *EEF1A1* gene which expresses the α subunit of eukaryotic elongation factor 1. The pHAGE2-EF-1αInt-ACE2-WT plasmid (BEI Resources number NR-52512) was used as a backbone to produce lentiviral vectors (Fig. 22).

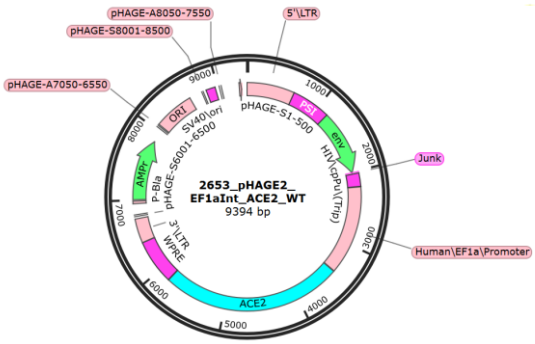

Fig. 22: Map of pHAGE2-EF-1αInt-ACE2-WT plasmid (Genbank format) used as a backbone to produce the lentiviral vector expressing human ACE2. The most important features of

the plasmid map are human EF-1α promoter, which allows a robust gene expression, human ACE2, which is the gene of interest, AMPr, which is the β-lactamase gene that confers ampicillin resistance. In the map some elements are not represented: HIV/U3, pHAGE-A0050-8050, pHAGE-S501-1000, HIV/R, Pa/Site, 5'/UTR, HIV/U5, G-T/cluster, PBS-K, pHAGE-A0550-0050 and other features [32].

For HEK 293T ACE2 cells development, VSV-G-pseudotyped lentiviral particles were produced by co-transfecting cells with the backbone plasmid and other lentiviral plasmids: the HDM-VSV-G (Addgene® catalogue code: 164440) that encodes the G glycoprotein from Vesicular Stomatitis Virus (VSV) under a CMV promoter, HDM-tat1b (BEI catalogue number NR-52518), that is a lentiviral helper plasmid expressing HIV Tat under a CMV promoter, HDM-Hgpm2 (BEI catalogue number NR-52517), which is a lentiviral helper plasmid expressing HIV Gag-Pol under a CMV promoter, and pRC-CMV-Rev1b (BEI catalogue number NR-52519), that is a lentiviral helper plasmid expressing HIV Rev under a CMV promoter. All these plasmids contain the β-lactamase gene that provides ampicillin resistance: this is useful to allow selection of the transformed *E.coli* cells during the amplification procedure. At 60 hours post infection, supernatants were harvested to collect lentiviral vectors, filtered with a 0.45 μm filter and stored at -80°C.
After transduction, cells were sorted in single cell to select only cells with the higher ACE2 expression. For the sorting, cells were stained with an anti-human ACE2 polyclonal goat IgG primary antibody (Bio-Techne) at 1 μg/mL and donkey anti-goat IgG conjugated to Alexa Fluor 488 secondary antibody at a 1:2500 dilution. When single cell clones had grown, they were screened for ACE2 expression through flow cytometry based on antibody staining, and the clones with the highest level of ACE2 were amplified and maintained in culture [32].
This HEK 293T ACE2 cell line has been used in this experimental study to produce other cell lines through transduction with lentiviral vectors and can be used as a negative control in cell-cell fusion assays. ACE2 levels have been periodically confirmed via antibody staining and flow cytometry.

All these adherent cell lines were maintained in culture with Dulbecco's Modified Eagle Medium (DMEM, Gibco™) at high glucose concentration ($4{,}5x10^3$ mg/L), supplemented with 10% v/v Fetal Bovine Serum (FBS, Gibco™) and 1X of Penicillin-Streptomycin (Pen-Strep 100X, $1x10^4$ U/ml, Thermofisher). Before assays with lentiviral particles, the medium was changed with fresh medium without Penicillin-Streptomycin. For an optimal growth, these cell lines were kept at 37°C in an atmosphere composed by 5% v/v CO_2 and 95% humidity. Cell lines were periodically tested for mycoplasma contamination using a PCR assay with primers for mycoplasmas detection and using positive control, and after electrophoresis gel were found to be mycoplasma free.

3.1.2 Plasmids

pLVx-Puro plasmids encoding GFP1-10 (pLVx GFP1-10, 9453 bp), GFP11 (pLVx GFP 11 MBP, 10.083 bp) or Spike Wuhan (pLVx-SWuhan, 12.641 bp), produced previously in the laboratory, were used in the study to produce HIV-1-based lentiviral vectors through the co-transfection of HEK 293T cells with other plasmids encoding HIV proteins necessary for virion formation. pLVx encoding GFP1-10 and GFP11 were also used to transiently transfect cells with calcium phosphate transfection protocols, to verify the expression of GFP11 or GFP1-10, respectively: HEK 293T GFP11/HEK 293T ACE2 GFP11 cell lines were transfected with pLVx GFP1-10, HEK 293T GFP1-10/HEK 293T ACE2 GFP1-10 cell lines were transfected with pLVx MBP GFP11 (the counterpart of the GFP). pLVx-Puro is an HIV-1-based lentiviral expression vector containing the constitutive CMV promoter and a puromycin resistance marker (Puro^r gene) (Fig. 23). The human cytomegalovirus immediate early promoter is located upstream of the multiple cloning site (MCS), allowing constitutive, high-level expression of the protein of interest.
The ppt CMV GFP plasmid, containing the CMV promoter, was used as a positive control in transient transfection protocols since it leads to the expression of the entire GFP so there is necessarily the detection of green fluorescence at fluorescence microscopy.

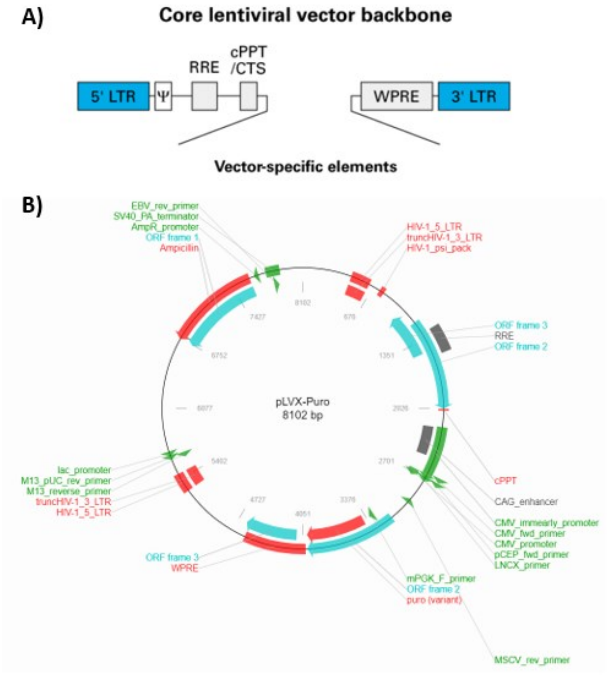

Fig. 23: A) Core lentiviral vector backbone: it contains 5' and 3' long terminal repeats (LTRs); the lentiviral packaging signal (Ψ); a Rev response element (RRE), which helps to increase titers by promoting the nuclear export unspliced viral genomic RNA; a central polypurine tract/central termination sequence (cPPT/CTS), that improves vector integration and transduction efficiency; a woodchuck hepatitis virus posttranscriptional

regulatory element (WPRE), which prevents polyA readthrough, allows RNA processing and maturation, increases nuclear export of RNA and increases the maturation of mRNA transcripts [33].
B) pLVx-Puro plasmid map according to Addgene. The main characteristics of this plasmid are puromycin resistance ($Puro^r$) and the constitutive CMV promoter.

3.1.3 Lentiviral vectors

Several HIV-1-based lentiviral vectors were used to transduce HEK 293T cell lines or HEK 293T ACE2 cell lines: lentiviral vectors containing GFP11 gene, GFP1-10 gene, or Spike Wuhan gene. They are efficient tools for transferring genetic material into the genome of virtually any cell type and for sustaining protein expression.
Lentiviral vectors LV GFP1-10, LV GFP11 and LV Spike Wuhan were produced with the Lenti-X™ Packaging Single Shots Protocol At-A-Glance. The protocol consists in the co-transfection of HEK 293T cells with a lentiviral backbone plasmid expressing the gene of interest, a plasmid encoding the G glycoprotein from Vesicular Stomatitis Virus (VSV-G) under a CMV promoter; and plasmids encoding the other HIV proteins necessary for virion formation: Tat under a CMV promoter, Gag-Pol under a CMV promoter, Rev under a CMV promoter. All these plasmids encoding HIV proteins were provided in a tube containing a pre-aliquoted and lyophilized Xfect^{TM} Transfection Reagent.

3.1.4 Antibodies

Anti-Human ACE2 Monoclonal Mouse IgG_{2A} primary antibody (Catalogue number: FAB9332P-100, Bio-Techne), conjugated with phycoerythrin (PE), was used in FACS to verify the stable expression of ACE2 in ACE2-expressing cell lines. The recommended concentration for the use in flow cytometry is 10 µL/10^6 cells. As a control, a Mouse anti-keyhole limpet hemocyanin IgG1 PE antibody was used (Catalogue Number: 345816, BD Biosciences).

3.2 Methods

3.2.1 Generation of lentiviral vectors: LV GFP1-10, LV GFP11, LV Spike Wuhan

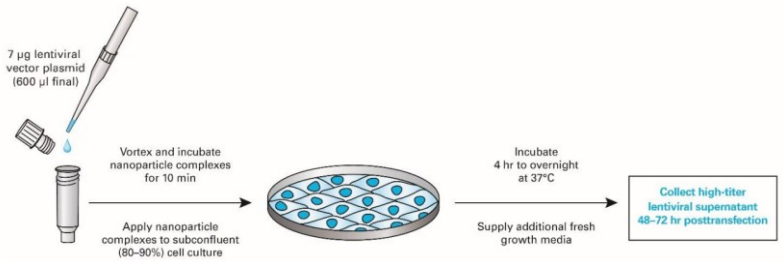

Fig. 24: Generation of lentiviral particles with Lenti-X Packaging Single Shots Protocol. The first step consists in the lentiviral vector plasmid addition to a tube containing the Lenti-X Packaging Single Shots. The mix is vortexed and incubated, then nanoparticle complexes are added to an 80-90% cell culture in a 10-cm dish. The subsequent step is the cell culture incubation for 24 hours, and then the final step includes the harvest of supernatants that contain lentiviral vectors. Lentiviral vectors are stored at -80°C and used for cell transduction [34].

The Lenti-X Packaging Single Shots Protocol (VSV-G) (Takara Bio USA, Catalogue number: 631275 and 631276) was used to generate lentiviral vectors expressing GFP1-10, GFP11 or Spike. The Protocol consists in the co-transfection of HEK 293T cells with the pLVx expressing the gene of interest (backbone) and the Lenti-X Packaging Single Shots (VSV-G). (Fig. 24, 25).
The pre-aliquoted and lyophilized Xfect^{TM} Transfection Reagent contains a premixed, optimized formulation of Lenti-X lentiviral packaging plasmids including lentiviral plasmids expressing VSV-G, Tat, Gag-Pol, and Rev. The packaging mix also contains a vector expressing the Tet-Off transcriptional activator (tTA): Tet-Off transactivation is used to produce high expression levels of specific packaging proteins.
24 hours before transfection, $4x10^6$ of HEK 293T cells were seeded in two 10-cm culture dishes in 8 mL of complete growth medium: one dish for transfection, the other dish as a negative control. Cells were incubated at 37°C, 5% CO_2 overnight, until they reach 80-90% confluence. 7.0 µg of the lentiviral vector plasmid DNA (pLVx containing the gene of interest) was diluted with sterile water to a final concentration of 7.0 µg in a sterile microfuge tube in a final volume of 600 µL. Nanoparticle complexes were vortexed for 20 seconds and incubated for 10 minutes at room temperature to allow nanoparticle formation. Then the solution was added drop by drop to the cell culture. For the negative control, no plasmid was added to the Lenti-X Packaging Single Shots tube. Cells were incubated overnight at 37°C, 5% CO. The day after, the culture medium was replaced with fresh medium. After 48 hours of transfection, the viral titer is the highest possible

and supernatants can be harvested and filtered with a 0,45 µm filter of cellulose acetate or polysulfone to collect lentiviral particles.

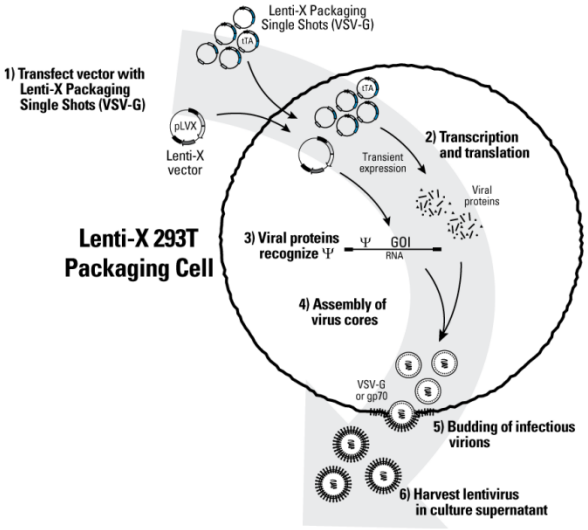

Fig. 25: Lentiviral vectors production with Lenti-X™ Packaging Single Shots Protocol-At-A-Glance. The first step is the co-transfection of HEK 293T cells with the pLVx expressing the gene of interest (backbone) and the Lenti-X Packaging Single Shots (VSV-G). The second step is the transcription and translation of the gene of interest and viral proteins for the envelope. The third step is the recognition of the packaging sequence by the packaging proteins. The fourth step is the assembly of virus core. The fifth step is the budding of infectious virions that have as an envelope with VSV-G proteins. The sixth step is the harvest of lentiviral vectors in culture supernatants [33].

3.2.2 Cell transduction with lentiviral vectors

Lentiviral vectors were used to transduce HEK 293T/HEK 293T ACE2 cells in the presence of 5 µg/mL polybrene (the optimal concentration of polybrene is usually in the 2-12 µg/mL range; exposure to polybrene for more than 24 hours can be toxic to cells). HEK 293T/HEK 293T ACE2 were transduced with a lentiviral vector expressing GFP11 to produce HEK 293T GFP11/HEK 293T ACE2 GFP11; or with a lentiviral vector expressing GFP1-10 to produce HEK 293T GFP1-10/HEK 293T ACE2 GFP1-10; and with a lentiviral vector expressing the Spike Wuhan to produce HEK 293T Spike. Once that the HEK 293T Spike cell line was generated, these cells transduced also with a lentiviral vector expressing either GFP11 or GFP1-10 to develop HEK 293T Spike GFP11 or HEK 293T Spike GFP1-10 cell lines, respectively. 24 hours before transduction, $3{,}5 \times 10^5$ cells/well were plated in a 6-well plate, in 2 mL of DMEM 10% FBS. The day after, the medium was removed from wells and cells were transduced with 1 mL of lentiviral vector (that was thawed from -80°C stock). At least one well was reserved for non-transduced negative control, in which the medium was replaced with 2 mL of fresh medium and the lentiviral vector was not added.

3.2.3 Calcium phosphate transient transfection

To verify the transduction with lentiviral vectors expressing the GFP11 or the GFP1-10, cells were transiently transfected with the pLVx plasmid expressing the counterpart of the GFP, GFP1-10 and GFP11 respectively. The calcium phosphate transient transfection method was used to introduce DNA into HEK 293T cells forming calcium phosphate-DNA precipitate. Calcium phosphate facilitates the binding of the DNA to the cell surface and then the DNA enters the cell by endocytosis. 24 hours before transient transfection, $2x10^5$ cells/well were seeded in a 12-well plate, in 1 mL/well of DMEM 10% FBS. The day after, the medium was replaced with 900 µL fresh medium and the transfection mix was added to the cells dropwise. The transfection mix for one well was composed of 714 ng of the pLVx plasmid containing the gene of interest, 4,42 µL $CaCl_2$ that was added dropwise and water to reach a final volume of 35,77 µL. The mix was vortexed and then an isovolume of HEPES Buffered Saline (HBS2X) was added dropwise. Gentle, continuous aeration of the phosphate buffer with a Pasteur pipette facilitates the entry of DNA in the cell, because it allows the formation of a small precipitate. 24 hours later, after a wash in PBS, fresh medium was added to cells to remove precipitates. One well was reserved as a negative control in which water was added instead of DNA, and a well was reserved as a positive control in which ppt CMV GFP plasmid was added. After transient transfection, cells were observed at the fluorescence microscopy to detect GFP signal and to verify the occurred transduction.

Calcium phosphate transient transfection was also used before cell sorting to select cells with a part of the GFP, GFP1-10 or GFP11. 24 hours before transient transfection, $2,5X10^6$ cells/dish were seeded in two 10-cm plates, in 10 mL/dish of DMEM 10% FBS. One dish was used as a control, the other dish was used for plasmid transient transfection. The medium was replaced with 9 mL of fresh medium and the transfection mix was added to the cells dropwise. The transfection mix for one dish was composed of 10 µg of the plasmid containing the gene of interest, 62 µL $CaCl_2$ that was added dropwise and water to reach a final volume of 500 µL. The mix was vortexed and then 500 µL HBS2X was added dropwise. 24 hours later, after a first wash with 5 mL of PBS and a second wash with 5 mL of DMEM serum free, 10 mL of DMEM 10% FBS were added to the cells to remove precipitates.

3.2.4 Fluorescence-activated cell sorting (FACS)

Cells previously transduced with lentiviral vector expressing GFP11 or GFP1-10 and transfected with the counterpart of the GFP were resuspended in DMEM 10% FBS, transferred in a 15 mL-falcon tube, and centrifuged at 900 rpm for 5 minutes at 4°C, then the supernatant was discarded by inversion. Cells were resuspended in

5 mL of fresh PBS and centrifuged at 900 rpm for 5 minutes at 4°C, then the supernatant was discarded by inversion. Cells were resuspended in 6 mL of PBS supplemented with EDTA (50 µL EDTA in 50 mL of PBS) and kept on ice until sorting.
ACE2-expressing cells were resuspended in DMEM 10% FBS, counted, and centrifuged at 500 rpm for 5 minutes at 4°C, then the supernatant was discarded. Cells were resuspended in 500 µL fresh PBS and centrifuged at 500 rpm for 5 minutes at 4°C, then the supernatant was discarded. 10^6 ACE2-expressing cells were resuspended in 100 µL PBS with the addition of 10 µL of anti-human ACE2 primary antibody conjugated with phycoerythrin (PE), that is a monoclonal mouse IgG_{2A} (10 µL antibody/10^6 cells). $3x10^5$ ACE2-expressing cells were resuspended in 100 µL PBS with the addition of 1,5 µL of an isotype antibody conjugated with phycoerythrin, (i.e., mouse IgG1 kappa isotype control (BD Biosciences, Catalogue Number: 345816)), as a negative control. $3x10^5$ HEK 293T cells (without ACE2 expression) were resuspended in 100 µL PBS with the addition of 3,3 µL of anti-human ACE2 primary antibody conjugated with phycoerythrin, as a negative control. Stained cells were incubated at 4°C for 40 minutes in the dark. $3x10^5$ HEK 293T cells (without ACE2 expression) not stained were resuspended in 100 µL PBS as a control. Cells were centrifuged at 500 rpm for 5 minutes at 4°C, then the supernatant was discarded. Cells were resuspended in 500 µL PBS, centrifuged at 500 rpm for 5 minutes at 4°C, then the supernatant was discarded. Finally, cells were resuspended in 500 µL PBS with the addition of EDTA and kept on ice until sorting.
Bulk cell sorting was performed with BD FACSAria™ IIIu Cell Sorter of the Veneto Institute of Molecular Medicine (VIMM), using a 100 µm-noozle. $1X10^4$ cells were sorted in an eppendorf tube containing FBS. FCS data were analyzed by an expert colleague of the VIMM using BD CellQuest™, BD FACSDiva™ and BD FlowJo™ Software.

3.2.5 Cloning by limiting dilution

After bulk sorting, cells were cloned by limiting dilution preparing a solution of 3 cells/mL of DMEM 10% FBS. 100 µL/well of the cell solution was plated in a 96-well plate. The experiment was performed in duplicate to obtain additional single clones. Every well was regularly screened with optic microscopy to select single cell clones. Once single cell clones had grown sufficiently, in general after two weeks, they were splitted in a 24-well plate, then in a 6-well plate and finally in a flask.

3.2.6 Flow cytometry

ACE2 levels in HEK 293T ACE2 initial cell line have been periodically confirmed via antibody staining and flow-cytometry. Cells were harvested using Trypsin-EDTA (0.05%, phenol red, catalogue number: 25300054), counted to obtain $3x10^5$ cells, and transferred in an eppendorf tube. Cells were pelleted at 500 rpm for 5 minutes at 4°C, then the supernatant was discarded. Cells were resuspended in 500 µL of fresh PBS and centrifuged at 500 rpm for 5 minutes at 4°C, then the supernatant was discarded. Cells were resuspended with 100 µL of fresh PBS supplemented with an anti-human ACE2 primary antibody conjugated with phycoerythrin (PE), that is a monoclonal mouse IgG_{2A} (10 µL antibody/10^6 cells). Cells were incubated for 40 minutes in the dark. Cells were centrifuged at 500 rpm for 5 minutes at 4°C, then the supernatant was discarded. Cells were resuspended in 500 µL PBS, centrifuged at 500 rpm for 5 minutes at 4°C, then the supernatant was discarded. Finally, cells were resuspended in 500 µL PBS and kept on ice. HEK 293T cells that were not stained were used as a control.
After cloning by limiting dilution, single cell clones were screened at flow cytometry for GFP signal, after transfecting them with the counterpart of the GFP in a 12-well plate. Cells were trypsinized and resuspended in DMEM 10% FBS, transferred in an eppendorf tube, and pelleted at 900 rpm for 5 minutes at 4°C, then the supernatant was discarded. Cells were resuspended in 1 mL of fresh PBS and centrifuged at 900 rpm for 5 minutes at 4°C, then the supernatant was discarded. Cells were resuspended in 500 µL PBS (the volume of PBS has been increased if the cell number was high) and kept on ice until flow cytometry lecture. Untransfected cells were used as a negative control.
Cells were analyzed with BD FACSCalibur™ Flow Cytometer. $1X10^4$ events were acquired using the FL-1 laser fluorescence (green) for GFP (peak emission wavelength at 508 nm) or the FL-2 laser fluorescence (red) for phycoerythrin (peak emission wavelength at 575 nm). Logarithmic scale was used to examine a single population of cells. Data were analyzed using FCSalyzer version 0.9.22-alpha.

3.2.7 DNA extraction and quantification

Cells that were previously transduced with a lentiviral vector expressing the Spike Wuhan were screened by PCR to verify the presence of the Spike gene. Genomic DNA was extracted from cell lines HEK 293T, HEK 293T Spike, and 10B and 4G clones of HEK 293T Spike GFP1-10 using DNeasy® Blood & Tissue kit (QIAGEN). $2.5X10^6$ cells were collected in eppendorf tubes and centrifuged for 5 minutes at 300 g. The pellet was resuspended in 200 µL PBS (pH 7.2, 50 mM potassium phosphate, 150 mM NaCl) and 20 µL Proteinase K were added (activity of 600 mAU/mL or 40 mAU/mg protein) to digest contaminating proteins. 200 µL Buffer AL without added ethanol (guanidine hydrochloride and maleic acid) were added

and eppendorf tubes were mixed thoroughly by vortexing to yield a homogeneous solution. Samples were incubated at 56°C for 10 minutes. 200 µL ethanol 96% (Carlo Erba Reagents) were added and samples were mixed thoroughly by vortexing to obtain a homogeneous solution. The mixtures were then added into DNeasy Mini spin columns with silica-based membranes placed in 2 mL collection tubes and centrifuged for 1 minute at 8000 rpm. The flow-throughs and the collection tubes were discarded and the columns were placed in new 2 mL collection tubes. 500 µL Buffer AW1 (Wash Buffer with guanidine hydrochloride) were added to wash away contaminants from the DNA, and samples were centrifuged for 1 minute at 8000 rpm, then the flow-throughs and the collection tubes were discarded, and the columns were placed in new 2 mL collection tubes. 500 µL Buffer AW2 (Wash Buffer 2) were added, and samples were centrifuged for 3 minutes at 13,200 rpm to dry the DNeasy membrane as residual ethanol may interfere with subsequent reactions. The flow-throughs and the collection tubes were discarded and the columns were placed in new eppendorf tubes. 200 µL buffer AE (Elution Buffer with 10 mM Tris-Cl and 0.5 mM EDTA, pH 9.0) were added in the centre of the columns, columns were incubated for 1 minutes at room temperature, and then samples were centrifuged for 1 minutes at 8000 rpm to elute DNA. DNA concentration (ng/µL) and yield ($A_{260/280}$ and $A_{260/230}$) were analysed using NanoDrop™ One/One^{C} Microvolume UV-Vis Spectrophotometer (Thermo Scientific™).

3.2.8 RNA extraction and quantification

Cells that were previously transduced with lentiviral vector expressing the Spike Wuhan were screened by Reverse Transcription (RT)-PCR to verify the presence of the Spike transcript. Total RNA was extracted from cell lines HEK 293T, HEK 293T Spike, and 10B and 4G clones of HEK 293T Spike GFP1-10 using TRIzol™ Reagent (Invitrogen™). Cells were collected in eppendorf tubes and centrifuged at 900 rpm for 5 minutes. The supernatants were discarded, 1 mL TRIzol™ Reagent (monophasic solution of phenol, guanidine isothiocyanate and ammonium thiocyanate) was added to the pellet, and the lysates were pipetted to homogenize it. Samples were incubated for 5 minutes to allow complete dissociation of nucleoproteins complexes. 0.2 mL chloroform (Carlo Erba Reagents) were added, samples were mixed thoroughly by shaking and incubated for 2-3 minutes. Samples were then centrifuged for 15 minutes at 12,000 x g at 4°C to allow the separation of the mixture into three different phases: a red lower organic phase containing DNA and proteins, an interphase layer containing DNA, and a clear upper aqueous phase containing RNA. The aqueous phases containing the RNA were transferred in new eppendorf tubes. To precipitate the RNA, 0.5 mL isopropanol were added to the aqueous phase, samples were incubated for 10 minutes at 4°C, centrifuged for 10 minutes at 12,000 x g at 4°C and then the

supernatants were discarded. To wash the RNA, the white-gel like pellets were resuspended in 1 mL ethanol 75% (Carlo Erba Reagents). Samples were vortexed and centrifuged for 5 minutes at 7500 g at 4°C, then the supernatants were discarded. The pellets containing RNA were air dried for 5-10 minutes. To solubilize RNA, pellets were resuspended in 25 µL of RNase-free water. Samples were incubated in a heat block at 60°C for 10 minutes. RNA concentration (ng/µL) and yield ($A_{260/280}$ and $A_{260/230}$) were analysed using NanoDrop™ One/One^{C} Microvolume UV-Vis Spectrophotometer (Thermo Scientific™).

3.2.9 Reverse transcription polymerase chain reaction (RT-PCR)

The first-strand cDNA synthesis was performed using a RT-PCR for 2 µg of RNA. The following components, except RNA, were mixed in a sterile RNase-free microfuge tube (final volume of 50 µL/sample):

COMPONENT	QUANTITY
Total RNA	2 µg
$MgCl_2$ solution [25 mM] (Roche)	11 µL
10X PCR Buffer II No Mg^{2+} (Roche), used at 1X	5 µL
dNTPs 2,5 mM (Roche): 25 µL of every dNTPs in a final volume of 400 Ml	10 µL
RNAse Inhibitor [2000 U, 20 U/Ml] (Roche)	1,5 µL
Moloney Murine Leukemia Virus Reverse Transcriptase (MuLV) (Celera)	1,5 µL
Random Hexamers [50 µM, 5 nMoles] (Roche)	2,5 µL
DEPC H_2O (with diethyl pyrocarbonate)	To a total volume of 50 µL

Table 1: Components of the mix for reverse transcription polymerase chain reaction.

The mix was aliquoted into individual PCR tubes and then the RNA was added last. RT-PCR reaction consists in three steps performed in a thermal cycler (Applied biosystems, Thermo Fisher Scientific):

STEP	TEMPERATURE (°C)	TIME (minutes)
Random hexamers annealing	25	10
Reverse transcription	42	60
Denaturation	95	3

Table 2: RT-PCR steps.

3.2.10 Polymerase chain reaction (PCR) and gel electrophoresis

The Spike Wuhan DNA and cDNA were amplified performing a polymerase chain reaction (PCR) with the following primers:

PRIMER	SEQUENCE (5' – 3')
Spike Forward (Life Technologies, catalogue number: 10336022)	AGACTCTTCTTGCCCTGCAC
Spike Reverse (Life Technologies, catalogue number: 10336022)	CGAAGCTGTCGGCATAAACG

Table 3: Primer forward and reverse used for Spike Wuhan DNA/cDNA amplification.

The following components, except DNA/cDNA, were mixed in a sterile microfuge tube (final volume of 50 µL/sample):

COMPONENT	QUANTITY
10X DreamTaq Buffer (which contains 20 mM $MgCl_2$, KCl and $(NH4)_2SO_4$) (Thermo Scientific), used at 1X	5 µL
dNTP Mix, 2 mM each (Thermo Scientific)	5 µL (0.2 mM of each)
Forward primer	0,1 µM
Reverse primer	0,1 µM
Template DNA/cDNA	a) 100 ng of DNA, b) or 1 µL of cDNA from HEK 293T, HEK 293T Spike, clone 10B of HEK 293T Spike GFP1-10 10B, diluted 1:10 c) or 1 µL of cDNA from clone 4G of HEK 293T Spike GFP1-10, diluted 1:5.
DreamTaq™ DNA Polymerase (5U/µl, 500 units) (Thermo Scientific)	1,25 µL
Nuclease-free H_2O	To a total volume of 50 µL

Table 4: Components of the PCR mix.

The mix was aliquoted into individual PCR tubes and then the DNA was added last. PCR reaction consists in these steps performed in a thermocycler:

STEP	TEMPERATURE (°C)	TIME	NUMBER OF CYCLES
Initial denaturation	95	3 minutes	1
Denaturation	95	30 seconds	30
Primer Annealing	60	30 seconds	
Extension	72	30 seconds	
Final extension	72	5 minutes	1

Table 5: PCR steps.

PCR products were loaded in gel electrophoresis. The gel was produced with 50 mL TRIS-Borate-EDTA buffer (TBE 20X, used at 1X), 1% of agarose (Sigma-Aldrich), and 2,5 µL SYBR™ Safe DNA Gel Stain (Invitrogen, Thermo Fisher Scientific). GeneRuler 1 kb DNA Ladder (Catalogue number: SM0311, Life Technologies) was used as a molecular weight marker. DNA Gel Loading Dye (6X, used at 1X, containing bromophenol blue and xylene cyanol FF) (ThermoFisher Scientific) was added to samples for visual tracking of DNA/cDNA migration in the agarose gel.

3.2.11 Pilot cell-cell fusion assays

After verifying presence of the Spike gene and transcript in transduced cells, pilot fusion tests were performed in a 24-well plate. In order to determine the best conditions for fusion tests, HEK 293T ACE2 GFP11 and clone 4G of HEK 293T Spike GFP1-10 were mixed in three different ratios in each well: $0.5x10^6$ cells/type, or $1x10^6$ cells/type, or $0.5x10^6$ HEK 293T ACE2 GFP11 and 0.75 $x10^6$ clone 4G of HEK 293T Spike GFP1-10 (excess of Spike). As negative controls, we seeded $0.5x10^6$ cells of the following cell lines, without mixing them: $0.5x10^6$ HEK 293T ACE2 GFP11, $0.5x10^6$ clone 4G of HEK 293T Spike GFP1-10, $0.5x10^6$ HEK 293T GFP11, $0.5x10^6$ HEK 293T ACE2 GFP1-10. In addition, also as negative controls, we mixed $0.5x10^6$ each of HEK 293T GFP11 and of clone 4G of HEK 293T Spike GFP1-10 (control without the ACE2 receptor), and $0.5x10^6$ each of HEK 293T ACE2 GFP1-10 and HEK 293T GFP11 (control without the Spike protein).
Cells were trypsinized, resuspended in DMEM 10% FBS, counted using a hemocytometer, and the required number of cells was harvested in eppendorf tubes. In fusion tests and negative fusion controls, cells were mixed in eppendorf tubes before centrifugation at 900 rpm for 5 minutes. After centrifugation, the pellet was resuspended in 500 µL of DMEM 10% FBS and transferred in the 24-well plate. Cells were monitored for 24 hours and screened for fusion and fluorescence signal detection every half an hour.
To study the dimension and the fluorescence signal of fused cells, a flow cytometry analysis was performed after 24 hours, using BD FACSCalibur™ Flow Cytometer. Cells were harvested from the 24-well plate and the procedure described in the chapter “3.2.6 Flow Cytometry” for GFP-expressing cells was used to prepare samples. $1x10^4$ events were acquired using the FL-1 laser fluorescence (green) for GFP (peak emission wavelength at 508 nm).
To determine the functionality of the pilot cell-cell fusion system, a test was performed in a 96-well black microplate in triplicate. Cells were separately centrifuged and resuspended in Opti-MEM™ (Reduced Serum Medium, Gibco™), which reduces fluorescent background. For fusion test, $8,3x10^4$ of each HEK 293T ACE2 GFP11 and HEK 293T Spike GFP1-10 (clone 4G) cell lines were mixed in microplate well, in triplicate. As controls, we used $16,6x10^4$ per well of each of the following single cell lines: HEK 293T ACE2 GFP11, HEK 293T Spike GFP1-10, and

HEK 293T GFP11. As a fusion control, we mixed 8,3x10^4/well each of HEK 293T Spike GFP1-10 and of HEK 293T GFP11 (control with cells lacking ACE2 receptor). Three wells were reserved for background control with only Opti-MEM. The test was monitored for 27 hours by Varioskan LUX, using SkanIt Software 6.1 (Thermo Fisher Scientific). The GFP fluorescent signal was detected (excitation: 485 nm, emission: 520 nm). A separate test was performed mixing cells before centrifugation at 900 rpm for 5 minutes, followed by seeding at the same cell densities mentioned above in a 96-well microplate and monitoring them for 48 hours with Varioskan.
To evaluate the presence of differences between the means of the fusion test and the means of controls, we performed a two-tailed paired Wilcoxon Test, using as a 95% of confidence interval.

3.2.12 Fluorescence microscopy

GFP signal was detected by fluorescence microscopy using Leica Application Suite X 3.7.5.24914, regulating the exposure time (measured in milliseconds, ms) and the fluorescence signal gain to allow optimised imaging. The exposure or scanning rate controls the time that the camera sensing elements are exposed to the specimen, while the fluorescence signal gain is a function for changing the brilliance of an image. Fluorescence microscopy was used to verify the cell transduction with a lentiviral vector expressing the GFP11 or the GFP1-10 after transient transfection with a plasmid encoding the counterpart of the GFP, and to monitor cell-cell fusion during pilot fusion tests.

4. RESULTS

4.1 Cell lines development

The first step of cell lines development included the lentiviral vectors generation through transfection procedure. A pLVx backbone plasmid expressing the GFP11, or the GFP1-10 or the Spike Wuhan was added to a tube containing the Lenti-X Packaging Single Shots, to generate lentiviral vectors expressing the GFP11, the GFP1-10 or the Spike Wuhan. HEK 293T cells or HEK 293T ACE2 cells, that were the two initial cell lines, were transduced with the lentiviral vectors to obtain cell lines stably and permanently expressing proteins of interest. Cells were transiently transfected with a plasmid expressing the counterpart of the GFP (pLVx MBP GFP11 or pLVx GFP1-10) and visualized with fluorescence microscopy to verify the transduction. When GFP1-10 and GFP11 are spatially close to each, complementation occurs reconstituting the entire GFP. Cells were then sorted for the GFP to select cells expressing proteins of interest. HEK 293T ACE2 have also been screened for an anti-ACE2 antibody conjugated with phycoerythrin to confirm the stable and permanent expression of the receptor. $1X10^4$ cells were sorted in an eppendorf tube containing FBS, then they were seeded in a flask and in limiting dilution in a 96-well plate in duplicate to allow the growing of single cell clones. After around two weeks, single cell clones had sufficiently grown, and they were screened using transient transfection with a plasmid expressing the counterpart of the GFP and with fluorescence microscopy to confirm the expression of a particular protein.
HEK 293T cells expressing the Spike protein have to be sorted in the future with an anti-Spike antibody conjugated with a fluorophore to select cells that highly express the Spike.
For every cell line, the clone that had a better growth in culture was expanded and stored at -80°C and in liquid nitrogen to have stocks of cells to use for pilot fusion tests.

4.1.1 Generation of HEK 293T GFP11 cell line

HEK 293T cells were transduced with a lentiviral vector derived from pLVx-EF1α-IRES-puro expressing GFP11. Cells were subsequently transiently transfected with a pLVx plasmid expressing GFP1-10 to confirm the expression of GFP11 in the cell line. The fluorescent signal revealed that cells have been transduced with the protein of interest (Fig. 26). In the negative control a fluorescent signal was no detected because these cells have not been transiently transfected with the pLVx GFP1-10 plasmid, so the complementation of GFP did not occur.

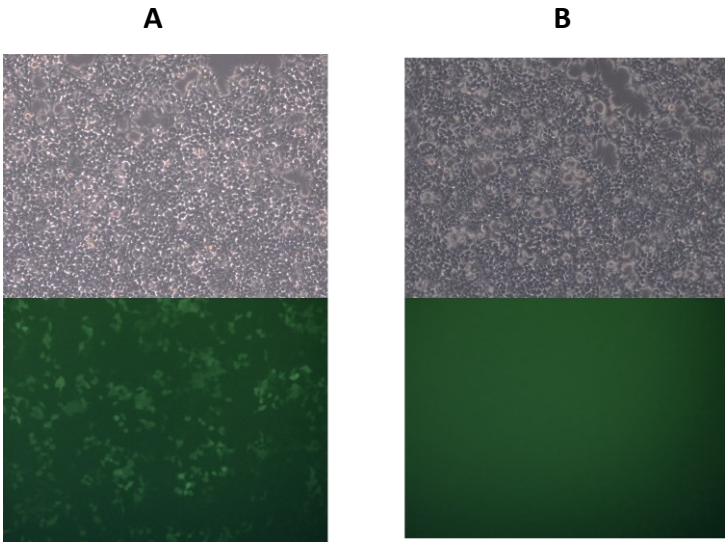

Fig. 26: HEK 293T GFP11, which have been transduced with a lentiviral vector expressing GFP11: top panels are images obtained without laser beam, while bottom panels are images obtained with a blue laser beam of the fluorescence microscope. A) HEK 293T GFP11 transiently transfected with pLVx GFP1-10. Cells efficiently transiently transfected were fluorescent. B) Untransfected HEK 293T GFP11, as a negative control. A fluorescent signal was not detected.

After confirming successful transduction with fluorescence microscopy, cells were sorted for GFP by flow cytometry, selecting cells with the highest signal of GFP (Fig. 27).

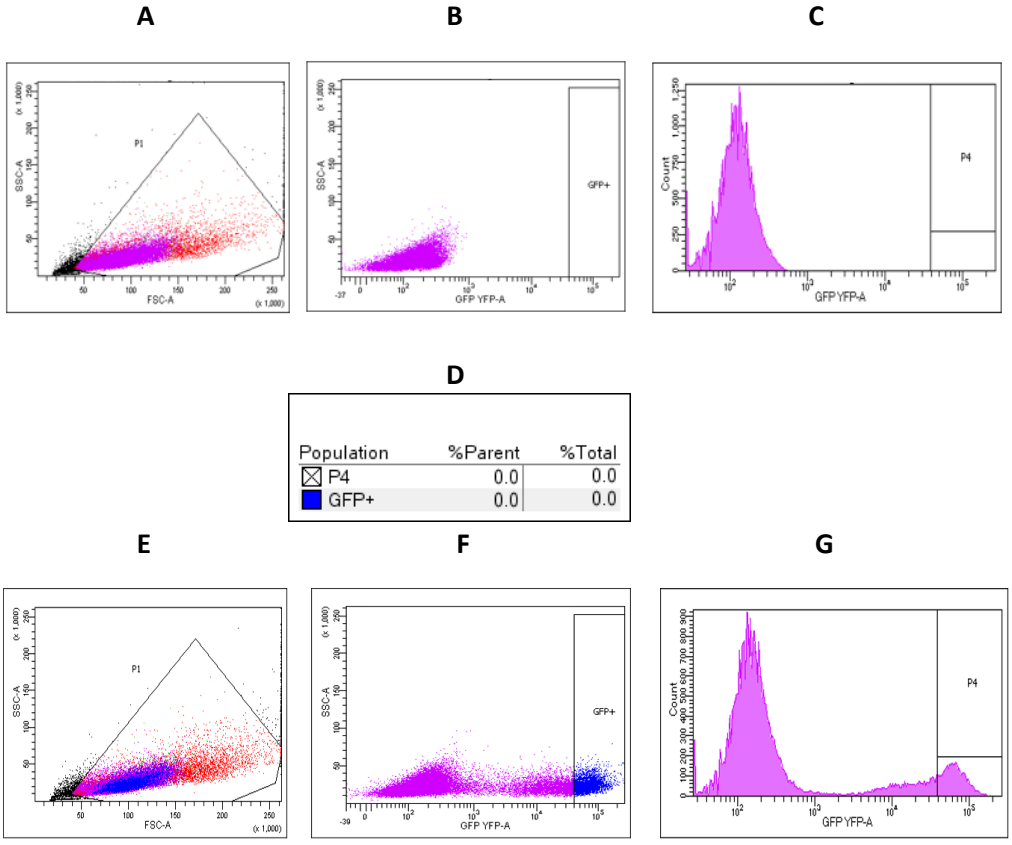

H

Population	%Parent	%Total
P4	11.1	8.0
GFP+	10.8	7.8

Fig. 27: Sorting plots showing GFP fluorescent signal by HEK 293T GFP11 cells (E, F, G, H) compared with control (A, B, C, D). A, E) Selection of cells of interest in control and in HEK 293T GFP11 cells, respectively. The Forward Scatter (FSC-A) is shown on the x axis, plotted against the side scatter (SSC-A) on the y axis. B, F) Selection of cells with the highest signal of GFP in control and in HEK 293T GFP11 cells, respectively. GFP signal is shown on the x axis, plotted against SSC-A on the y axis. C, G) The signal of GFP is shown on the x axis, plotted against cell counts on the y axis. In control cells (C) there is a peak interpreted as GFP negative cells, while in HEK 293T GFP11 cells a distinct second peak on the right includes cells with a high signal of green fluorescence. D, H) Percentage of GFP-positive cells in control and in the sample, respectively. 0% of cells are GFP-positive in control, while 7.8% of HEK 293T GFP11 are strongly GFP-positive.

Based on flow cytometry analysis, 7.8% of HEK 293T GFP11 cells were strongly positive for GFP. Cells were sorted and cloned by limiting dilution to obtain single cell clones that stably and permanently express the GFP11. Clones have been screened with transient transfection procedure to allow the generation of the entire GFP that has been detected by fluorescence microscopy (Fig. 28) to confirm the expression of GFP11.

A **B**

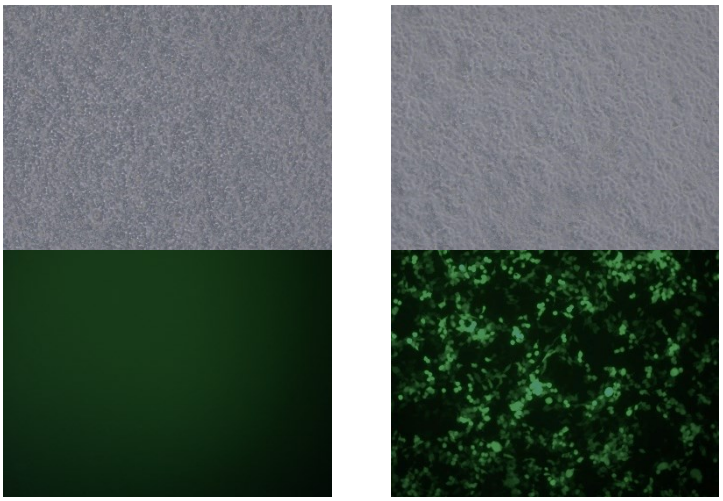

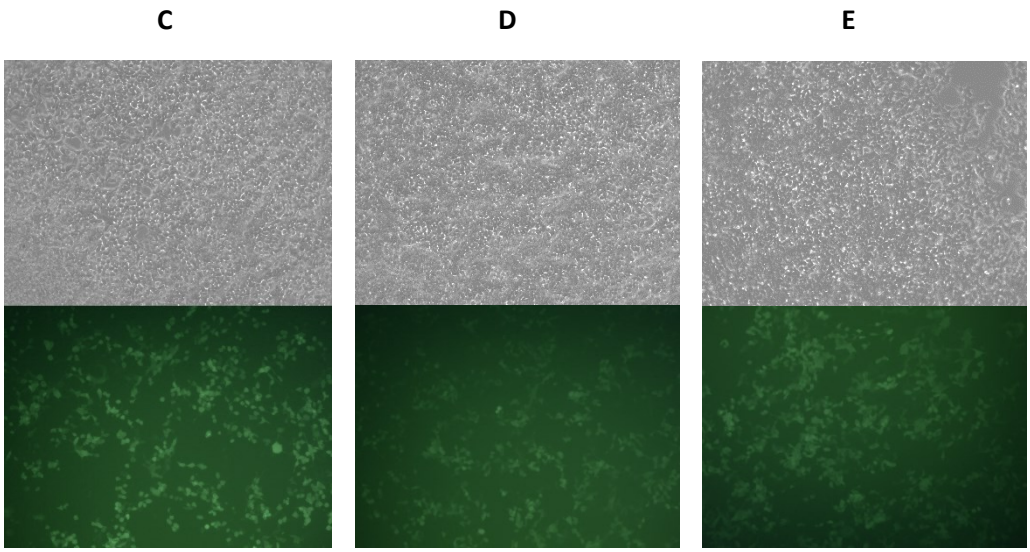

Fig. 28: Screening of single cell clones derived from HEK 293T GFP11 cell line after transient transfection. Top panels are images obtained without laser beam, while bottom panels are images obtained with a blue laser beam of fluorescence microscope. A) Untransfected HEK 293T GFP11 (negative control). B) HEK 293T GFP11 transfected with ppt CMV GFP (positive control). C, D, E) HEK 293T GFP11 cells (B3 clone, C10 clone and B10 clone, respectively), transiently transfected with pLVx GFP1-10 plasmid.

To confirm GFP expression of single cell clones after transient transfection, an initial determination was performed by fluorescence microscopy followed by flow cytometry analyses (Fig. 29).

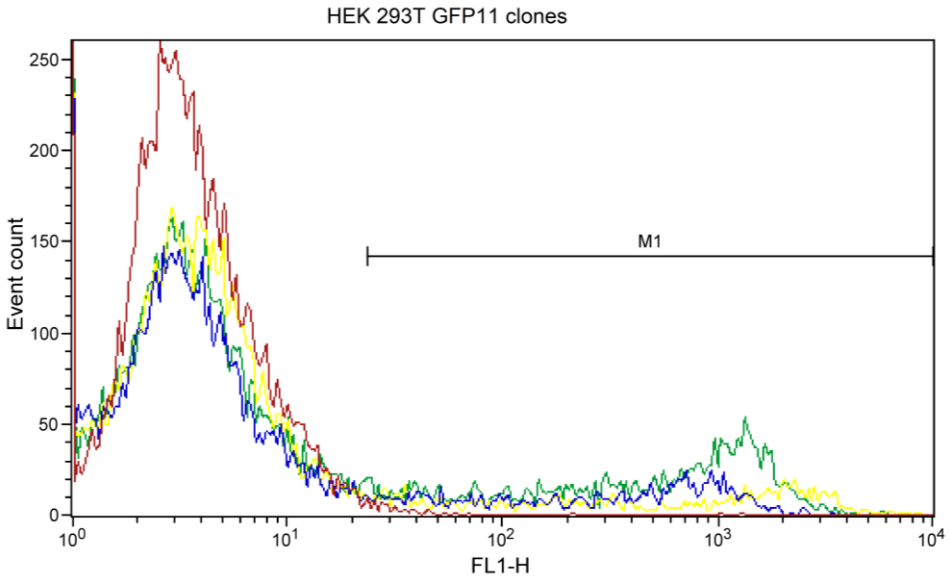

Fig. 29: The FL1-H laser fluorescence signal is shown on the x axis, plotted against event count on the y axis. The red line represents the negative control, the blue line the C10 clone of HEK 293T GFP11 cells, the green line the B10 clone of HEK 293T GFP11 cells, and the yellow line the B3 clone of HEK 293T GFP11 cells.

In this way a basic cell line was obtained, and it can be used to generate other cell lines with different combinations of protein expression.

4.1.2 Generation of HEK 293T GFP1-10 cell line

HEK 293T cells were transduced with a lentiviral vector derived from pLVx-EF1α-IRES-puro expressing GFP1-10. Cells were subsequently transiently transfected with a pLVx plasmid expressing GFP11 to confirm the expression of GFP1-10 in the cell line. The fluorescent signal revealed that cells have been transduced with the protein of interest (Fig. 30).

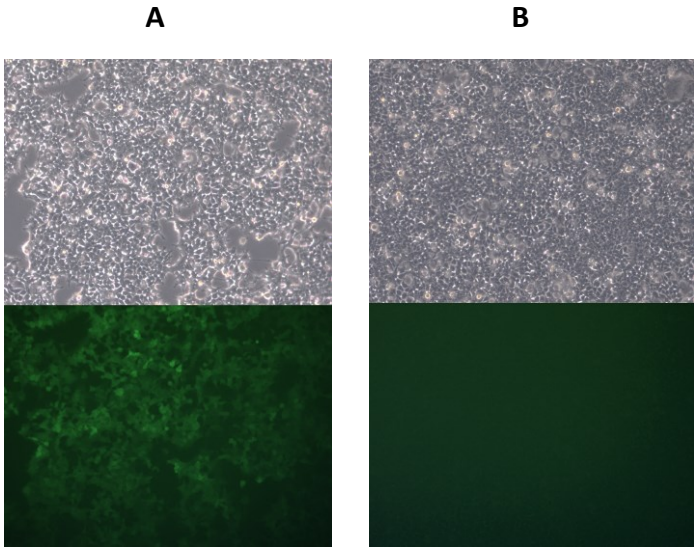

Fig. 30: HEK 293T GFP1-10, which have been transduced with a lentiviral vector expressing GFP1-10: top panels are images obtained without laser beam, while bottom panels are images in fluorescence microscopy. A) HEK 293T GFP1-10 transiently transfected with pLVx MBP GFP11. Cells efficiently transiently transfected were fluorescent. B) Untransfected HEK 293T GFP1-10, as a negative control without fluorescent signal.

After confirming successful transduction with fluorescence microscopy, cells were sorted for GFP by flow cytometry, selecting cells with the highest GFP signal (Fig. 31). As a negative control, untransfected HEK 293T GFP11 cell line was used (Fig. 27 A, B, C, D).

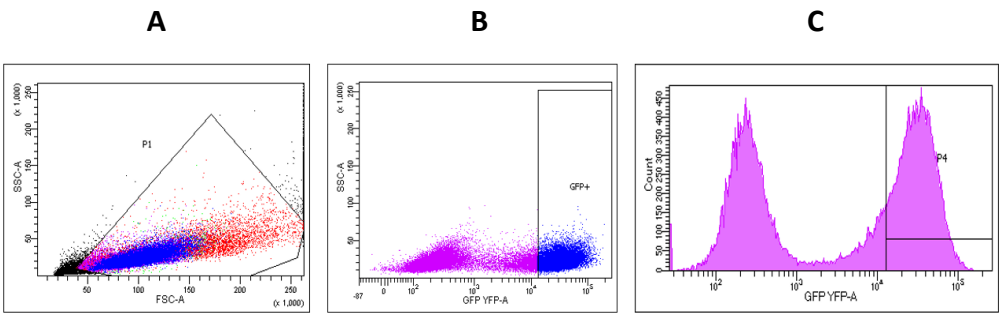

D

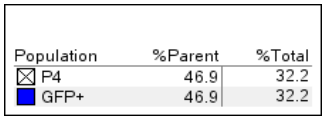

Population	%Parent	%Total
P4	46.9	32.2
GFP+	46.9	32.2

Fig. 31: Sorting plots showing GFP fluorescent signal by HEK 293T GFP1-10 cells. A) Selection of cells of interest. The Forward Scatter (FSC-A) is shown on the x axis, plotted against the side scatter (SSC-A) on the y axis. B) Selection of cells with the highest signal of GFP. The GFP signal is shown on the x axis, plotted against the SSC-A on the y axis. C) GFP signal is shown on the x axis, plotted against cell counts on the y axis. There are two peaks: the peak on the right includes cells with a high signal of green fluorescence, the peak on the left includes cells GFP-negative. D) Percentage of 32.2 % GFP-strongly positive cells on the total.

Based on flow cytometry analysis, 32.2 % of HEK 293T GFP1-10 cells were strongly positive for GFP. Cells were sorted and cloned by limiting dilution to obtain single cell clones that stably and permanently express the GFP1-10. Clones were screened using transient transfection with a plasmid expressing the counterpart of the GFP and with fluorescence microscopy (Fig. 32) to confirm the expression of GFP1-10. As a negative control, untransfected HEK 293T GFP11 cell line was used (Fig. 28 A).

A B C

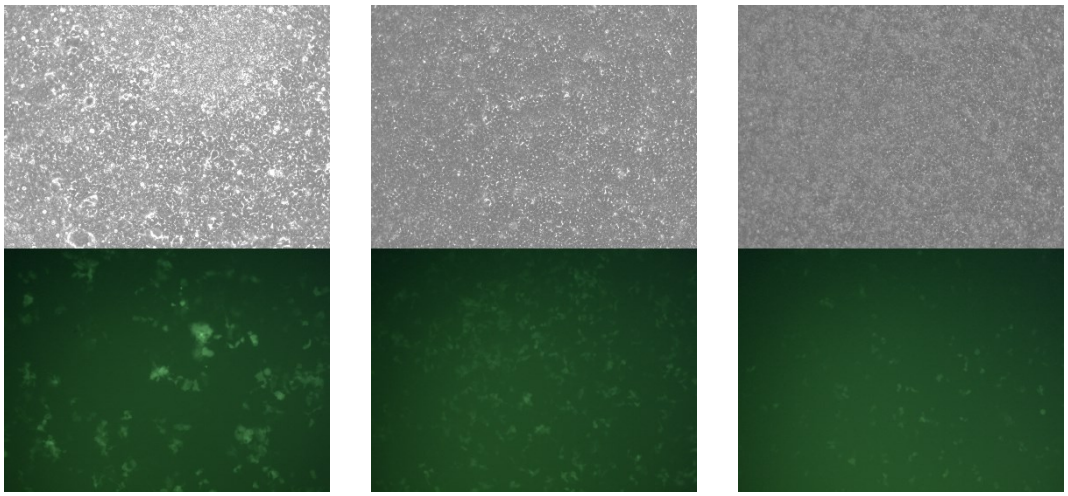

Fig. 32: Screening of single cell clones derived from HEK 293T GFP1-10 cell line. Top panels are images obtained without laser beam, while bottom panels are images obtained with a blue laser beam of fluorescence microscope. A) B9 clone, B) E9 clone, C) F9 clone.

To verify reconstituted GFP expression in single cell clones, flow cytometry analyses were performed after identification of positive clones by fluorescence microscopy (Fig. 33).

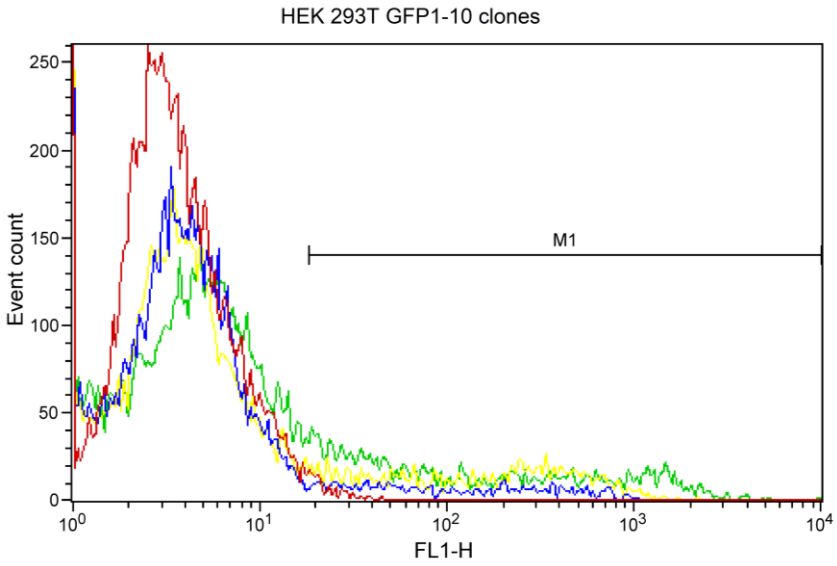

Fig. 33: The FL1-H laser fluorescence signal is shown on the x axis, plotted against event count on the y axis. The red line represents the negative control, the blue line the F9 clone of HEK 293T GFP1-10 cells, the green line the B9 clone of HEK 293T GFP1-10 cells, and the yellow line the E9 clone of HEK 293T GFP1-10 cells.

In this way a basic cell line was obtained, and it can be used to generate other cell lines with different combinations of protein expression.

4.1.3 Generation of HEK 293T ACE2 GFP11 cell line

HEK 293T ACE2 cells were transduced with a lentiviral vector derived from pLVx-EF1α-IRES-Puro expressing GFP11. Cells were subsequently transiently transfected with a pLVx plasmid expressing GFP1-10 to confirm the expression of GFP11 in the cell line. The fluorescent signal revealed that cells have been transduced with the protein of interest (Fig. 34).

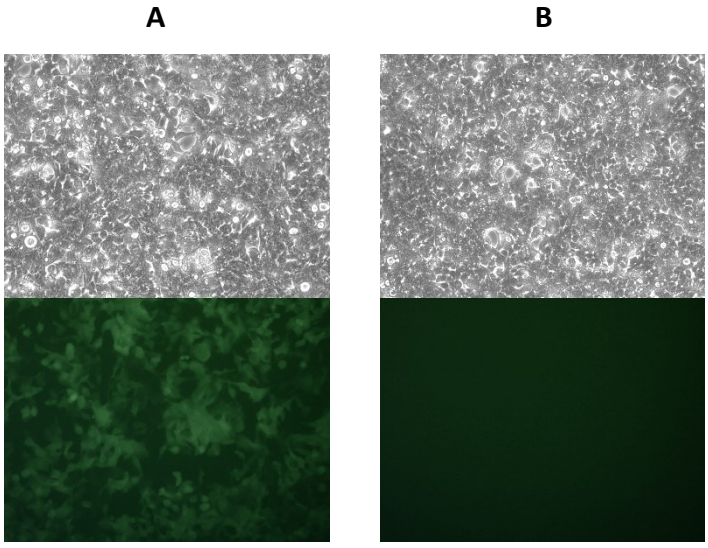

Fig. 34: HEK 293T ACE2 GFP11, which have been transduced with a lentiviral vector expressing GFP11: top panels are images obtained without laser beam, while bottom panels are images obtained with a blue laser beam of the fluorescence microscope. A) HEK 293T ACE2 GFP11 transiently transfected with pLVx GFP1-10. Cells efficiently transiently transfected were fluorescent. B) Untransfected HEK 293T ACE2 GFP11, as a negative control. A fluorescent signal was not detected.

After confirming successful transduction with fluorescence microscopy, cells were sorted for GFP signal by flow cytometry, selecting cells with the highest fluorescence intensity. Cells were also sorted for ACE2-PE to verify the expression of ACE2 in the cell line (Fig.35).

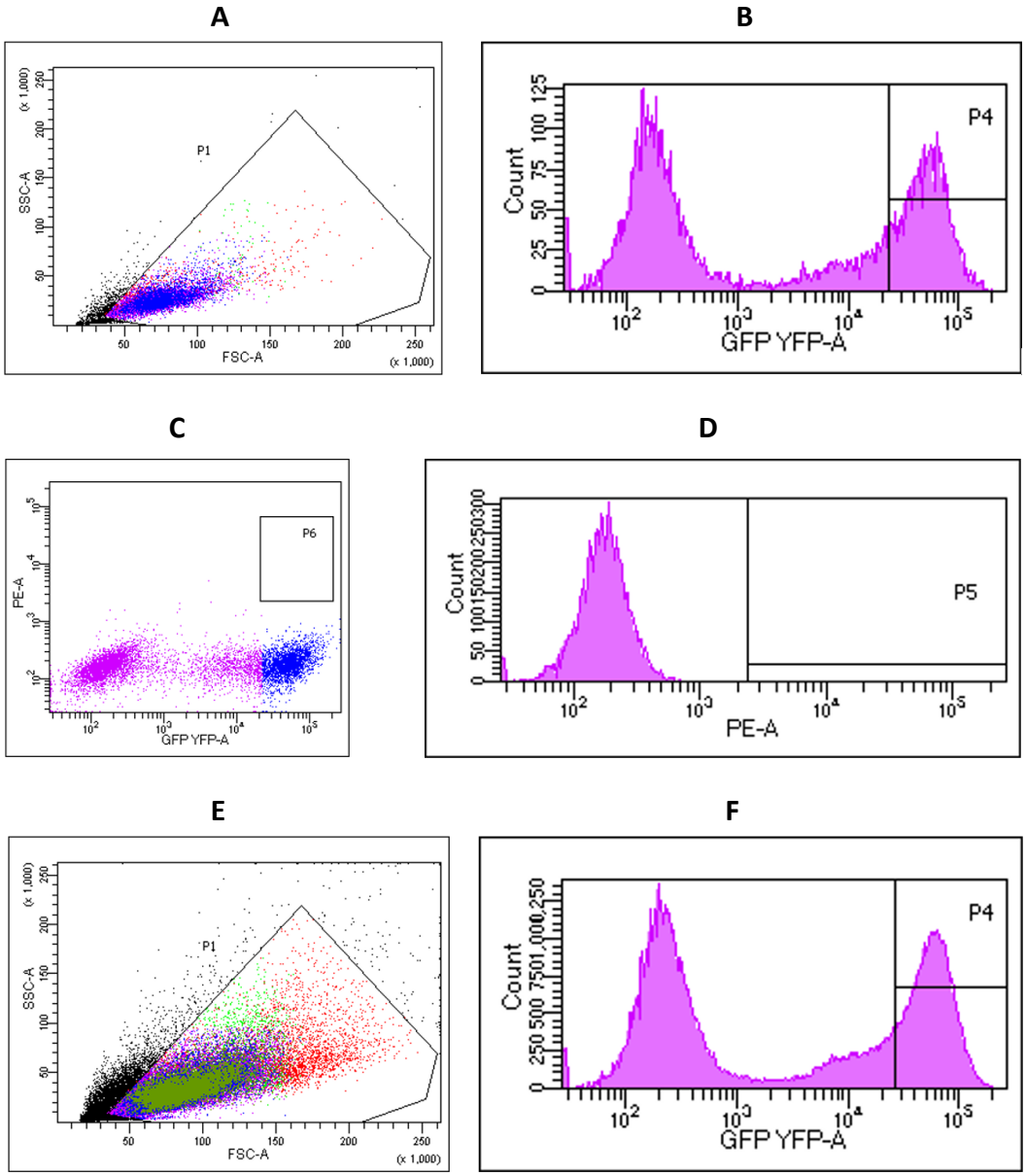

G

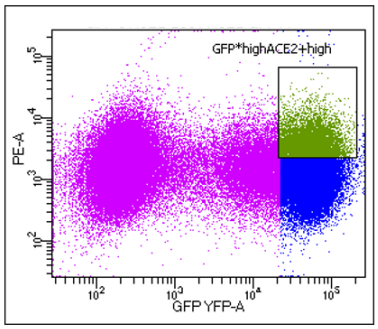

H

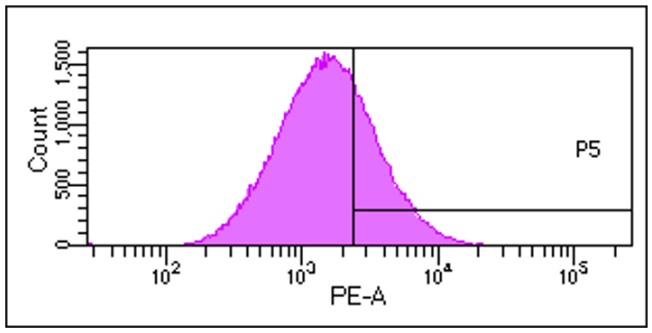

I

Tube: 293T ACE2 GFP11

Population	#Events	%Parent	%Total
All Events	106,270	####	100.0
P1	95,306	89.7	89.7
P2	91,223	95.7	85.8
P3	90,176	98.9	84.9
P4	31,476	34.9	29.6
GFP+	33,213	36.8	31.3
P5	25,088	27.8	23.6
GFP*highACE2+high	9,125	10.1	8.6

Fig. 35: Sorting plots showing the fluorescent signal of GFP and the ACE2-PE of HEK 293T ACE2 GFP11 cells (E, F, G, H) compared with control (A, B, C, D). A, E) Selection of cells of interest in control and in HEK 293T ACE2 GFP11 cells, respectively. The Forward Scatter (FSC-A) is shown on the x axis, plotted against the side scatter (SSC-A) on the y axis. B, F) GFP signal is shown on the x axis, plotted against counts in the y axis, in control and in HEK 293T ACE2 GFP11 cells, respectively. C, G) Selection of cells with the highest signal of GFP and ACE2-PE in control and in HEK 293T ACE2 GFP11 cells, respectively. The GFP YFP-A is shown on the x axis, plotted against the PE-A on the y axis. D, H) The PE-A is shown on the x axis, plotted against cell counts on the y axis. The unimodal distribution of HEK 293T ACE2 GFP11 is shifted on the right because cells are positive to ACE2. I) Percentage of HEK 293T ACE2 GFP11 GFP-strongly positive and ACE2-PE-positive.

All HEK 293T ACE2 GFP11 cells were ACE2 positive as shown by the unimodal distribution at relatively high fluorescence intensity, indicating that ACE2-expression remained stable in time.

Based on flow cytometry analysis performed when sorting cells, 31.3 % of HEK 293T ACE2 GFP11 cells were strongly positive for GFP. Cells were sorted and cloned by limiting dilution to obtain single cell clones that stably and permanently express the GFP11. Clones have been screened with transient transfection procedures to allow the generation of an entire GFP that has been detected by fluorescence microscopy (Fig. 36) to confirm the expression of GFP11. As a negative control, untransfected HEK 293T GFP11 cell line was used (Fig. 28 A).

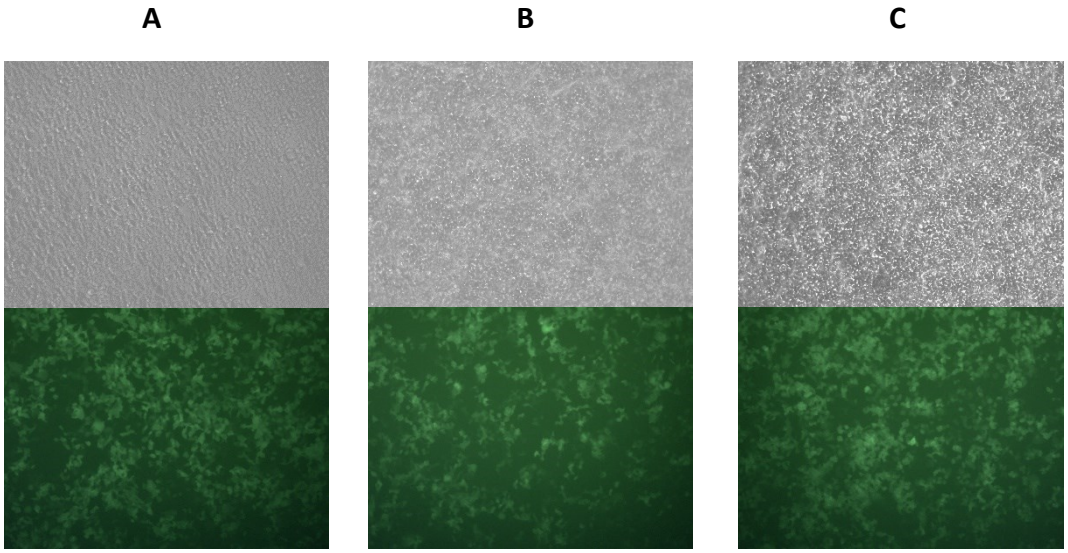

Fig. 36: Screening of single cell clones derived from HEK 293T ACE2 GFP11 cell line. Top panels are images obtained without laser beam, while bottom panels are images obtained with a blue laser beam of fluorescence microscope. A) C10 clone, B) E10 clone, C) G9 clone. Single cell clones were transiently transfected with pLVx GFP1-10 plasmid.

To confirm GFP expression of single cell clones after transient transfection, an initial determination was performed by fluorescence microscopy followed by flow cytometry analyses (Fig. 37).

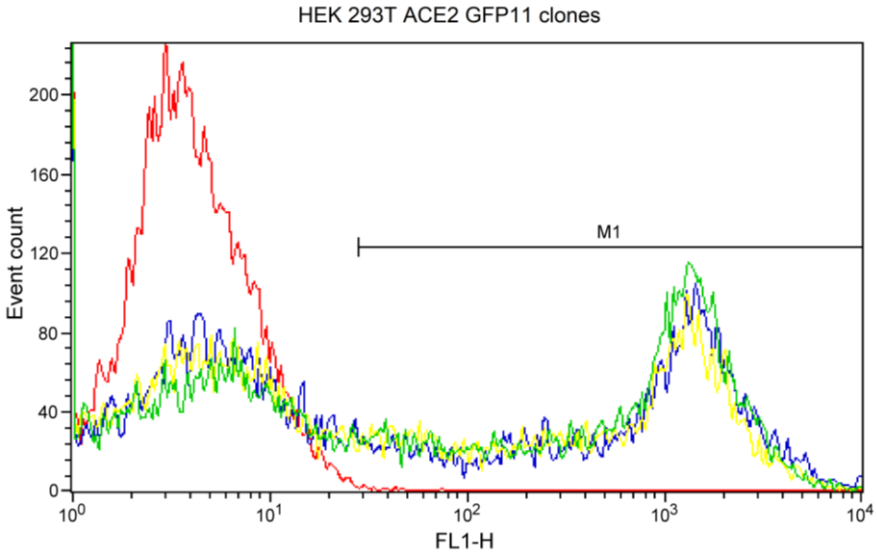

Fig. 37: The FL1-H laser fluorescence signal is shown on the x axis, plotted against event count on the y axis. The red line represents the negative control, the blue line the C10 clone of HEK 293T ACE2 GFP11 cells, the green line the G9 clone of HEK 293T ACE2 GFP11 cells, and the yellow line the E10 clone of HEK 293T ACE2 GFP11 cells.

4.1.4 Generation of HEK 293T ACE2 GFP1-10 cell line

HEK 293T ACE2 cells were transduced with a lentiviral vector derived from pLVx-EF1α-IRES-Puro expressing GFP1-10, and subsequently transiently transfected with a pLVx plasmid expressing GFP11 to confirm the expression of GFP1-10 in the cell line. Cells that have been efficiently transiently transfected were detected by fluorescence microscopy (Fig. 38).

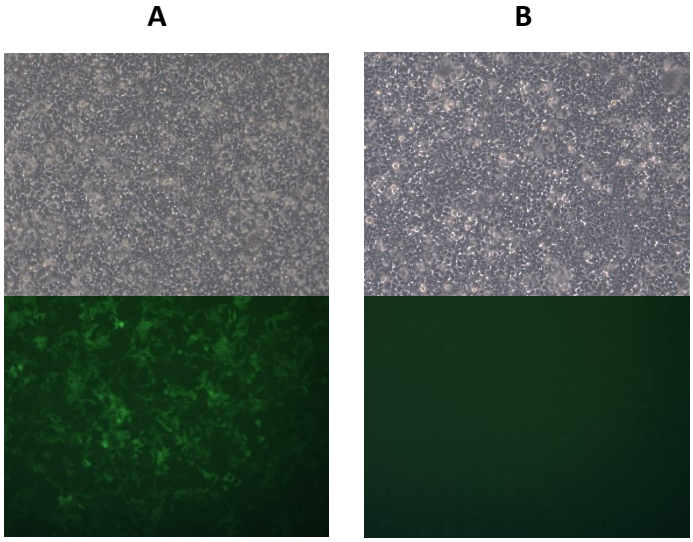

Fig. 38: HEK 293T ACE2 GFP1-10, which have been transduced with a lentiviral vector expressing GFP1-10: top panels are images obtained without laser beam, while bottom panels are images obtained with a blue laser beam of fluorescence microscope. A) HEK 293T ACE2 GFP1-10 transiently transfected with pLVx MBP GFP11. Cells efficiently transiently transfected were fluorescent. B) Untransfected HEK 293T ACE2 GFP1-10, as a negative control without fluorescent signal.

After confirming successful transduction, cells were sorted for GFP signal and for ACE2 using an antibody by flow cytometry, selecting cells with the highest fluorescent signal (Fig. 39). As a negative control, untrasfected HEK 293T GFP11 cell line was used (Fig. 27 A, B, C, D).

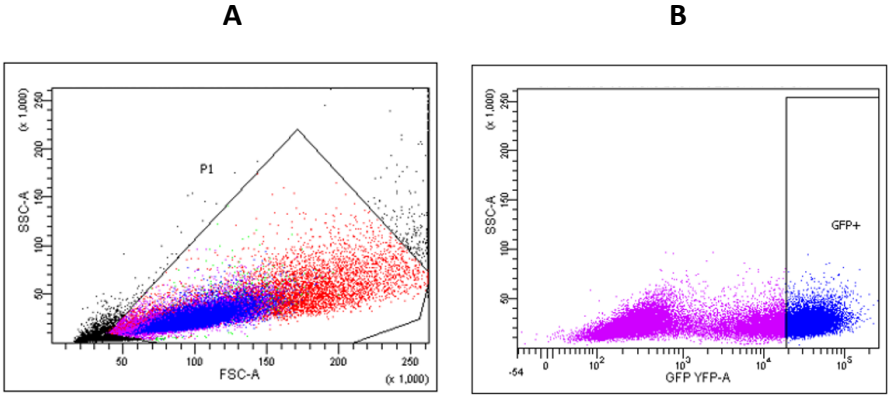

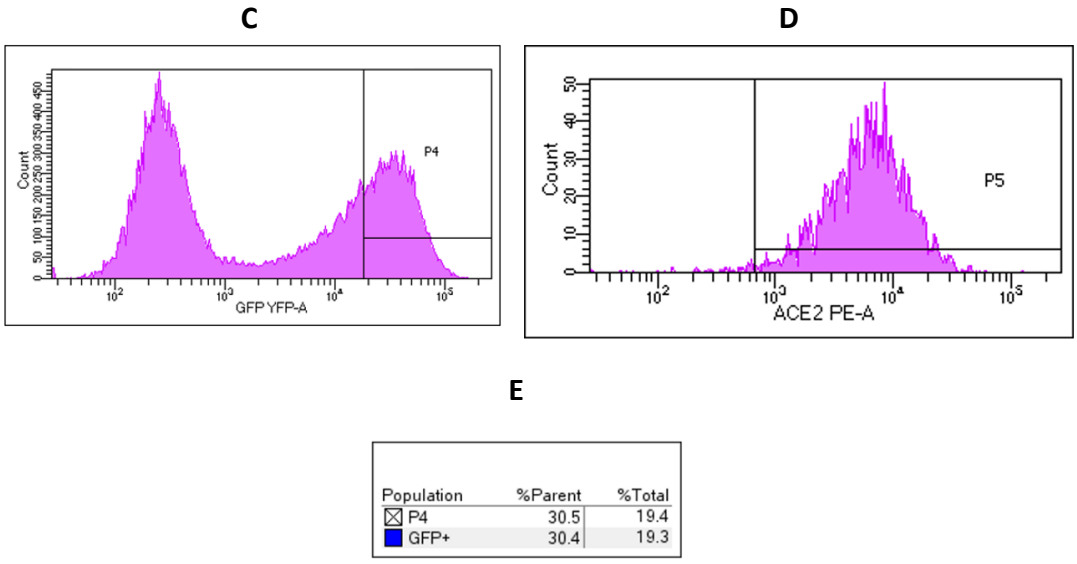

Fig. 39: Sorting plots showing GFP fluorescent signal by HEK 293T ACE2 GFP1-10 cells. A) Selection of cells of interest. The FSC-A is shown on the x axis, plotted against the SSC-A on the y axis. B) Selection of cells with the highest signal of GFP. The GFP signal is shown on the x axis, plotted against the SSC-A on the y axis. C) GFP signal is shown on the x axis, plotted against cell counts on the y axis. There are two peaks: the peak on the right includes cells with a high signal of green fluorescence, while the peak on the left includes GFP-negative cells. D) ACE2 PE-A signal is shown on the x axis, plotted against cell counts on the y axis. The unimodal distribution shows that all cells express ACE2. E) Percentage of 19.3 % GFP-strongly positive cells on the total.

Based on flow cytometry analyses performed at the time of sorting, 19.3 % of HEK 293T ACE2 GFP1-10 cells were strongly positive for GFP. Cells were sorted and cloned by limiting dilution to obtain single cell clones that stably and permanently express the GFP1-10. Clones were screened using transient transfection with a plasmid expressing the counterpart of the GFP and with fluorescence microscopy (Fig. 40) to confirm the expression of GFP1-10. As a negative control, untransfected HEK 293T ACE2 GFP11 cell line was used (Fig. 28 A).

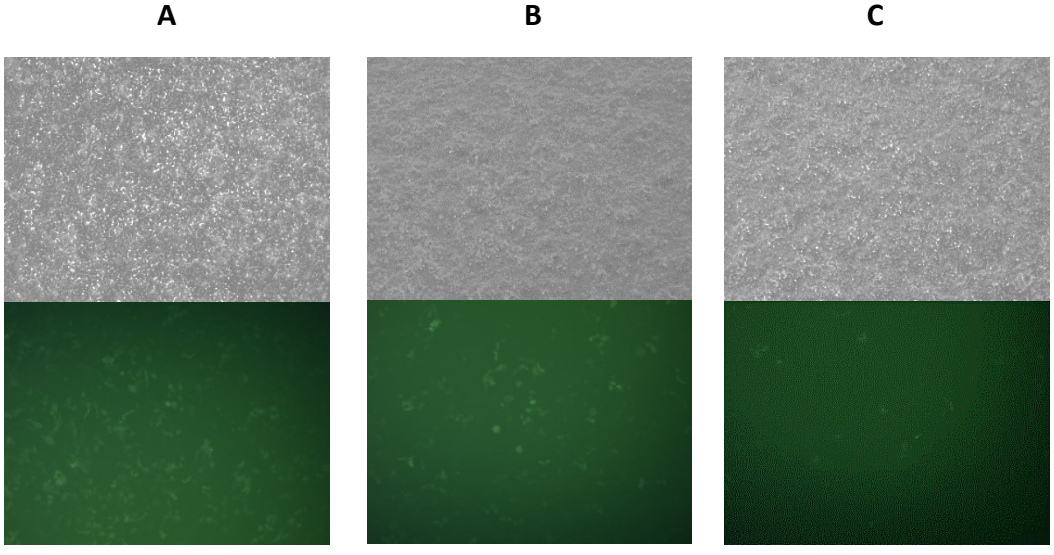

Fig. 40: Screening of single cell clones derived from HEK 293T ACE2 GFP1-10 cell line. Top panels are images obtained without laser beam, while bottom panels are images obtained with a blue laser of fluorescence microscope. A) D9 clone, B) F5 clone, C) D6 clone.

To verify reconstituted GFP expression in single cell clones, flow cytometry analyses were performed after identification of positive clones by fluorescence microscopy (Fig. 41).

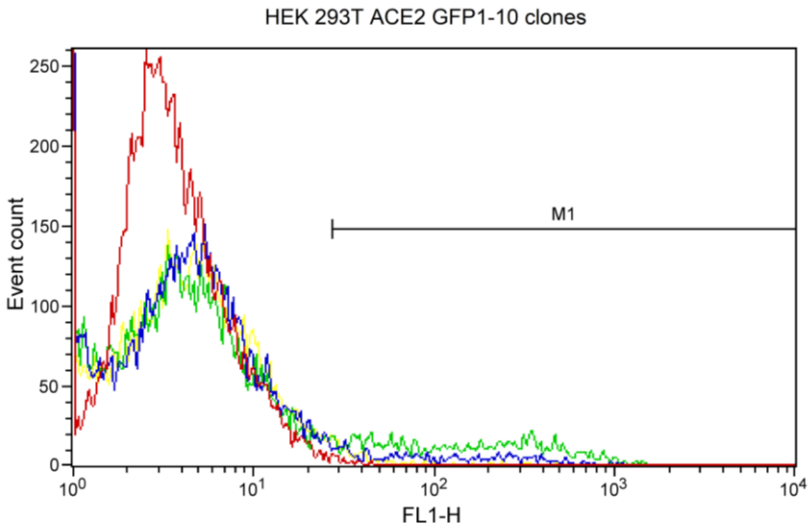

Fig. 41: The FL1-H laser fluorescence signal is shown on the x axis, plotted against event count on the y axis. The red line represents the negative control, the blue line the F5 clone of HEK 293T ACE2 GFP1-10 cells, the green line the D9 clone of HEK 293T ACE2 GFP1-10 cells, and the yellow line the D6 clone of HEK 293T GFP1-10 cells.

4.1.5 Generation of HEK 293T Spike GFP11 cell line

HEK 293T cells were transduced with a lentiviral vector derived from pLVx-EF1α-IRES-Puro expressing the Spike Wuhan protein to generate HEK 293T Spike cell line.

The basic cell line expressing the Spike was transduced with a lentiviral vector derived from pLVx-EF1α-IRES-Puro expressing GFP11. Cells were subsequently transiently transfected with a pLVx plasmid expressing GFP1-10 to confirm the expression of GFP11 in the cell line. The fluorescent signal indicates that cells have been transduced with the protein of interest, due to complementation of GFP11 with GFP1-10 (Fig. 42).

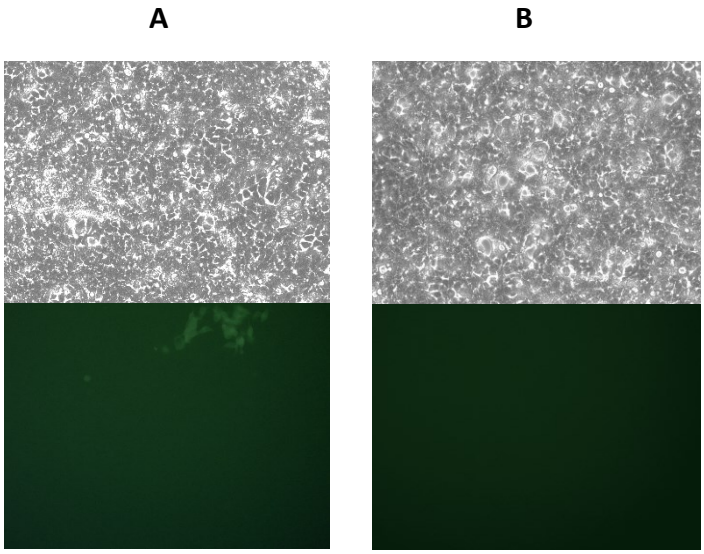

Fig. 42: HEK 293T Spike GFP11, which have been transduced with a lentiviral vector expressing GFP11: top panels are images obtained without laser beam, while bottom panels are images obtained with a blue laser beam of the fluorescence microscope. A) HEK 293T Spike GFP11 transiently transfected with pLVx GFP1-10. Cells efficiently transiently transfected were fluorescent. B) Untransfected cells, as a negative control without fluorescent signal.

After confirming the successful transduction with fluorescence microscopy, cells were sorted for GFP by flow cytometry, selecting cells with the highest signal of GFP (Fig. 43). As a negative control, untransfected HEK 293T GFP11 cell line was used (Fig. 27 A, B, C, D).

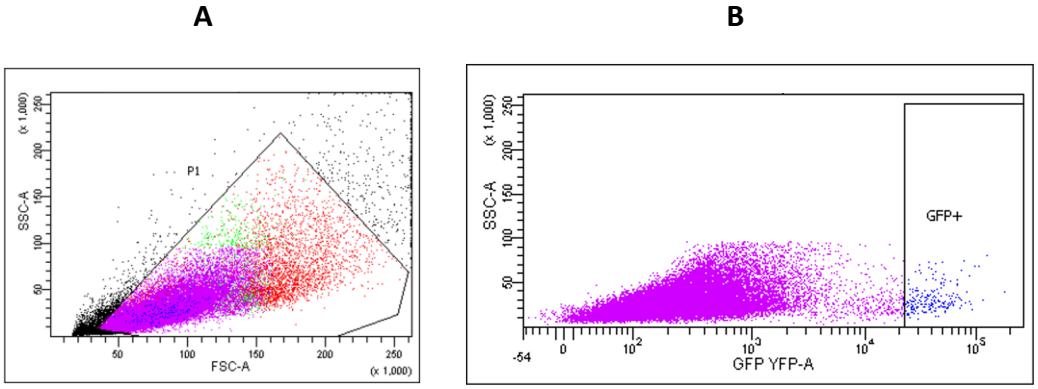

C

Tube: 293T Spike GFP11

Population	#Events	%Parent	%Total
All Events	50,000	###	100.0
P1	45,176	90.4	90.4
P2	41,094	91.0	82.2
P3	40,342	98.2	80.7
P4	185	0.5	0.4
GFP+	215	0.5	0.4
P5	14	0.0	0.0
GFP*highACE2+high	0	0.0	0.0

Fig. 43: Sorting plots showing GFP fluorescent signal by HEK 293T Spike GFP11 cells. A) Selection of cells of interest. The Forward Scatter (FSC-A) is shown on the x axis, plotted

against the side scatter (SSC-A) on the y axis. B) Selection of cells with the highest signal of GFP (in blue). GFP signal is shown on the x axis, plotted against SSC-A on the y axis. C) Percentage of 0.4% GFP-strongly positive cells on the total.

Based on flow cytometry analysis, 0.4% of HEK 293T Spike GFP11 cells were strongly positive to GFP. Cells were sorted and cloned by limiting dilution to obtain single cell clones that stably and permanently express the GFP11.

4.1.6 Generation of HEK 293T Spike GFP1-10 cell line

HEK 293T Spike cell line was transduced with a lentiviral vector derived from pLVx-EF1α-IRES-Puro expressing GFP1-10. Cells were subsequently transiently transfected with a pLVx plasmid expressing GFP11 to confirm the expression of GFP1-10 in the cell line. The fluorescent signal indicates that cells have been transduced with the protein of interest, due to complementation of GFP1-10 with GFP11 (Fig. 44).

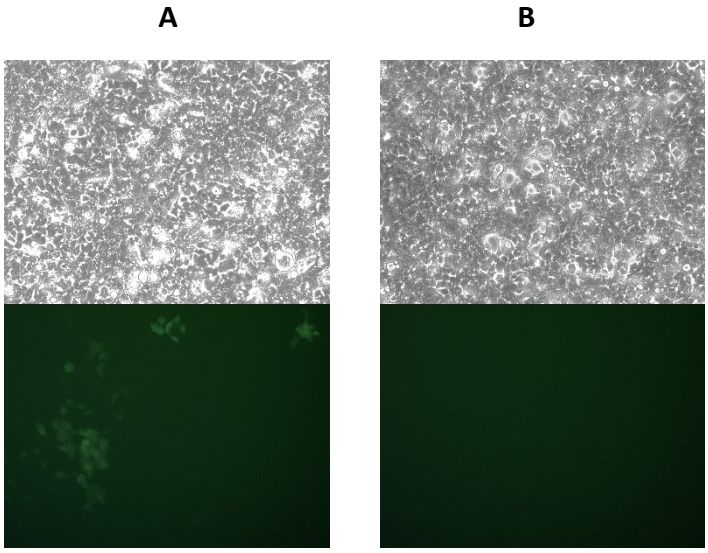

Fig. 44: HEK 293T Spike GFP1-10, which have been transduced with a lentiviral vector expressing GFP1-10: top panels are images obtained without laser beam, while bottom panels are images obtained with a blue laser beam of the fluorescence microscope. A) HEK 293T Spike GFP1-10 transiently transfected with pLVx MBP GFP11. Cells efficiently transiently transfected were fluorescent. B) Untransfected cells, as a negative control without fluorescent signal.

After confirming the successful transduction with fluorescence microscopy, cells were sorted for GFP signal by flow cytometry, selecting cells with the highest signal of GFP (Fig. 45). As a negative control, untrasfected HEK 293T GFP11 cell line was used (Fig. 27 A, B, C, D).

A B

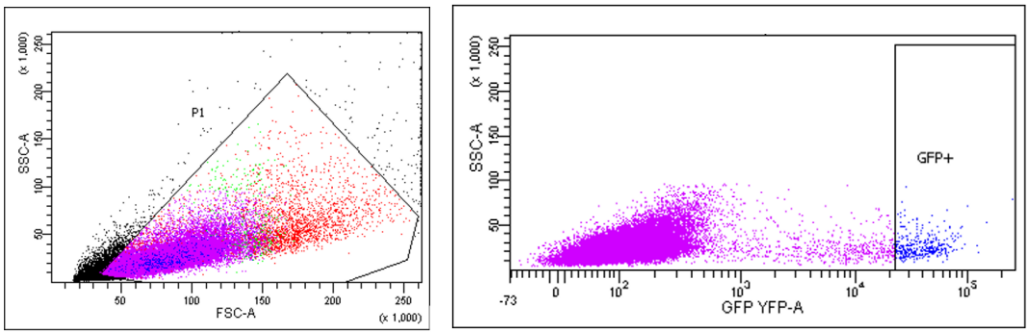

C

Tube: 293T Spike GFP1-10

Population	#Events	%Parent	%Total
All Events	50,000	####	100.0
P1	44,856	89.7	89.7
P2	41,075	91.6	82.2
P3	40,508	98.6	81.0
P4	320	0.8	0.6
GFP+	376	0.9	0.8
P5	3	0.0	0.0
GFP*highACE2+high	0	0.0	0.0

Fig. 45: Sorting plots showing GFP fluorescent signal by HEK 293T Spike GFP1-10 cells. A) Selection of cells of interest. The Forward Scatter (FSC-A) is shown on the x axis, plotted against the side scatter (SSC-A) on the y axis. B) Selection of cells with the highest signal of GFP (in blue). GFP signal is shown on the x axis, plotted against SSC-A on the y axis. C) Percentage of 0.8% GFP-strongly positive cells on the total.

Based on flow cytometry analysis, 0.8% of HEK 293T Spike GFP1-10 cells were strongly positive to GFP. Cells were sorted and cloned by limiting dilution to obtain single cell clones (clones 10B and 4G) that stably and permanently express the GFP1-10.

4.2 Detection of Spike Wuhan gene and transcript in HEK 293T Spike GFP1-10 cell line

To verify the presence of Spike Wuhan gene in HEK 293T Spike GFP1-10 clones (10B and 4G), DNA was extracted from cells, quantified, and amplified with a PCR, using Spike Forward and Spike Reverse primers. A future goal is to sort cells with an anti-Spike antibody to select cells that highly express the Spike protein and to perform final fusion tests.

The quantity and the yield of DNA was measured using a Nanodrop spectrophotometer, measuring concentration (ng/µL), $A_{260/280}$ and $A_{260/230}$. Adequate amounts of DNA were obtained for every cell line and with an

acceptable purity. $A_{260/280}$ values were around 1,8 and 2, while $A_{260/230}$ values were around 2, indicating good quality of DNA preparations (Tab. 6).

CELL LINE	DNA CONCENTRATION (ng/µL)	$A_{260/280}$	$A_{260/230}$
HEK 293T	84	1,98	2,03
HEK 293T Spike	100	1,99	1,88
HEK 293T Spike GFP1-10, clone 10B	180,8	2,08	2,25
HEK 293T Spike GFP1-10, clone 4G	88,2	1,99	2,08

Table 6: Quantification and analysis of yield of DNA by absorbance with Nanodrop Spectrophotometer.

HEK 293T cells, which do not have the Spike gene, were used as a control. HEK 293T Spike, HEK 293T Spike GFP1-10 clone 10B and HEK 293T Spike GFP1-10 clone 4G were screened for the presence of the Spike gene, whose presence has been verified in every cell line (Fig. 46). 20 µL PCR of every sample were loaded in the gel electrophoresis. pLVx Spike Wuhan plasmid (diluted 1:20.000 from the maxiprep of 3,8 µg/µl) was used as a positive control and 4 µL of its PCR were loaded.

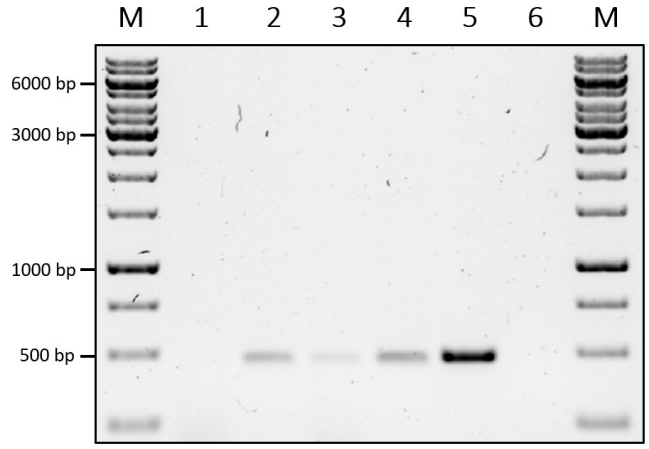

Fig. 46: Gel electrophoresis after DNA extraction and PCR to determine the presence of Spike gene in HEK 293T (1), HEK 293T Spike (2), HEK 293T Spike GFP1-10 clone 10B (3) and HEK 293T Spike GFP1-10 clone 4G (4). pLVx Spike Wuhan plasmid (5) was used as a positive control. A negative control with water was used (6). The GeneRuler 1kb Ladder (M) was used as a molecular weight marker. The expected band is 486 bp.

To verify the presence of Spike Wuhan transcript in HEK 293T Spike GFP1-10 clones, RNA was extracted from cells, quantified, reverse transcribed into cDNA, and amplified with PCR, using Spike Forward and Spike Reverse primers.

The quantity and the yield of RNA was measured using a Nanodrop spectrophotometer, measuring concentration (ng/µL), $A_{260/280}$ and $A_{260/230}$. Adequate amounts of RNA were obtained for every cell line and with an acceptable purity. $A_{260/280}$ values were all around 2, indicating good preparations of RNA (Tab. 7).

CELL LINE	RNA CONCENTRATION (ng/µL)	$A_{260/280}$	$A_{260/230}$
HEK 293T	1495,8	2,04	2,06
HEK 293T Spike	1602,4	2,05	1,93
HEK 293T Spike GFP1-10, clone 10B	69,2	1,92	0,64
HEK 293T Spike GFP1-10, clone 4G	608,9	2	1,74

Table 7: Quantification and analysis of yield of RNA by absorbance with Nanodrop Spectrophotometer.

HEK 293T cells, which do not have the Spike transcript, were used as a control. HEK 293T Spike, HEK 293T Spike GFP1-10 clone 10B and HEK 293T Spike GFP1-10 clone 4G were screened for the presence of the Spike transcript, whose presence has been verified in every cell line (Fig. 47). 5 µL PCR of every sample were loaded in the gel electrophoresis.

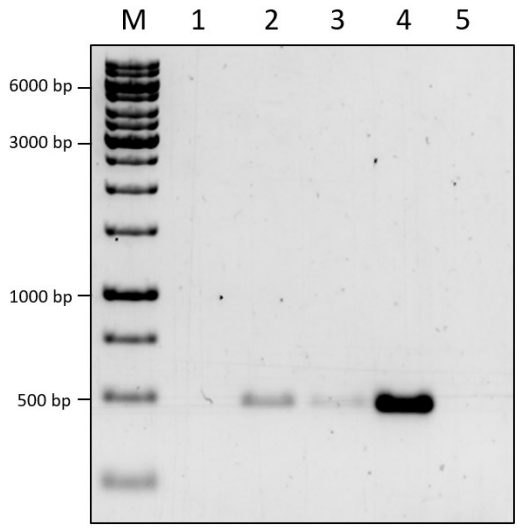

Fig. 47: Gel electrophoresis after RNA extraction, reverse transcription, and PCR to determine the presence of Spike transcript in HEK 293T (1), HEK 293T Spike (2), HEK 293T Spike GFP1-10 clone 10B (3) and HEK 293T Spike GFP1-10 clone 4G (4). A negative control with water was used (5). The GeneRuler 1kb Ladder (M) was used as a molecular weight marker. The expected band is 486 bp.

After confirming the presence of the Spike gene and transcript, pilot fusion tests have been performed with HEK 293T Spike GFP1-10 clone 4G.

4.3 Spike-ACE2 mediated fusion and subsequent GFP complementation produce a fluorescent signal after 3 hours

Pilot fusion tests were performed in a 24-well plate with HEK 293T ACE2 GFP11 and clone 4G of HEK 293T Spike GFP1-10 in different ratios to study a possible relation between the number of cells and the presence of more Spike-expressing cells than ACE2-expressing cells: $0.5x10^6$ cells/type, $1x10^6$ cells/type, and $0.5x10^6$ of HEK 293T ACE2 GFP11 mixed with $0.75\ x10^6$ HEK 293T Spike GFP1-10 (excess of Spike-expressing cells). As negative controls, we seeded $0.5x10^6$ cells of the following cell lines, without mixing them: HEK 293T ACE2 GFP11, HEK 293T Spike GFP1-10, HEK 293T GFP11, HEK 293T ACE2 GFP1-10. As a first fusion control, $0.5x10^6$ HEK 293T GFP11 (without ACE2 receptor) were mixed with $0.5x10^6$ HEK 293T Spike GFP1-10 to verify if the fusion (and then the complementation between the GFP1-10 and the GFP11) occurs in absence of ACE2 protein. A second fusion control was prepared mixing $0.5x10^6$ HEK 293T ACE2 GFP1-10 with $0.5x10^6$ HEK 293T GFP11 (without Spike protein) to verify if the fusion (and then the complementation between GFP1-10 and GFP11) occurs in absence of Spike protein.

In a previous study of cell-cell fusion performed with CD4-expressing cells and gp160-expressing cells to study HIV virion fusion with cellular membrane, syncytia formation occurred after 1-3 hours after cell mixing [25]. In this experimental study, fusion occurred at 2 to 3 hours after mixing of the appropriate cells. The green, fluorescent signal of GFP indicated that the complementation of GFP1-10 and GFP11, due to the fusion between a GFP1-10-expressing cell line and a GFP11-expressing cell line, occurred. In the fusion controls lacking, respectively, ACE2 or SARS-CoV-2 Spike, fluorescence was not detected (Fig. 48). This reveals that the binding/fusion kinetic between Spike protein and ACE2-receptor requires at least 2-3 hours in this system.

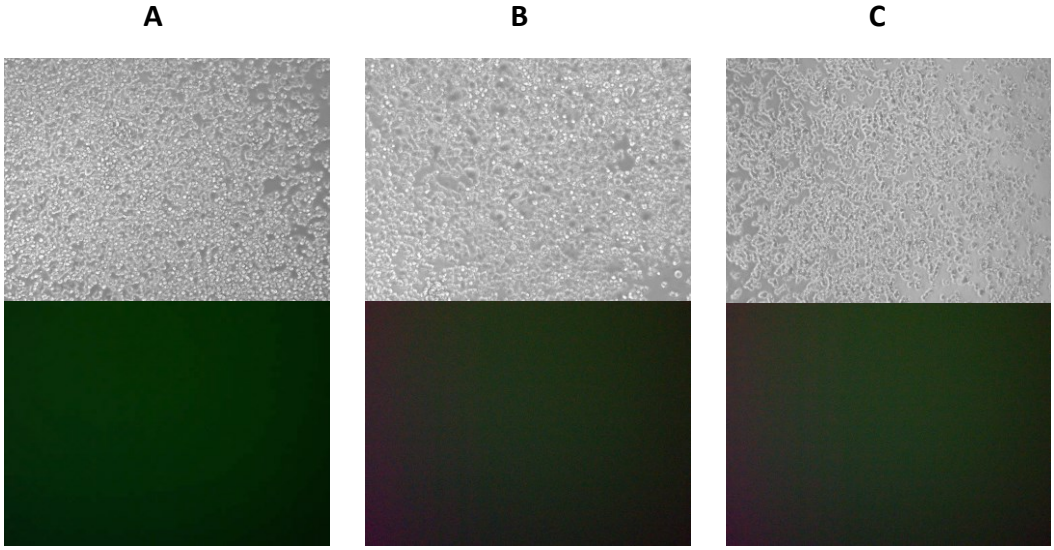

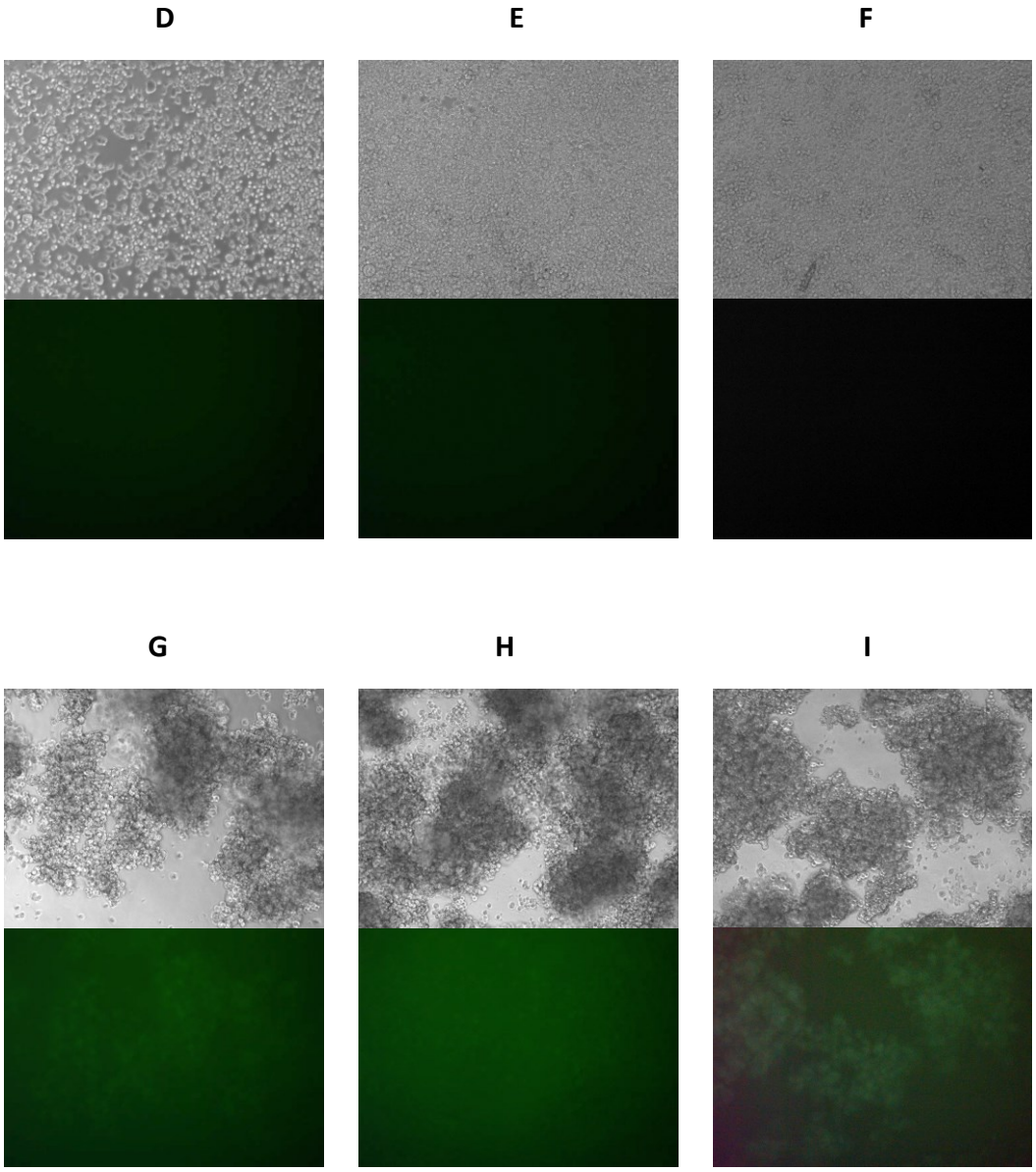

Fig. 48: Pilot fusion tests after 3 hours. Top panels are images obtained with optical microscopy, while bottom panels are images obtained with a fluorescence microscope (10X objective). Single-cell line controls ($0.5x10^6$ cells): A) HEK 293T ACE2 GFP11, B) HEK 293T Spike GFP1-10, C) HEK 293T GFP11, D) HEK 293T ACE2 GFP1-10. Fusion controls: E) $0.5x10^6$ HEK 293T GFP11 mixed with $0.5x10^6$ HEK 293T Spike GFP1-10, F) $0.5x10^6$ HEK 293T ACE2 GFP1-10 mixed with $0.5x10^6$ HEK 293T GFP11. Fusion tests: G) $0.5x10^6$ HEK 293T ACE2 GFP11 cells mixed with $0.5x10^6$ HEK 293T Spike GFP1-10, H) $1x10^6$ cells HEK 293T ACE2 GFP11 cells mixed with 1 $X10^6$ HEK 293T Spike GFP1-10, I) $0.5x10^6$ HEK 293T ACE2 GFP11 cells mixed with 0.75 $x10^6$ HEK 293T Spike GFP1-10.

The peak of GFP intensity was observed after 4-5 hours by fluorescence microscopy (Fig. 49). Fluorescence seemed to be comparable in the two fusion

conditions with $0.5x10^6$ cells/type and $0.5x10^6$ ACE2-expressing cells - $0.75 x10^6$ Spike-expressing cells, while in the fusion condition with $1X10^6$ cells/type a high background signal was observed, and we hypothesized that this was probably due to the elevated number of cells in the well. The relation between number of cells and fusion efficiency has to be further studied because successful fusion can depend on different factors such as membrane fluidity, adhesion components and surface changes [36].

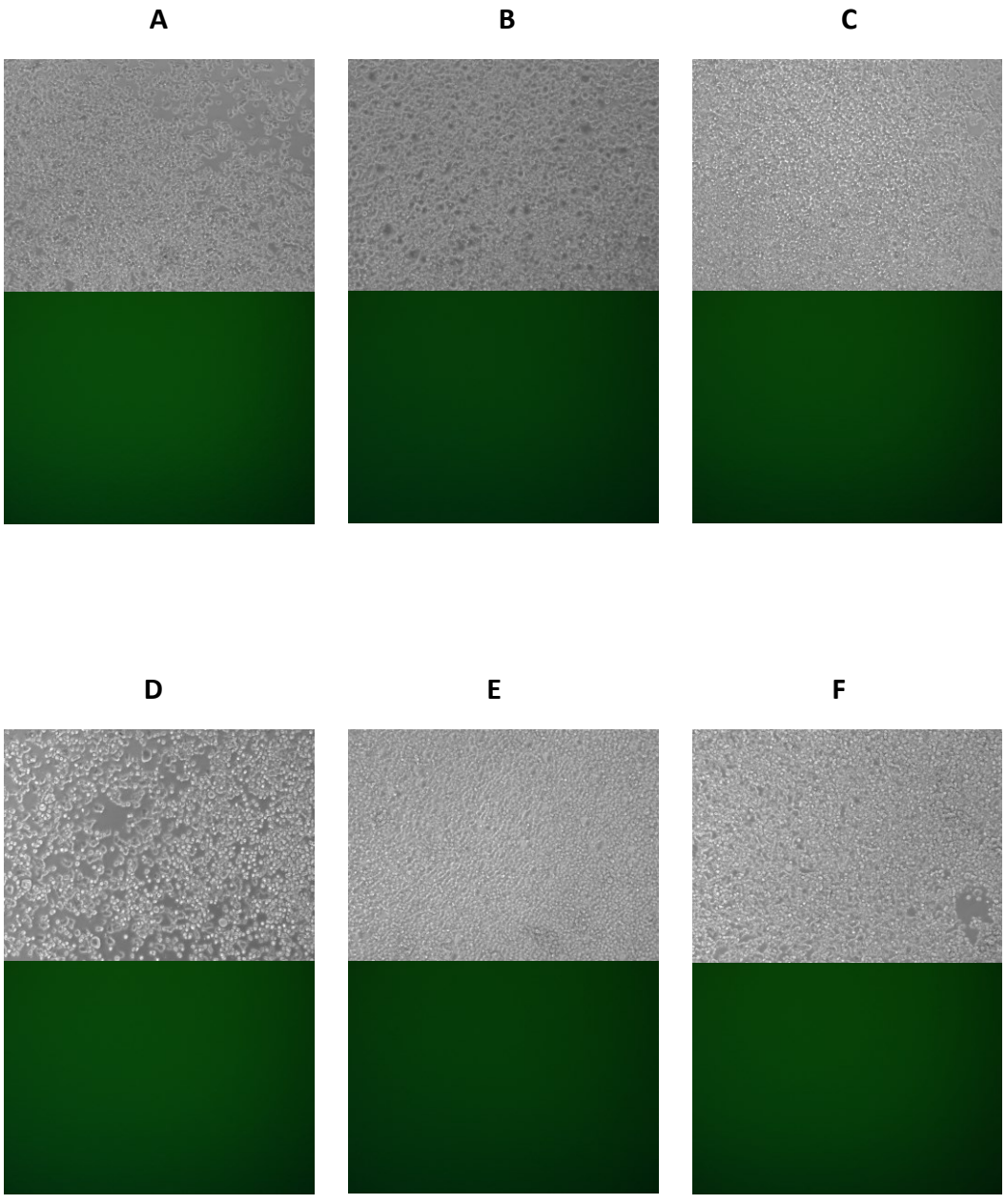

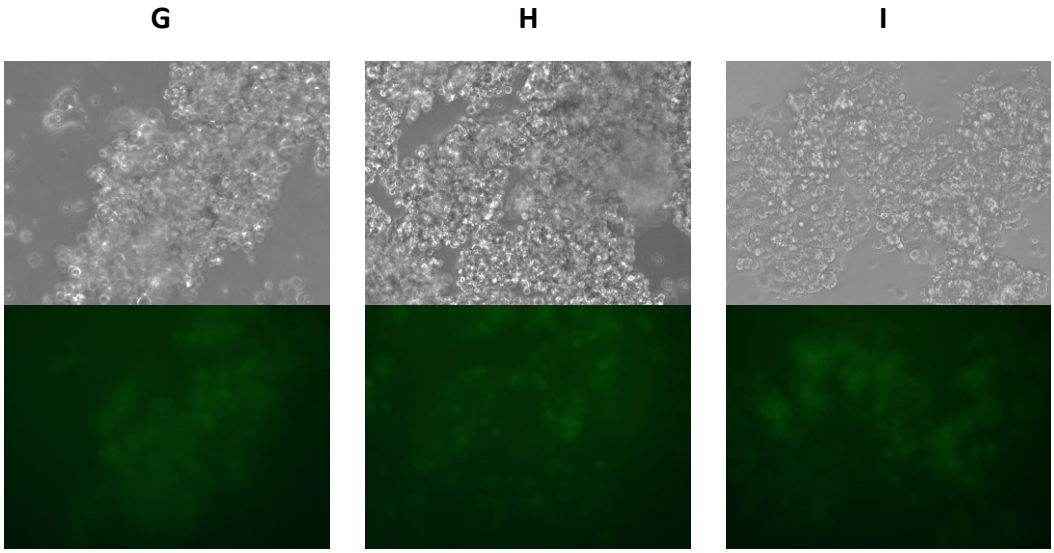

Fig. 49: Pilot fusion tests after 5 hours. Top panels are images obtained with optical microscope, while bottom panels are images obtained with a fluorescence microscope (10X objective for controls, 20X objective for fusion tests). Single-cell line controls ($0.5x10^6$ cells): A) HEK 293T ACE2 GFP11, B) HEK 293T Spike GFP1-10, C) HEK 293T GFP11, D) HEK 293T ACE2 GFP1-10. Fusion controls: E) $0.5x10^6$ HEK 293T GFP11 mixed with $0.5x10^6$ HEK 293T Spike GFP1-10, F) $0.5x10^6$ HEK 293T ACE2 GFP1-10 mixed with $0.5x10^6$ HEK 293T GFP11. Fusion tests: G) $0.5x10^6$ cells/type. H) $1X10^6$ cells/type. I) $0.5x10^6$ HEK 293T ACE2 GFP11 mixed with 1 $X10^6$ clone 4G of HEK 293T Spike GFP1-10.

Controls remained negative at all time points. After 24 hours, a labile fluorescent signal was revealed also in small number of cells of the fusion control lacking ACE2, between HEK 293T GFP11 and HEK 293T Spike GFP1-10. This signal could be due to the fusogenicity of the Spike protein in the absence of ACE2-receptor. A recent study has demonstrated that Spike-expressing HEK 293T cells can rarely lead to an ACE2-independent membrane fusion in a small proportion of neighbouring cells [35]. In alternative, this could also be related with cell death, that could cause GFP1-10 and GFP11 to be released out of the cell and then complement extracellularly to generate the entire GFP. Another possibility is that autofluorescence of cells, enhanced by the phenol-red containing culture medium, could contribute to the spurious fluorescence signal we observed. To optimize the system, a medium with a reduced percentage of phenol red, such as FluoroBrite™ DMEM, could be used in the next experiments. Furthermore, to avoid background detection, we selected a window of 2-7 hours after cell mixing to study cell-cell fusion by fluorescence microscopy.

In fusion tests, we used a high number of cells to promote contacts between cells, Spike-ACE2 binding and the subsequent fusion. Fused cells seemed to be aggregated, multinucleated, with a granular aspect, and tightly associated in clumps (Fig. 50).

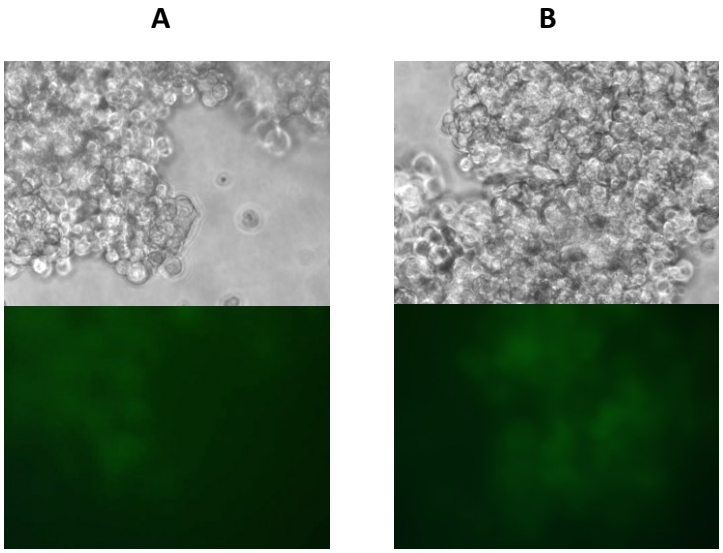

Fig. 50: A) Pilot fusion tests with $0.5x10^6$ HEK 293T ACE2 GFP11 and $0.5x10^6$ HEK 293T Spike GFP1-10. Top panels are images obtained with optical microscope, while bottom panels are images obtained with a fluorescence microscope (objective 40X).

4.4 Analysis by flow cytometry reveals that fused, green, fluorescent cells have the biggest dimension and internal complexity

The large size and granularity of cells after pilot fusion tests were also detected with flow cytometry, which showed the presence of distinct cell subpopulations in relation to GFP signal, cell dimension, and cell granularity. Cells were prepared for flow cytometry analysis with the protocol for GFP-expressing cells, and FL-1 signal was detected in $1X10^4$ events.

While in controls we observed only a population of cells, in fusion experiments the population of cells can be divided into 4 subpopulations, which we defined as R0-4 (Figure 51 C), with different characteristics of granularity, dimension and GFP signal (FL1-H signal). The R0 subpopulation is characterized by small dimension of cells and little granularity; the R1 subpopulation is characterized by high dimension of cells and little granularity; the R2 subpopulation is characterized by high dimension of cells and high granularity, correlated with a higher signal of fluorescence than other cells; the R3 subpopulation is characterized by small dimension of cells and high granularity (Fig. 51 C). Cells with the highest surface area/size and granularity had the highest GFP signal (FL1-H signal) (Fig. 51 D and E). In fusion controls, in which HEK 293T GFP11 and HEK 293T Spike GFP1-10 or HEK 293T ACE2 GFP11 and HEK 293T GFP1-10 were mixed cells have a small size and a reduced granularity/internal complexity (Fig. 51 A, B).

A) Fusion control: HEK 293T GFP11 and HEK 293T Spike GFP1-10

B) Fusion control: HEK 293T ACE2 GFP11 and HEK 293T GFP1-10

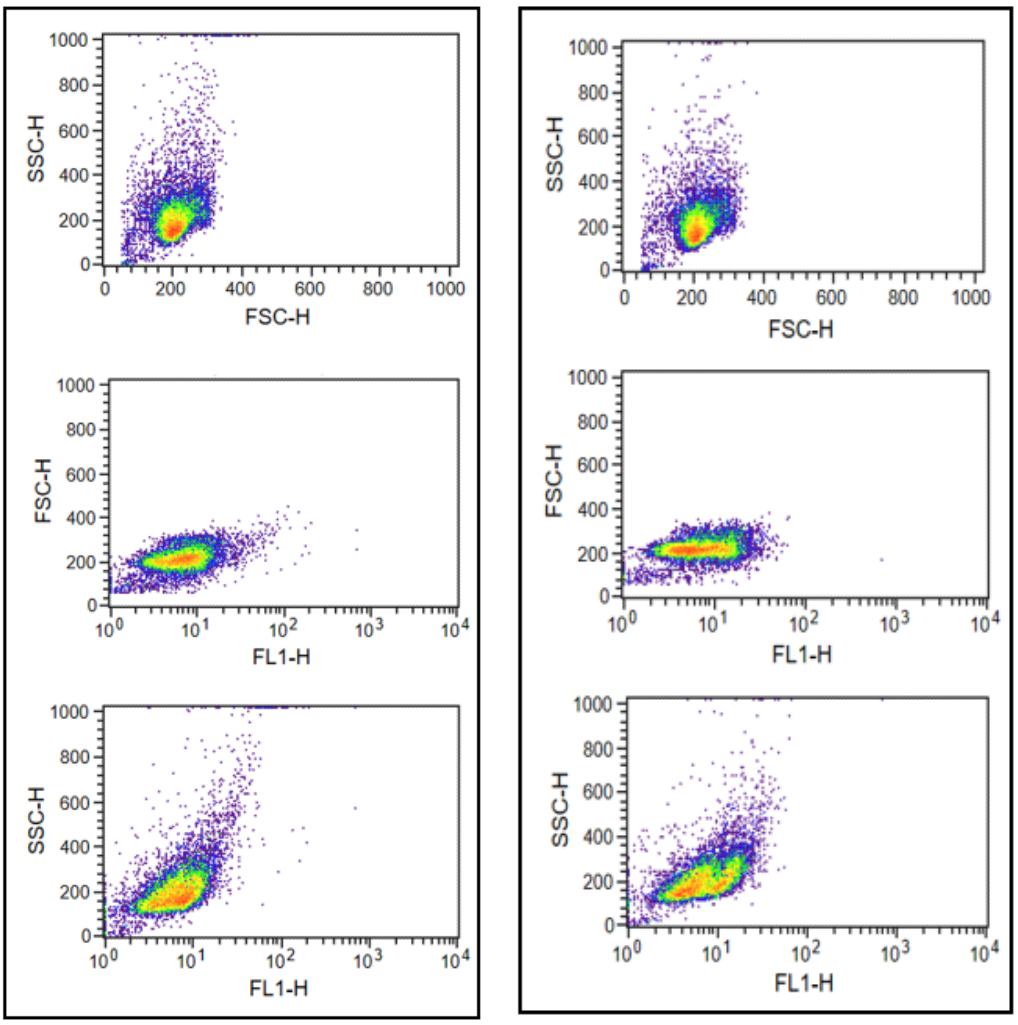

C

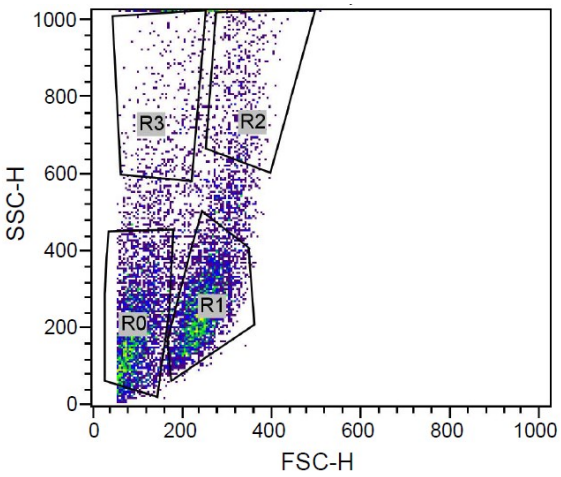

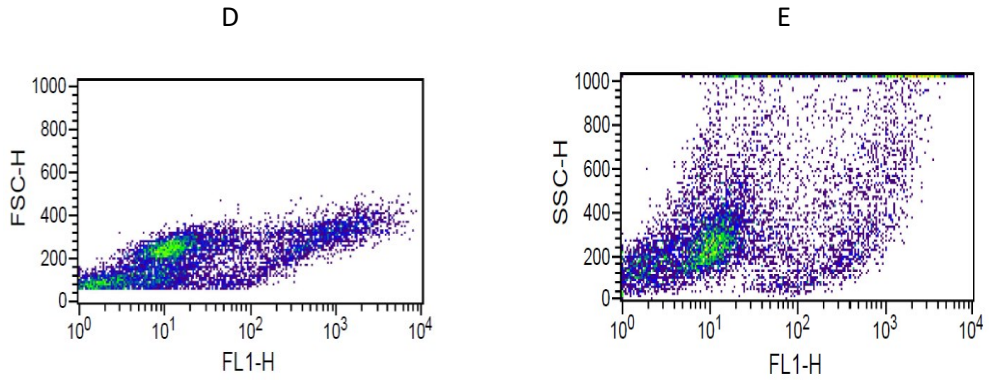

Fig. 51: Density plots of fusion controls and fusion tests: colours show cell density. A, B) Density plots of fusion controls in which HEK 293T GFP11 were mixed with HEK 293T Spike GFP1-10, and in which HEK 293T ACE2 GFP11 were mixed with HEK 293T GFP1-10, respectively: in the first plot the FSC-H is shown on the x axis, plotted against the SSC-A on the y axis; in the second plot the FL1-H is shown on the x axis, plotted against the FSC-H on the y axis; in the third plot the FL1-H is shown on the x axis, plotted against the SSC-H on the y axis. A relation between dimension and fluorescence signal, and a relation between granularity and fluorescence signal are not shown in fusion controls. C, D, E) Density plots of fusion test between HEK 293T ACE2 GFP11 and HEK 293T Spike GFP1-10. C) Selection of cells of interest of four distinct subpopulations (R0, R1, R2 and R3). The FSC is shown on the x axis, plotted against the SSC-A on the y axis. D) The FL1-H is shown on the x axis, plotted against the FSC-H on the y axis. E) The FL1-H is shown on the x axis, plotted against the SSC-H on the y axis.

When analysing fluorescent signal (FL1-H) in relation to event count in fusion tests, we observed a subpopulation of cells with a high fluorescent signal (high FL1-H) visible in the right part of the histogram (Fig. 52 G). On the contrary, analysing fluorescent signal (FL1-H) in relation to event count in all negative controls, we observed a single population with low signal (Fig. 52 A, B, C, D, E, F).

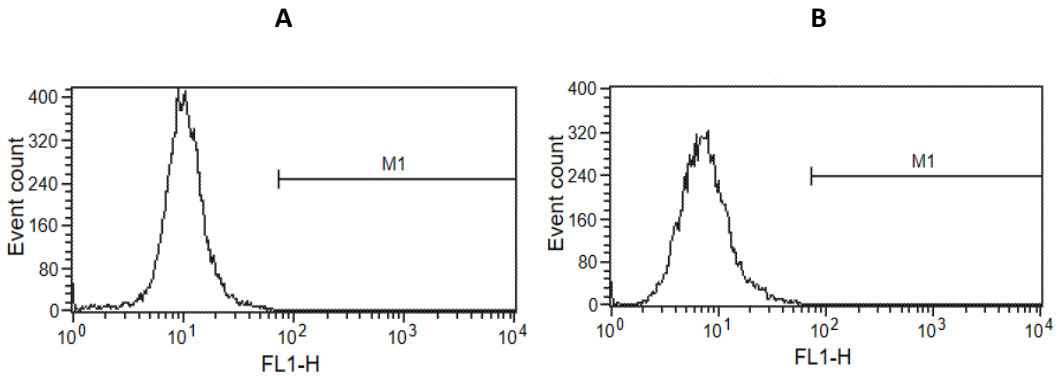

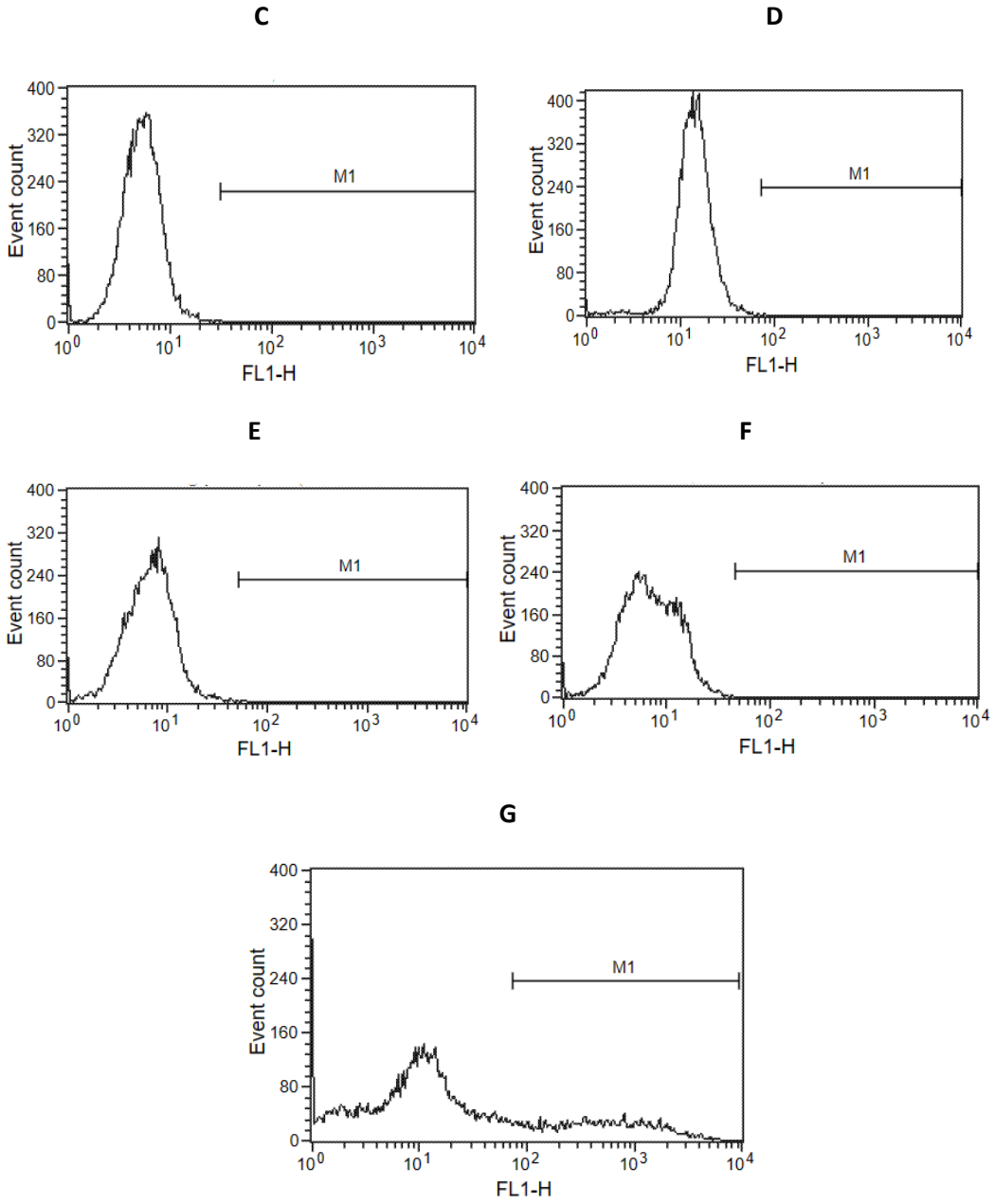

Fig. 52: Histograms of controls and fusion test. The FL1-H is shown on the x axis, plotted against event count on the y axis. A) HEK 293T Spike GFP1-10, B) HEK 293T ACE2 GFP11, C) HEK 293T GFP11, D) HEK 293T ACE2 GFP1-10, E) HEK 293T GFP11 mixed with HEK 293T Spike GFP1-10, F) HEK 293T GFP11 mixed with HEK 293T ACE2 GFP1-10, G) Fusion test with HEK 293T ACE2 GFP11 mixed with HEK 293T Spike GFP1-10.

The four subpopulations of fusion test (R0, R1, R2 and R3) were analysed with histograms to determine their main cellular characteristics. The R2 subpopulation is likely composed of fused, green, fluorescent cells with a high signal of FL1-H. There are some peaks in the x axis between 10^3 and 10^4, that have the highest FL1-H values respect other subpopulations (Fig. 53). A peak of FL1-H signal is also visible in the histogram of R1 subpopulation between 10^2 and 10^3 indicating that also these cells have a significant GFP signal.

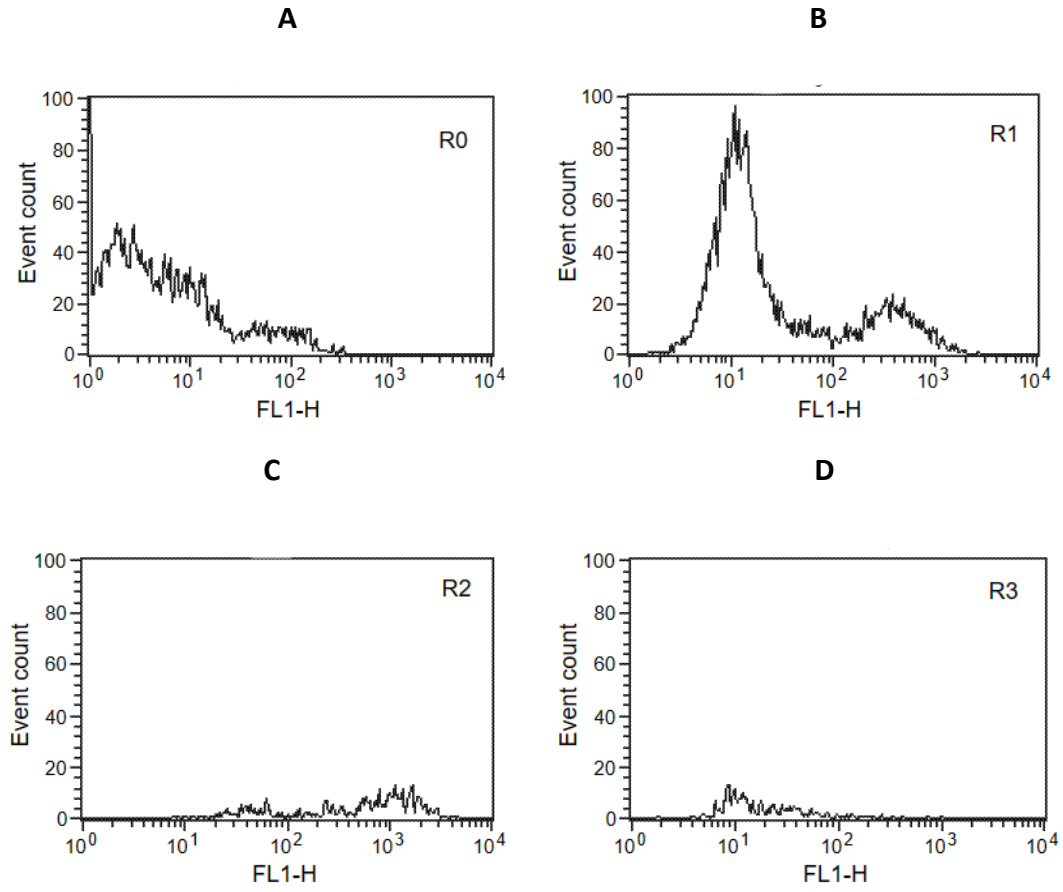

Fig. 53: Histograms of the four subpopulations of fusion test between HEK 293T ACE2 GFP11 and HEK 293T Spike GFP1-10: A) R0, B) R1, C) R2 and D) R3. The FL1-H is shown on the x axis, plotted against event count on the y axis.

Collectively, flow cytometry data and fluorescent microscopy had shown that fused cells have a green, fluorescent signal due to the complementation between the GFP1-10 and the GFP11 to form the entire GFP. Furthermore, fusion, as it may be expected, results in cells of bigger size and internal complexity.

4.5 Analysis of the pilot cell-cell fusion system efficiency and reproducibility through detection of Fluorescence Intensity

To verify the functionality of the pilot cell-cell-fusion system, fusion tests were quantitatively analysed by Varioskan, detecting GFP fluorescence intensity at time points over 27 hours. We observed a visible increase in fluorescent signal between 22-27 hours after mixing $8{,}3x10^4$ of each HEK 293T ACE2 GFP11 and HEK 293T Spike GFP1-10 (clone 4G) cells/well. In fusion controls, in which we mixed $8{,}3x10^4$ of each HEK 293T GFP11 (cells lacking ACE2 receptor) and HEK 293T Spike GFP1-10 cells/well, the fluorescent signal remained stable, at values comparable to these measured at t=0, at all time points. Fluorescent intensity (RFU) was detected

for every triplicate of the experiment, the mean of the three measurements and the standard deviations were calculated and plotted (Fig. 54). The mean of the fluorescence intensity of the fusion test detected at the first time point, i.e at time of mixing, was 0,2918, increasing up to 0,6130 at 27 hours. The mean of the fluorescence intensity of the fusion control at the same time points was 0,3249 at time of mixing, and 0,3015 27 hours post-mixing. These data are consistent with the assumption that in absence of ACE2 receptor the fusion with cells expressing SARS-CoV-2 Spike does not occur, as this signal is comparable to that measured in the wells containing only Opti-MEM (Fig. 54).

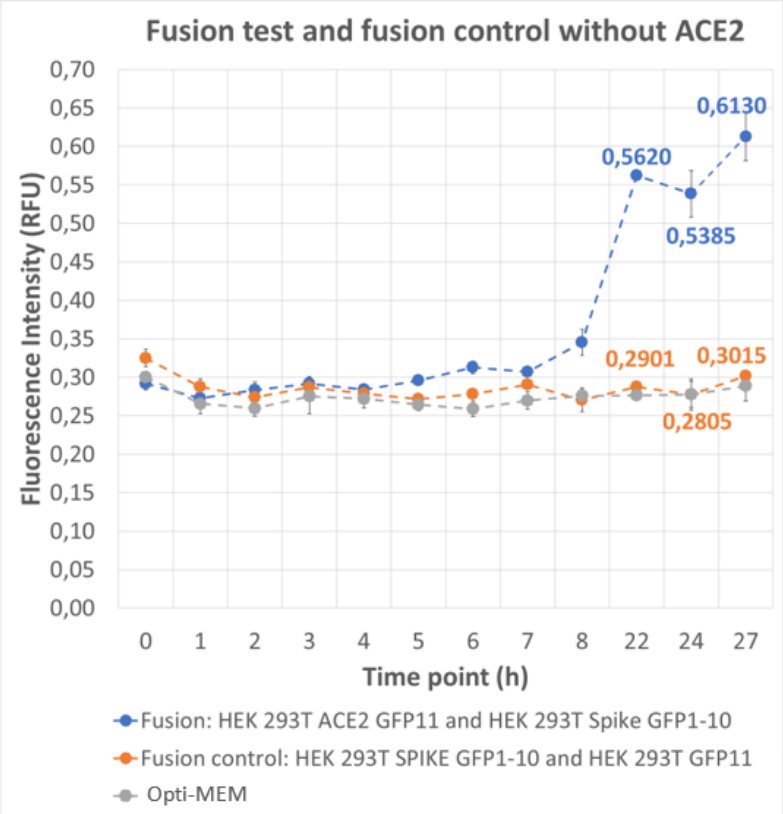

Fig. 54: Graph with fusion test, fusion control, and Opti-MEM fluorescence intensity, monitored for 27 hours with Varioskan LUX, using SkanIt Software 6.1. In this case cells have been mixed in the well. The time point (h) is shown on the x axis (the axis is not drawn to scale), plotted against fluorescence intensity (RFU) on the y axis. After 22 hours, an increase in fluorescence intensity can be seen in the fusion test (blue dots), while the fusion control (orange dots) and the background of Opti-MEM (grey dots) remain stable in time. Data are represented as means of a triplicate. Errors bars indicate ± Standard Deviation of the three measurements. Two-tailed Wilcoxon test, with 95% of confidence interval, was used to evaluate differences between the means of the fusion test and the means of controls.

The single cell lines controls have shown a stable fluorescent intensity during all the time points. The mean of the fluorescence intensity of HEK 293T ACE2 GFP11 detected at the first time point was 0,3012, and at the final time point was 0,2798; the value of HEK 293T Spike GFP1-10 detected at the first time point was 0,3053 and the final value 0,2781; the initial value of HEK 293T GFP11 was 0,3115 and the final value 0,3035. Collectively, these results have shown that the single cell lines were all GFP-negative (Fig. 55).

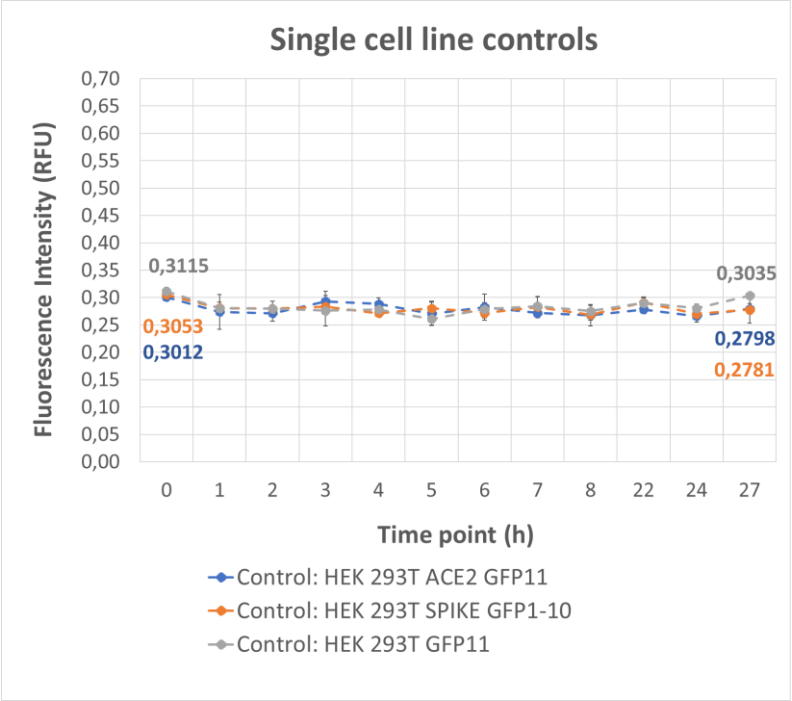

Fig. 55: Graph with the fluorescence intensity of single cell line controls, monitored for 27 hours with Varioskan LUX, using SkanIt Software 6.1. The time point (h) is shown on the x axis (the axis is not drawn to scale), plotted against fluorescence intensity (RFU) on the y axis. All controls remain stable in time. Data are represented as means of a triplicate. Errors bars indicate ± Standard Deviation of the three measurements.

Another pilot cell-cell fusion test was performed and analysed with Varioskan at different time points for 48 hours. In this case, HEK 293T ACE2 GFP11 and HEK 293T Spike GFP1-10 were not mixed in the well, but they were centrifuged together at 900 rpm for 5 minutes, which may have facilitated the binding between the Spike and the ACE2. Also in this test, we observed a considerable increase in fluorescence intensity in cell-cell fusion wells after 22-27 hours. Furthermore, the initial fluorescent intensity at time of mixing was 0,3513, increasing up to 0,8770 at 48 hours. A stable fluorescent intensity, comparable to that of cells at the time of initial mixing, was observed in all controls (Fig. 56).

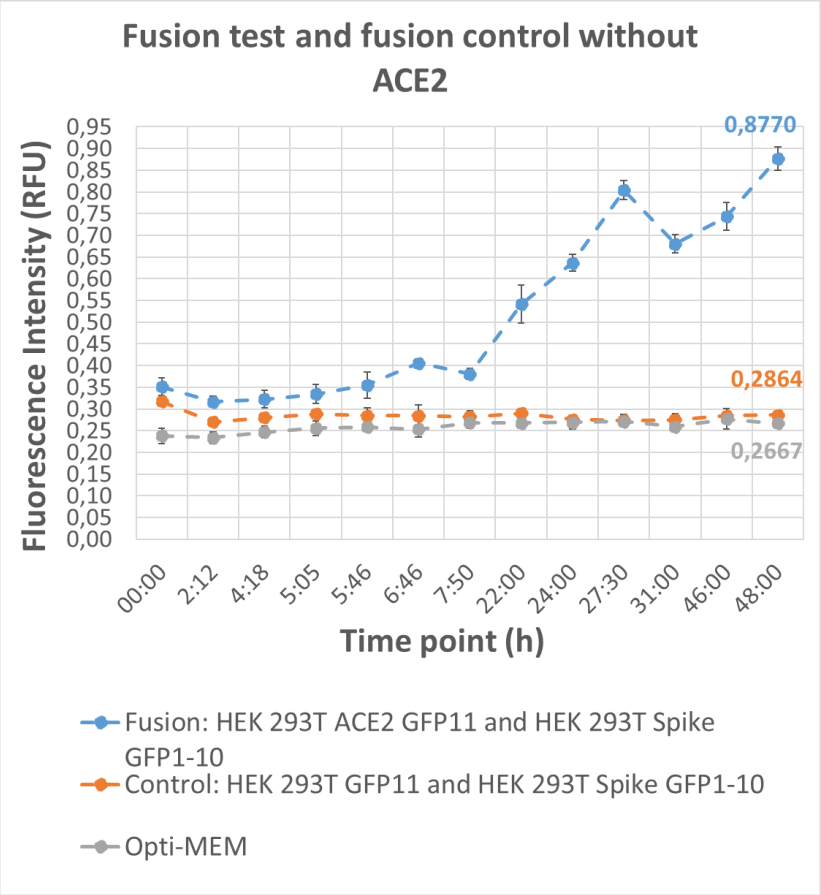

Fig. 56: Graph with fusion test, fusion control, and Opti-MEM fluorescence intensity, monitored for 48 hours with Varioskan LUX, using SkanIt Software 6.1. In this case cells have been mixed before centrifugation. The time point (h) is shown on the x axis (the axis is not drawn to scale), plotted against fluorescence intensity (RFU) on the y axis. After 22 hours an increase in fluorescence intensity can be seen in the fusion test (blue dots), while the fusion control (orange dots) and the background of Opti-MEM (grey dots) are stable in time. Data are represented as means of a triplicate. Errors bars indicate ± Standard Deviation of the three measurements. Two-tailed Wilcoxon test, with 95% of confidence interval, was used to evaluate differences between the means of the fusion test and the means of controls.

Collectively, the results of the two experiments have demonstrated the reproducibility of the pilot cell-cell fusion system because the fluorescence intensity has increased only in the fusion test. In the next step of optimization, it is important to consider the optimal range of time for highest signal-to-noise ratio, as the fluorescence signal increases significantly between 24 and 48 hours post-mixing, as shown by the two experiments. Furthermore, it is essential to further address the optimal condition of mixing the two partner cells, promoting the fusion and then the complementation of the GFP.

5. DISCUSSION

Cell-cell fusion systems have been developed in virology, and adapted to study several viruses, like in the case of HIV-induced fusion mediated by the binding between gp120, which is the HIV envelope glycoprotein, and CD4, which is the human host receptor [25], [26]. The same method has been used in this experimental study, developing a cell line expressing the viral protein and a cell line expressing the host cell receptor through transduction with lentiviral vectors. Since it is well known that the SARS-CoV-2 Spike protein binds to the human ACE2 receptor to induce the fusion between the viral and the cell membrane, a cellular system based on the binding between these two proteins can be easily generated. The aim of this experimental study was to develop a pilot cell-cell fusion system based on the split-GFP. The principle behind this system is that GFP can be made into a split protein into two subunits, i.e., one with the β sheets 1-10, and the other with the 11^{th} β sheet. The two subunits can be expressed in two separate cell lines that also express either the viral protein Spike or its receptor ACE2. When the fusion occurs due to the binding between the Spike and the ACE2 receptor, the signal of the complemented GFP can be easily detected by fluorescence microscopy, flow cytometry or plate readers.

After generating stable cell lines and verifying the presence of the proteins of interest, syncytia formation was thoroughly evaluated by fluorescence microscopy and flow cytometry. Flow cytometry analysis revealed that fused, green, fluorescent cells have shown increased size and internal complexity. The pilot fusion test has revealed that, when HEK 293T ACE2 GFP11 and HEK 293T Spike GFP1-10 are co-cultured, they can fuse due to the recognition between the SARS-CoV-2 Spike and the human ACE2 receptor, leading to a fluorescent signal visible in fluorescence microscopy after 3 hours. The assay can be easily performed because the two types of cells require simple mixing, without the need of lysing the cells. Furthermore, analysing fusion test with a fluorescence plate reader, we verified the increase in fluorescence intensity, especially 22-27 hours after mixing the two partner cells. Therefore, the current vision of the entry-fusion system requires about 24 hours to develop a signal statistically different from the negative controls. A further characterization and optimization of the system could be performed in real-time with a confocal microscope and a plate reader where cells can be kept at 37°C and in an atmosphere of 5% CO_2 and 95% humidity.

The next step is to validate the system with neutralizing antibodies that have a known activity against the Spike or the ACE2 receptor and using antibodies that do not have an effect (like an anti-vinculin antibody or an anti-GAPDH) as negative controls. Moreover, another future goal is to create a dose-response curve with neutralizing antibodies quantifying the fluorescence intensity signal. This cell-cell fusion system would allow high-throughput screening drugs libraries for inhibitors of Spike-ACE2 binding in a short time. It is important to develop this type of system

to screen antiviral drugs in an easy and fast way. In effect, current therapeutic efforts to reduce COVID-19 morbidity and mortality include neutralizing antibodies, peptides, aptamers, and small molecules, that are mostly in the preclinical or clinical phase [30] and that have the need to be screen in a rapid way to make them available for patients.

In conclusion, this cell-cell fusion system can be adapted for every virus that uses ACE2 as the entry receptor (like SARS-CoV), and potentially for every enveloped-virus that uses membrane fusion process to enter host cells: to set the system is sufficient to produce a cell line expressing the viral protein and a cell line expressing the host receptor, in addition to control cell lines. It would be easy and rapid to do that because, in addition to final cell lines for fusion test and fusion controls, we have also generated basic cell lines, like HEK 293T GFP1-10 and HEK 293T GFP11, that can be used for future implementation of the system. In this way, we could screen therapeutics, against different viruses, that target the fusion between the viral and the host cell membrane.

6. RIASSUNTO

Il virus SARS-CoV-2 (Severe Acute Respiratory Syndrome Coronavirus 2), appartenente alla famiglia dei *Coronaviridae* e al genere dei *Betacoronavirus,* è l'agente eziologico della malattia da COVID-19. Il virus si trasmette per via aerea e può causare sintomi quali tosse secca, febbre, stanchezza. Mentre negli individui che sono stati precedentemente infettati o vaccinati contro il virus SARS-CoV-2 si osserva una forte diminuzione dei casi di sindrome respiratoria severa e della mortalità dovuta a COVID-19, negli individui non infettati e/o non vaccinati, e nei soggetti immunocompromessi o anziani, il virus può causare manifestazioni severe a livello di organi vitali che possono portare anche alla morte.

Il genoma di SARS-CoV-2 è un genoma a polarità positiva a singolo filamento (+ssRNA) che codifica 16 non-structural proteins (nsps), le quattro proteine strutturali e proteine accessorie. La particella virale è caratterizzata da quattro proteine: la proteina Spike (S), la proteina dell'envelope (E), la proteina del nucleocapside (N) e la proteina di membrana (M). La proteina Spike è fondamentale nel processo di ingresso del virus nella cellula ospite, in quanto è implicata nel riconoscimento del recettore ACE2 (Angiotensin-converting like enzyme 2), presente in maniera quasi ubiquitaria nelle cellule umane, e nella fusione tra la membrana virale e la membrana cellulare.

Dalla sua origine fino ad oggi, il virus del SARS-CoV-2 si è diffuso in tutto il mondo e ha acquisito numerose mutazioni, dando origine a diverse varianti, comprese le cosiddette VOC (Variants Of Concern), fino alle odierne varianti del lignaggio Omicron e le loro ricombinanti. Malgrado l'immunità da infezione naturale e/o in seguito a vaccinazione proteggano da sintomi gravi e mortalità, le popolazioni vulnerabili sopracitate sono ancora ad alto rischio di complicazioni da COVID-19. È per questo essenziale continuare a studiare e sviluppare nuovi approcci terapeutici contro il SARS-CoV-2. Di particolare interesse sono i farmaci antivirali che hanno come target il riconoscimento tra la proteina Spike del SARS-CoV-2 e il recettore umano ACE2, perché vanno a inibire il primo step di ingresso del virus nella cellula dell'ospite e perché il loro target è facilmente accessibile dallo spazio extracellulare. Soltanto poche molecole antivirali contro l'ingresso-fusione sono state sviluppate e la maggior parte di esse sono ancora allo stadio preclinico.

Lo scopo dello studio sperimentale è quello di sviluppare un sistema di fusione cellulare basato sulla complementazione della proteina GFP (Green Fluorescent Protein) per lo screening di nuovi farmaci che hanno come target il legame tra la proteina Spike e il recettore ACE2. Il sistema è caratterizzato dalla presenza di una linea cellulare esprimente la proteina Spike del SARS-CoV-2 e la GFP1-10 (porzione della GFP dal residuo 1 al 215, comprendente i foglietti β dall'1 al 10) e dalla presenza di un'altra linea cellulare esprimente il recettore umano ACE2 e la GFP11 (porzione della GFP dal residuo 216 al 230, comprendente l'undicesimo foglietto

β). Quando sono separate spazialmente, nessuna subunità della GFP è fluorescente, quando invece sono vicine tra loro possono spontaneamente riassemblarsi a dare la proteina GFP fluorescente. Quando le due linee cellulari sono mescolate assieme, avviene il riconoscimento tra la proteina Spike e il recettore ACE2 e la successiva fusione cellulare, e questo porta all'avvicinamento della GFP1-10 e della GFP11 e alla loro complementazione. Il risultato della fusione è quindi un segnale fluorescente che è facilmente rilevabile alla microscopia a fluorescenza o su lettore di piastre a fluorescenza. In presenza di farmaci antivirali che inibiscono la Spike, l'ACE2 o la loro interazione, non si avrà fusione cellulare e quindi la GFP1-10 e la GFP11 non saranno in grado di complementarsi, di conseguenza non si avrà nessun segnale di fluorescenza o si avrà una sua diminuzione significativa.

Il primo passo per la generazione del sistema di fusione cellulare consiste nella produzione dei vettori lentivirali esprimenti la GFP1-10, la GFP11 o la Spike Wuhan, tramite il Lenti-X Packaging Single Shots Protocol, che prevede di trasfettare le cellule HEK 293T con una miscela costituita dal plasmide pLVx (backbone) contenente il gene di interesse e da plasmidi essenziali per la sintesi del virione maturo. Le cellule HEK 293T ed HEK 293T ACE2 sono poi state trasdotte con i vettori lentivirali prodotti, per ottenere le seguenti linee cellulari: HEK 293T GFP11, HEK 293T GFP1-10, HEK 293T ACE2 GFP11, HEK 293T ACE2 GFP1-10, HEK 293T SPIKE GFP11 ed HEK 293T Spike GFP1-10. Per verificare l'avvenuta trasduzione con il plasmide esprimente la GFP1-10 o la GFP11, le cellule sono state trasfettate transientemente con un plasmide esprimente la controparte della GFP e monitorate tramite microscopia a fluorescenza e citometria a flusso. In seguito a trasfezione transiente, le cellule sono state sottoposte a FACS (Fluorescence-Activated Cell Sorting) per selezionare le cellule con il segnale più elevato di GFP. Dopo il sorting, le cellule sono state clonate effettuando una diluzione limite, ed è stato selezionato un singolo clone per linea cellulare. In assenza di un anticorpo contro la Spike efficiente per il sorting, le cellule che erano state precedentemente trasdotte con un vettore lentivirale esprimente la Spike Wuhan sono state testate per la presenza del gene della Spike tramite una PCR su DNA, tecnica che ha rivelato la presenza effettiva del gene. Dalle stesse cellule è stata anche effettuata l'estrazione dell'RNA, la sua retrotrascrizione in cDNA tramite la RT-PCR (Reverse Transcription Polymerase Chain Reaction) e poi è stata eseguita una PCR sul cDNA, dimostrando la presenza del trascritto della Spike. Dopo aver ottenuto le linee cellulari di interesse, è stato effettuato un test di fusione pilota. Il saggio è stato eseguito in una MW24 mescolando tra loro le due linee cellulari HEK 293T ACE2 GFP11 ed HEK 293T Spike GFP1-10 in diverse quantità: $0.5x10^6$ cellule/tipo, $1X10^6$ cellule/tipo, $0.5x10^6$ HEK 293T ACE2 GFP11 e $0.75 x10^6$ HEK 293T Spike GFP1-10 (eccesso di cellule esprimenti la Spike). Come controlli negativi sono stati utilizzati i seguenti: $0.5x10^6$ HEK 293T ACE2 GFP11, $0.5x10^6$ HEK 293T Spike GFP1-10, $0.5x10^6$ HEK 293T GFP11, $0.5x10^6$ HEK 293T ACE2 GFP1-10, $0.5x10^6$ HEK 293T

GFP11 mescolate con $0.5x10^6$ HEK 293T Spike GFP1-10 (controllo senza il recettore ACE2), e $0.5x10^6$ HEK 293T ACE2 GFP1-10 mescolate con $0.5x10^6$ HEK 293T GFP11 (controllo senza la proteina Spike). La fluorescenza è stata monitorata per 24 ore tramite microscopia a fluorescenza e il segnale fluorescente nelle cellule in fusione è stato visualizzato dopo 3 ore dall'inizio del test, con un picco dopo le 4-5 ore. Le cellule del test di fusione sono state inoltre analizzate tramite citometria a flusso, rivelando che le cellule fuse, che presentano un segnale di fluorescenza (FL1-H) più elevato, sono caratterizzate da una dimensione e granularità maggiore rispetto alle cellule non fuse. Per avere una prima conferma dell'efficienza e della riproducibilità del sistema, il test di fusione è stato analizzato tramite un lettore di piastre a fluorescenza, che ha rivelato un segnale di intensità di fluorescenza significativamente differente tra le cellule in fusione e le cellule di controllo.
Il sistema, una volta ottimizzato e validato con anticorpi neutralizzanti contro la Spike o l'ACE2, potrà essere utilizzato per lo screening di farmaci che hanno come target l'ingresso-fusione del virus nella cellula ospite.

7. BIBLIOGRAPHY

[1] D. Singh and S. V. Yi, “On the origin and evolution of SARS-CoV-2,” *Experimental and Molecular Medicine*, vol. 53, no. 4. Springer Nature, pp. 537–547, Apr. 01, 2021. doi: 10.1038/s12276-021-00604-z.

[2] P. V’kovski, A. Kratzel, S. Steiner, H. Stalder, and V. Thiel, “Coronavirus biology and replication: implications for SARS-CoV-2,” *Nature Reviews Microbiology*, vol. 19, no. 3. Nature Research, pp. 155–170, Mar. 01, 2021. doi: 10.1038/s41579-020-00468-6.

[3] B. Hu, H. Guo, P. Zhou, and Z. L. Shi, “Characteristics of SARS-CoV-2 and COVID-19,” *Nature Reviews Microbiology*, vol. 19, no. 3. Nature Research, pp. 141–154, Mar. 01, 2021. doi: 10.1038/s41579-020-00459-7.

[4] R. Chilamakuri and S. Agarwal, “Covid-19: Characteristics and therapeutics,” *Cells*, vol. 10, no. 2, pp. 1–29, Feb. 2021, doi: 10.3390/cells10020206.

[5] M. Ruiz-Aravena *et al.*, “Ecology, evolution and spillover of coronaviruses from bats,” *Nature Reviews Microbiology*, vol. 20, no. 5. Nature Research, pp. 299–314, May 01, 2022. doi: 10.1038/s41579-021-00652-2.

[6] A. C. Brant, W. Tian, V. Majerciak, W. Yang, and Z. M. Zheng, “SARS-CoV-2: from its discovery to genome structure, transcription, and replication,” *Cell and Bioscience*, vol. 11, no. 1. BioMed Central Ltd, Dec. 01, 2021. doi: 10.1186/s13578-021-00643-z.

[7] I. Jungreis *et al.*, “Conflicting and ambiguous names of overlapping ORFs in the SARS-CoV-2 genome: A homology-based resolution,” *Virology*, vol. 558, pp. 145–151, Jun. 2021, doi: 10.1016/j.virol.2021.02.013.

[8] Y. Cao *et al.*, “Characterization of the SARS-CoV-2 E Protein: Sequence, Structure, Viroporin, and Inhibitors,” *Protein Science*, vol. 30, no. 6. John Wiley and Sons Inc, pp. 1114–1130, Jun. 01, 2021. doi: 10.1002/pro.4075.

[9] M. Takeda, “Proteolytic activation of SARS-CoV-2 spike protein,” *Microbiology and Immunology*, vol. 66, no. 1. John Wiley and Sons Inc, pp. 15–23, Jan. 01, 2022. doi: 10.1111/1348-0421.12945.

[10] J. P. Evans and S. L. Liu, “Role of host factors in SARS-CoV-2 entry,” *Journal of Biological Chemistry*, vol. 297, no. 1. American Society for

Biochemistry and Molecular Biology Inc., Jul. 01, 2021. doi: 10.1016/j.jbc.2021.100847.

[11] A. Vicco *et al.*, "Genomic surveillance of SARS-CoV-2 in patients presenting neurological manifestations," *PLoS One*, vol. 17, no. 6 June, Jun. 2022, doi: 10.1371/journal.pone.0270024.

[12] C. A. Devaux and L. Camoin-Jau, "An update on angiotensin-converting enzyme 2 structure/functions, polymorphism, and duplicitous nature in the pathophysiology of coronavirus disease 2019: Implications for vascular and coagulation disease associated with severe acute respiratory syndrome coronavirus infection," *Frontiers in Microbiology*, vol. 13. Frontiers Media S.A., Nov. 28, 2022. doi: 10.3389/fmicb.2022.1042200.

[13] I. Gintoni, M. Adamopoulou, and C. Yapijakis, "The Impact of ACE and ACE2 Gene Polymorphisms in Pulmonary Diseases including COVID-19," *In Vivo*, vol. 36, no. 1. International Institute of Anticancer Research, pp. 13–29, Feb. 01, 2022. doi: 10.21873/INVIVO.12672.

[14] B. Bakhshandeh *et al.*, "Variants in ACE2; potential influences on virus infection and COVID-19 severity," *Infection, Genetics and Evolution*, vol. 90, p. 104773, Jun. 2021, doi: 10.1016/j.meegid.2021.104773.

[15] S. Beyerstedt, E. Barbosa Casaro, and É. Bevilaqua Rangel, "COVID-19: angiotensin-converting enzyme 2 (ACE2) expression and tissue susceptibility to SARS-CoV-2 infection", doi: 10.1007/s10096-020-04138-6/Published.

[16] M. A. Aziz and M. S. Islam, "Association of ACE1 I/D rs1799752 and ACE2 rs2285666 polymorphisms with the infection and severity of COVID-19: A meta-analysis," *Molecular Genetics and Genomic Medicine*, vol. 10, no. 11. John Wiley and Sons Inc, Nov. 01, 2022. doi: 10.1002/mgg3.2063.

[17] J. M. White, S. E. Delos, M. Brecher, and K. Schornberg, "Structures and mechanisms of viral membrane fusion proteins: Multiple variations on a common theme," *Critical Reviews in Biochemistry and Molecular Biology*, vol. 43, no. 3. Taylor and Francis Inc., pp. 189–219, 2008. doi: 10.1080/10409230802058320.

[18] C. B. Jackson, M. Farzan, B. Chen, and H. Choe, "Mechanisms of SARS-CoV-2 entry into cells," *Nature Reviews Molecular Cell Biology*, vol. 23, no. 1. Nature Research, pp. 3–20, Jan. 01, 2022. doi: 10.1038/s41580-021-00418-x.

[19] W. Shi *et al.*, “Cryo-EM structure of SARS-CoV-2 postfusion spike in membrane,” *Nature*, Jun. 2023, doi: 10.1038/s41586-023-06273-4.

[20] Y. Cai *et al.*, “Distinct conformational states of SARS-CoV-2 spike protein,” *Science (1979)*, vol. 369, no. 6511, Sep. 2020, doi: 10.1126/science.abd4251.

[21] W. T. Harvey *et al.*, “SARS-CoV-2 variants, spike mutations and immune escape,” *Nature Reviews Microbiology*, vol. 19, no. 7. Nature Research, pp. 409–424, Jul. 01, 2021. doi: 10.1038/s41579-021-00573-0.

[22] A. M. Carabelli *et al.*, “SARS-CoV-2 variant biology: immune escape, transmission and fitness,” *Nature Reviews Microbiology*. Nature Research, Mar. 01, 2023. doi: 10.1038/s41579-022-00841-7.

[23] Y. Araf *et al.*, “Omicron variant of SARS-CoV-2: Genomics, transmissibility, and responses to current COVID-19 vaccines,” *Journal of Medical Virology*, vol. 94, no. 5. John Wiley and Sons Inc, pp. 1825–1832, May 01, 2022. doi: 10.1002/jmv.27588.

[24] J. Ngiam, A. Al-Mubaarak, S. Maurer-Stroh, and P. Tambyah, “Does the COVID-19 XBB Omicron subvariant signal the beginning of the end of the pandemic?,” *Singapore Med J*, vol. 0, no. 0, p. 0, 2023, doi: 10.4103/singaporemedj.smj-2022-180.

[25] P. A. Ashorn, E. A. Berger, and B. Moss, “Human Immunodeficiency Virus Envelope Glycoprotein/CD4-Mediated Fusion of Nonprimate Cells with Human Cells,” 1990. [Online]. Available: https://journals.asm.org/journal/jvi

[26] P. Ashorn, E. A. Berger, and B. Moss, “2 VIRUS AND VIRAL PROTEIN MEDIATED CELL-CELL FUSION [2]] Vaccinia Virus Vectors for Study of Membrane Fusion Mediated by Human Immunodeficiency Virus Envelope Glycoprotein and CD4,” 1993.

[27] M. Zhao *et al.*, “Rapid, reliable, and reproducible cell fusion assay to quantify SARS-Cov-2 spike interaction with hACE2,” *PLoS Pathog*, vol. 17, no. 6, Jun. 2021, doi: 10.1371/journal.ppat.1009683.

[28] S. V. Avilov and N. Aleksandrova, “Fluorescence protein complementation in microscopy: applications beyond detecting bi-molecular interactions,” *Methods Appl Fluoresc*, vol. 7, no. 1, 2019, doi: 10.1088/2050-6120/aaef01.

[29] S. Bettati, E. Pasqualetto, G. Lolli, B. Campanini, and R. Battistutta, “Structure and single crystal spectroscopy of Green Fluorescent Proteins,” *Biochimica et Biophysica Acta - Proteins and Proteomics*,

vol. 1814, no. 6. pp. 824–833, Jun. 2011. doi: 10.1016/j.bbapap.2010.10.002.

[30] S. Xiu *et al.*, “Inhibitors of SARS-CoV-2 Entry: Current and Future Opportunities,” *Journal of Medicinal Chemistry*, vol. 63, no. 21. American Chemical Society, pp. 12256–12274, Nov. 12, 2020. doi: 10.1021/acs.jmedchem.0c00502.

[31] S. S. Toussi, J. L. Hammond, B. S. Gerstenberger, and A. S. Anderson, “Therapeutics for COVID-19,” *Nat Microbiol*, vol. 8, no. 5, pp. 771–786, May 2023, doi: 10.1038/s41564-023-01356-4.

[32] K. H. D. Crawford *et al.*, “Protocol and reagents for pseudotyping lentiviral particles with SARS-CoV-2 spike protein for neutralization assays,” *Viruses*, vol. 12, no. 5, May 2020, doi: 10.3390/v12050513.

[33] T. Bio Inc, “Lenti-X^{TM} Lentiviral Expression System User Manual Lenti-X Lentiviral Expression Systems User Manual.”

[34] T. Bio USA, “Lenti-X^{TM} Packaging Single Shots Protocol-At-A-Glance.”

[35] N. Reuter *et al.*, “SARS-CoV-2 Spike Protein Is Capable of Inducing Cell-Cell Fusions Independent from Its Receptor ACE2 and This Activity Can Be Impaired by Furin Inhibitors or a Subset of Monoclonal Antibodies,” *Viruses*, vol. 15, no. 7, Jul. 2023, doi: 10.3390/v15071500.